

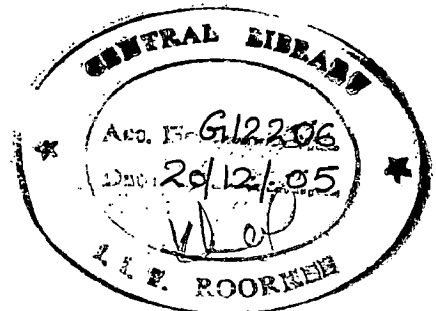
SPATIALLY DISTRIBUTED RAINFALL-RUNOFF MODELLING USING REMOTE SENSING AND GIS - A CASE STUDY

A DISSERTATION

*Submitted in partial fulfillment of the
requirements for the award of the degree*
of
MASTER OF TECHNOLOGY
in
**WATER RESOURCES DEVELOPMENT
(CIVIL)**

By

DWI HARI SHANTI



**DEPARTMENT OF WATER RESOURCES DEVELOPMENT & MANAGEMENT
INDIAN INSTITUTE OF TECHNOLOGY ROORKEE
ROORKEE - 247 667 (INDIA)
JUNE, 2005**

CANDIDATE'S DECLARATION

I hereby certify that the work which is being presented in the dissertation entitled :
“SPATIALLY DISTRIBUTED RAINFALL-RUNOFF MODELLING USING REMOTE SENSING AND GIS - A CASE STUDY”, is in partial fulfillment of the requirement for the award of the degree of the Master of Technology in Water Resources Development and Management (WRD&M) Department, Indian Institute of Technology Roorkee, is an authentic record of my own work carried out during period from July 2004 – July 2005 under the supervision and guidance of Dr. S.K. Mishra and Dr. M.K. Jain.

The matter embodied in this dissertation has not been submitted by me for the award of any other degree.

Date : 20 JUNE 2005

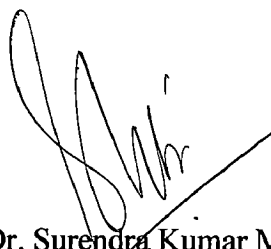
Place : Roorkee


Dwi Hari Shanti

Certified that the above declaration given by the candidate is correct to the best of my/our knowledge,



(Dr. Manoj Kumar Jain)
Scientists E1
National Institute of Hydrology Roorkee
Roorkee,
India



(Dr. Surendra Kumar Mishra)
Assistant Professor,
Department of Water Resources Development
and Management
Indian Institute of Technology, Roorkee
India

ACKNOWLEDGEMENTS

My greatest gratitude goes to my guides Dr. S.K. Mishra (Assistant Professor, Department of Water Resources Development and Management) and Dr. M.K. Jain (Scientist E1, National Institute of Hydrology, Roorkee) for their critical comments and inputs in the preparation and completion of this dissertation, and for encouraging, inspiring, motivating and providing valuable guidance and help. I am highly indebted to both of my guides for providing full cooperation and valuable suggestions from time to time.

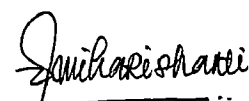
This study could not have been accomplished without the efforts of Dr. M.K. Jain who gave me illuminating insights into the problem. His regular guidance helped to find ways and means to solve the problems. Also for providing me satellite data, rainfall-runoff data, topographical data and other information needed in dissertation work. And I extend my thanks to authorities of National Institute of Hydrology Roorkee for providing necessary facilities during the study period.

I am greatly thankful to the Head of WRD&M Department and other Professors for always encouraging and motivating me.

I am highly grateful to Colombo Plan for providing me the scholarship, Board of Director PT. INDRA KARYA (Persero) and Ministry of Resettlements and Regional Infrastructure Republic Indonesia, for providing an opportunity to undertake and complete the Master's Degree in Water Resources Development and Management Department at Indian Institute of Technology Roorkee, India.

I, of course, should not hesitate to thank my colleagues in 48th batch WRD&M-Civil, Mechanical & Electrical and 24th batch WRD&M-IWM.

A final word of heartfelt thanks goes to my son Fahrizal Afkar, my parents and my family members who always encouraged me to work hard and for their patience during my study period.


Dwi Hari Shanti

CONTENTS

CANDIDATE DECLARATION.....	i
AKCNOWLEDGMENT.....	ii
ABSTRACT	iii
CONTENTS.....	v
LIST OF FIGURE	ix
LIST OF TABLES.....	xi

CHAPTER 1

INTRODUCTION.....	1
1.1. BACKGROUND	1
1.2. NEED OF GIS IN HYDROLOGY.....	2
1.2.1. HYDROLOGICAL INVENTORY AND ASSESSMENT	2
1.2.2. HYDROLOGIC PARAMETER DETERMINATION.....	2
1.2.3. LOOSELY COUPLED HYDROLOGIC MODELS.....	2
1.2.4. INTEGRATED GIS-HYDROLOGIC MODELS	3
1.3. DISTRIBUTED UNIT HYDROGRAPH.....	3
1.4. OBJECTIVE.....	4
1.5. ORGANIZATION OF THESIS	5

CHAPTER 2

REVIEW OF LITERATURE	6
2.1. BACKGROUND	6
2.2. UNIT HYDROGRAPH.....	7
2.2.1. LIMITATION OF UNIT HYDROGRAPH.....	9
2.2.1.1. AREA.....	9
2.2.1.2. WATERSHED LINEARITY.....	10
2.2.1.3. SUPERPOSITION	10
2.3. SPATIALLY DISTRIBUTED UNIT HYDROGRAPH.....	10
2.4. TIME TO EQUILIBRIUM.....	11
2.5. TIME-AREA DIAGRAM.....	13

CHAPTER 3

REMOTE SENSING AND GIS CONCEPT	15
3.1. REMOTE SENSING CONCEPT	15
3.2. THE REMOTE SENSING PROCESS	16
3.3. IDENTIFYING THE PROBLEM	16
3.4. DATA COLLECTION.....	18
3.4.1. IN-SITU DATA	18
3.4.2. REMOTELY SENSED DATA	19
3.5. DATA ANALYSIS IN REMOTE SENSING	21
3.5.1. ANALOG IMAGE PROCESSING.....	21
3.5.2. DIGITAL IMAGE PROCESSING	23
3.5.2.1. PREPROCESSING	23
3.5.2.2. INFORMATION ENHANCEMENT	24
3.5.2.3. INFORMATION EXTRACTION	24
3.6. GEOGRAPHIC INFORMATION SYSTEM (GIS) CONCEPT	24
3.7. DATA STRUCTURE USED IN A GIS.....	26
3.7.1. VECTOR DATA STRUCTURE.....	26
3.7.2. RASTER DATA STRUCTURE	27
3.8. COORDINATE SYSTEM AND GEOREFERENCE	28
3.9. DIGITAL ELEVATION MODEL (DEM).....	30
3.9.1. DATA SOURCES.....	30
3.9.2. DATA STRUCTURES.....	31
3.10. HYDROLOGICAL TERRAIN PARAMETERS	32

CHAPTER 4

METHODOLOGY.....	33
4.1. TRAVEL TIME.....	37
4.1.1. ANALYTICAL FORMULATION	37
4.1.2. OVERLAND FLOW.....	40
4.1.3. CHANNEL FLOW.....	41
4.2. TIME AREA DIAGRAM	41
4.3. UNIT HYDROGRAPH.....	44
4.4. DIRECT RUNOFF HYDROGRAPH.....	46
4.5. LINEAR RESERVOIR ROUTING.....	47

CHAPTER 5

THE STUDY AREA AND DATA AVAILABILITY	49
5.1. THE TEMUR BASIN	49
5.2. DATA AVAILABILITY	51

CHAPTER 6

DATA PROCESSING.....	54
6.1 SPATIAL DATA INPUT.....	54
6.1.1 SCANNING.....	54
6.1.2 COORDINATE SYSTEM AND GEOREFERENCE.....	55
6.1.3 DIGITIZING POINT MAP	55
6.1.4 DIGITIZING SEGMENT MAP.....	56
6.1.5 VECTOR TO RASTER CONVERSION	57
6.2 CREATING DIGITAL ELEVATION MODEL (DEM)	58
6.2.1 DEM OPTIMATIZATION.....	58
6.2.2 FILL SINK.....	59
6.2.3 FLOW DIRECTION	61
6.2.4 FLOW ACCUMULATION.....	63
6.3 CHANNEL DELINEATION	64
6.4 CREATING SLOPE MAP	65
6.5 IMAGE CLASSIFICATION.....	65

CHAPTER 7

ANALYSIS AND DISCUSSION OF RESULTS.....	68
7.1 DETERMINATION OF TRAVEL TIME	68
7.1.1 DETERMINATION OF EXCESS RAINFALL	68
7.1.2 DIFFERENTIAL MAPS OF TRAVEL TIME	68
7.1.2.1 OVERLAND FLOW.....	70
7.1.2.2 CHANNEL FLOW	70
7.1.3 CUMULATIVE TRAVEL TIME MAP	72
7.1.4 DEVELOPMENT OF RELATIONSHIP BETWEEN TIME OF CONCENTRATION AND RAINFALL EXCESS INTENSITIES.....	73

7.2	SENSITIVITY ANALYSIS	74
7.3	TIME AREA DIAGRAM	75
7.4	SPATIAL UNIT HYDROGRAPH.....	77
7.5	UNIT HYDROGRAPH SIMULATION.....	77
7.6	MODEL PERFORMANCE EVALUATION.....	79

CHAPTER 8

CONCLUSIONS.....	88
------------------	----

REFERENCES

APPENDICES

LIST OF FIGURE

Figure 2.1 Hydrology Cycle.....	6
Figure 3.1 Schematic representation of Taking Remotely Sensed Data	15
Figure 3.2 The Remote Sensing Process.....	16
Figure 3.3 Methodologies in Remote Sensing	17
Figure 3.4 Reflectance Curves Produced	20
Figure 3.5 Basic Steps in Analog and Digital Image Processing	23
Figure 3.6 The Concept of Layer	26
Figure 3.7 Vector Representations	27
Figure 3.8 Raster Representations.....	28
Figure 3.9 Determination by The Longitude and Latitude.....	20
Figure 3.10 Schematic of Contribution Cells and Effective Contour Lengths	32
Figure 4.1 Flow Chart of Methodology.....	36
Figure 4.2 Watershed Time-Area Relationships	43
Figure 4.3 The Time-Area Diagram and The Unit Hydrograph	45
Figure 4.4 Space Time Discretization in the Method of Cascade of Linear Reservoir.....	48
Figure 5.1 The Study Area	50
Figure 5.2 Satellite Map	51
Figure 6.1 Georeference and Coordinate System of Temur Basin.....	55
Figure 6.2 Contour Line of Temur Basin	57
Figure 6.3 Raster Contour of Temur Basin	57
Figure 6.4 Effect of Buffer Distance, Smooth Drop & Sharp Drop.....	59
Figure 6.5 Fill Sink Calculation Process.....	60
Figure 6.6 Steepest Slope Calculation Process	62
Figure 6.7 Lowest Height Calculation Process	62
Figure 6.8 Flow Accumulation Calculation Process.....	63
Figure 6.9 DEM Map, Flow Direction & Accumulation Map of Temur Basin.....	63
Figure 6.10 Temur Basin DEM-based stream network & digitized.....	64
Figure 6.11 Slope Map of Temur Basin	65

Figure 6.12	Sampling Corresponding Remote Sensing Map	66
Figure 6.13	Classified Land use map of Temur Basin	67
Figure 7.1	Equilibrium Discharge Map of Temur Basin.....	69
Figure 7.2	Manning's Map of Temur Basin.....	69
Figure 7.3	Relationship between R/h and W/h	71
Figure 7.4	Maps of Travel Time for $I=0.20$ cm/hr.....	71
Figure 7.5	Isochrone Map of Temur Basin ($I=0.20$ cm/hr).....	72
Figure 7.6	Variation of T_c with difference Rainfall Excess Intensities	73
Figure 7.7	Respond of T_c causes of Manning's Coefficient.....	74
Figure 7.8	Slicing Isochrone Map of Temur Basin	76
Figure 7.9	TAD for difference Rainfall Excess Intensities	76
Figure 7.10	Storage Coefficient (K) vs Maximum Rainfall Excess.....	79
Figure 7.11	Runoff Hydrograph for Event 5.09.1962.....	81
Figure 7.12	Runoff Hydrograph for Event 30.08.1965	82
Figure 7.13	Runoff Hydrograph for Event 14.08.1964.....	83
Figure 7.14	Runoff Hydrograph for Event 7.09.1965.....	84
Figure 7.15	Runoff Hydrograph for Event 20.07.1964.....	85
Figure 7.16	Runoff Hydrograph for Event 23.7.1962.....	86
Figure 7.17	Runoff Hydrograph for Event 24.08.1961	87

LIST OF TABLE

Table 3.1 Elements of Image Interpretation.....	22
Table 3.2 Typical Elevation Accuracy of Different Data Sources to Derive DEM.....	31
Table 5.1 Spatially Average Rainfall Data for Seven Events	52
Table 5.2 Observed Discharge Data for Seven Events	53
Table 7.1 Manning's Coefficient Value for Temur Basin.....	74
Table 7.2 Peak Discharge & Time to Peak of Simulated Data	77
Table 7.3 Different Value of K for Seven Events	78
Table 7.3 Error Statistics between Observed and Computed Hydrograph Series.....	80

ABSTRACT

Ever since its conception, the Sherman unit hydrograph (UH) has been widely used in rainfall-runoff modeling. Unit hydrograph of a watershed is defined as direct runoff hydrograph resulting from a unit depth of rainfall-excess generated uniformly over the drainage area at a constant rate for an effective duration. The unit hydrograph is a lumped linear model of a watershed where it is assumed that a catchment acts on an input of effective precipitation in a linear and time invariant manner to produce an output of direct storm runoff. Methods for determining a UH from storm events with observed direct runoff hydrograph and effective rainfall hyetograph are umpteen.

The unit hydrograph theory suffers from limitation that the response function is lumped over the whole watershed properties. Efforts have been made to overcome this limitation of unit hydrograph theory by introducing of geographical information system for spatial discretization of watershed into an inter-linked system of grid cells. It is now becoming common to represent land surface elevation over the watershed by grid based digital elevation model (DEM). Standardized algorithm are available in geographical information systems, which use the local terrain slope to link each cell with one of its neighbor along the line of steepest descent, thus creating a one-dimensional flow network over the entire land surface. It had been shown that this terrain representation can be utilized for runoff computation under spatially varying, but time and discharge invariant velocity field. The linear system response at the watershed outlet can be spatially decomposed into a set of cell based linear systems whose individual response functions summation give the watershed response function.

This study derives spatially distributed unit hydrograph using the isochrones varying in time with rainfall intensity, overcoming the stationary constraint of unit hydrograph concept. The model uses digital elevation model (DEM) data, ground slope, flow direction and flow accumulation maps to characterize the watershed terrain in a geographical information system (GIS). A raster based approach deals with spatial domain discretization and supports rainfall-runoff simulation in a modular distributed model. The translation characteristics of the catchment are accounted by time area (TA) concept. The TA diagram is a graph of cumulative drainage area contributing to discharge at the watershed outlet

within a specified time of travel. The isochrones of travel time are allowed to vary with temporal changes in intensity of rainfall-excess. The storage-induced time delay and catchment diffusion effects on the resultant flood hydrograph are accounted by routing the time variant TA diagram through a conceptual reservoir. Overland flow travel times are calculated by the kinematic wave equation for time to equilibrium, and channel flow times are based on Manning and continuity equations, which is an improvement over the existing isochrone extraction technique. The time series of travel time (or isochrones) maps constitute the basis for incremental and total runoff hydrograph computations. The data of a meso-scale catchment located in Madhya Pradesh (Temur river, tributary of Narmada river) were used to test the proposed method. Results obtained indicate that introduction of two reservoirs in series to account for catchment-induced storage effects on runoff hydrograph has significantly improved model computed results indicating use of simple kinematic wave derived travel time histogram for derivation of unit hydrograph is not sufficient for a mid-sized catchment exhibiting storage induced diffusion. The overall very high values of R^2 and Nash-Sutcliffe efficiency for most of the storm events indicate suitability of the proposed model to Temur catchment which exerts substantial amount of storage-induced diffusion effects on runoff hydrographs due to flatter topography in the middle to southern parts of the catchment.

CHAPTER 1

INTRODUCTION

1.1. BACKGROUND

The flow of water on the surface of earth has long perplexed the human mind. The desire to understand the movement of water has mainly arisen from the need to evaluate the amount of water available at a particular location to meet local demand as well as the risk of flooding due to excess water. Hydrologists have always been concerned with the discharge rates and runoff created by rainfall. The two most important parameters of hydraulic interest are the peak flow and the time to peak. This information is needed for a variety of design applications like dams, spillways and culverts (Ajward, 1996). But most of the rivers are not gauged and even if the gauge is in place the record period is too short to estimate the different hydraulic parameters (Muzik, 1995) or to predict extreme future events (Ajward, 1996). Using historical flow data we can predict future events with a certain return period using frequency analysis. But in the absence of such data we need to develop hydrologic models that would simulate the watershed characteristics and predict the flow rates at any given location in the watershed.

Since the precipitation data is more widely available (because of larger number of gauging stations and the longer record periods) than the stream flow data, many rainfall-runoff models have been developed to estimate the runoff. The type of model used and the complexity it manifests is convenient to the available data. Some hydrologic models try to estimate the watershed response based on the geo-morphological characteristics of the watershed. The other type of the model can be the empirical model, which works on the mathematical formulae developed using a range of data, which restricts its use. The concepts of Sherman (1932) Unit Hydrograph and Regression Analysis are the two examples. The physical models on the other hand are based on the physical laws and since they represent the hydrologic process in situ, they produce the whole hydrograph and not only the peak flow and the time to peak. With the increase in the computing power, hydrologists have developed many distributed models. These distributed models have the ability to incorporate information about the spatial variability of the soil, land use,

topography, etc. Geographic Information System (GIS) is commonly utilized to store the distributed information and making computations in spatial domain.

1.2. NEED OF GIS IN HYDROLOGY

As the interest in distributed hydrologic models increased, there was also an increase in the use of GIS for modeling and spatial analysis (McDonnell, 1996). Maidment (1993) suggested a scheme to classify the different uses of GIS in hydrology:

- (a) Hydrological inventory and assessment,
- (b) Hydrological parameter determination,
- (c) Loosely coupled GIS and hydrological models, and
- (d) Integrated GIS and hydrological models.

1.2.1. HYDROLOGICAL INVENTORY AND ASSESSMENT

Measuring the spatial extent of hydrologic variables, from paper maps may be tedious, labor-intensive and error-prone. A GIS may be used as a way to automatically derive the required information. It can be used as a method to integrate, visualize, and derive spatial and non-spatial data (McDonnell, 1996).

1.2.2. HYDROLOGIC PARAMETER DETERMINATION

The use of GIS for model parameter estimation is a very active area of research (McDonnell, 1996). Distributed parameter models require a large amount of data. A GIS may be used to manage and manipulate the large quantities of data that distributed models demand. Values such as slope and cumulative area above a point may be difficult to estimate with paper maps and manual methods. They are however easily determined with a GIS.

1.2.3. LOOSELY COUPLED HYDROLOGIC MODELS

One of the major limitations of the integration of GIS and hydrologic models is that current GIS technology cannot represent the continuous temporal element of modeling. It can only represent time as a series of "snapshots" (McDonnell, 1996). A loosely coupled system forms one of the most popular ways for use of GIS in hydrologic modeling where the model and GIS maintain two separate databases and interact through some form of a file exchange or conversion process.

1.2.4. INTEGRATED GIS-HYDROLOGIC MODELS

In an integrated GIS-hydrologic model, both components share one database and there is no data export between the two. The major limitation of this type of system is that current GISs often have limited modeling capabilities. Drayton et al. (1992) developed an integrated model that calculated the runoff volume and hydrograph for a watershed. The model uses satellite imagery and digital elevation data for the model inputs.

1.3. DISTRIBUTED UNIT HYDROGRAPH

Ever since its conception by Sherman (1932), the unit hydrograph (UH) has been widely used in rainfall-runoff modeling. Unit hydrograph of a watershed is defined as direct runoff hydrograph resulting from a unit depth of excess rainfall generated uniformly over the drainage area at a constant rate for an effective duration (Chow et al., 1988). The unit hydrograph is a lumped linear model of a watershed where it is assumed that a catchment acts on an input of effective precipitation in a linear and time-invariant manner to produce an output of direct storm runoff (Dooge, 1959). Methods for determining a UH from storm events with observed direct runoff hydrograph and effective rainfall hyetograph are umpteen. Singh (1988) has systematically categorized them.

The unit hydrograph theory suffers from limitation that the response function is lumped over the whole watershed and does not explicitly account for the spatially distributed nature of the watershed properties. Efforts have been made to overcome this limitation of unit hydrograph theory by introduction of geographical information system for spatial discretization of watershed into an inter-linked system of grid cells (Maidment, 1993; Maidment et al., 1996; Muzik, 1996; Olivera and Maidment, 1999; Saghafian, 2002). It is now becoming common to represent land surface elevation over the watershed by grid based digital elevation model (DEM). Standardized algorithms are available in geographic information systems, which use the local terrain slope to link each cell with one of its neighbors along the line of steepest descent, thus creating a one dimensional flow network over the entire land surface. It has been shown by Maidment et al. (1996) that this terrain representation can be utilized for runoff computation under spatially varying, but time- and discharge-invariant velocity field. The linear system response at the

watershed outlet can be spatially decomposed into a set of cell based linear systems whose individual response functions summation give the watershed response function.

1.4. OBJECTIVES

The overall objective of this study is to derive spatially distributed unit hydrograph using the isochrones varying in time with rainfall intensity, overcoming the stationary constraint of unit hydrograph concept. To attain the above objective the following subsidiary objectives need to be satisfied:

- To generate digital elevation model (DEM) for the watershed under study.
- To generate slope, flow direction, flow accumulation and channel network to characterize the study watershed terrain using a GIS.
- To generate land use map of the study watershed using digital analysis of satellite data.
- To generate overland and channel flow travel time using kinematic wave equation for time to equilibrium, for spatially varied watershed characteristics and temporally varied excess rainfall intensity.
- To generate isochrones and time-area (TA) diagram for developing spatially distributed unit hydrograph.
- To account for the storage-induced time delay and catchments diffusion effects on the resultant spatially distributed unit hydrograph by routing the time variant TA diagram through two conceptual reservoirs in series, one each for overland and channel regions.
- To generate direct runoff hydrographs of the storm by convoluting the spatially distributed unit hydrograph with the rainfall-excess hyetograph.
- To compare the simulated direct runoff hydrographs with the observed direct runoff hydrographs.

1.5. ORGANIZATION OF THESIS

The aforesaid objectives are addressed through the following chapters.

- CHAPTER 2** : presents a literature review of unit hydrograph, spatially distributed unit hydrograph, time to equilibrium for overland flow and channel flow, and time area diagram.
- CHAPTER 3** : presents a conceptual understanding of the basic principles of remote sensing and GIS, data analysis in remote sensing, data structure used in GIS, coordinate system and georeferences, digital elevation model (DEM), and hydrological terrain parameter.
- CHAPTER 4** : contains methodology followed in this study showing as flow chart, modeling framework, modeling steps, analytical formulation of time equilibrium, time-area diagram, unit hydrograph, direct runoff hydrograph and linear reservoir routing.
- CHAPTER 5** : presents details of study area of Temur basin and its data availability.
- CHAPTER 6** : discusses the data processing involving spatial data input in GIS software (ILWIS 3.2), creating digital elevation model (DEM), channel delineation, creating slope and aspect map, and image classification for classification of land use derived from the satellite image.
- CHAPTER 7** : presents the analysis and discusses the result, including determination of time to equilibrium, time area diagram, spatially distributed unit hydrograph, direct surface runoff hydrograph, routing through two conceptual linear reservoirs, sensitivity analysis and an evaluation based on dimensionless coefficient and Nash & Sutcliffe efficiency.
- CHAPTER 8** : concludes the study.

CHAPTER 2

REVIEW OF LITERATURE

2.1. BACKGROUND

The most basic equation in hydrology is the continuity equation, which states that over any time interval the difference in the volume of the water entering a (hydrologic or any other) system I , and leaving the system, O must equal the change in the volume of water stored in the system, ΔS

$$I - O = \Delta S \quad \dots \dots \dots (2-1)$$

If the hydrologic system is a small catchment, the inflow to the system would be precipitation. The outflow from the system would be stream-flow, deep seepage and evapotranspiration. Storage within the system would include soil water, ground water, ponds, lakes, reservoirs, channel storage, surface storage, detention storage and interception (Haan et al., 1994). A pictorial depiction of such a system referred from Chow (1988) is depicted in Figure 2.1.

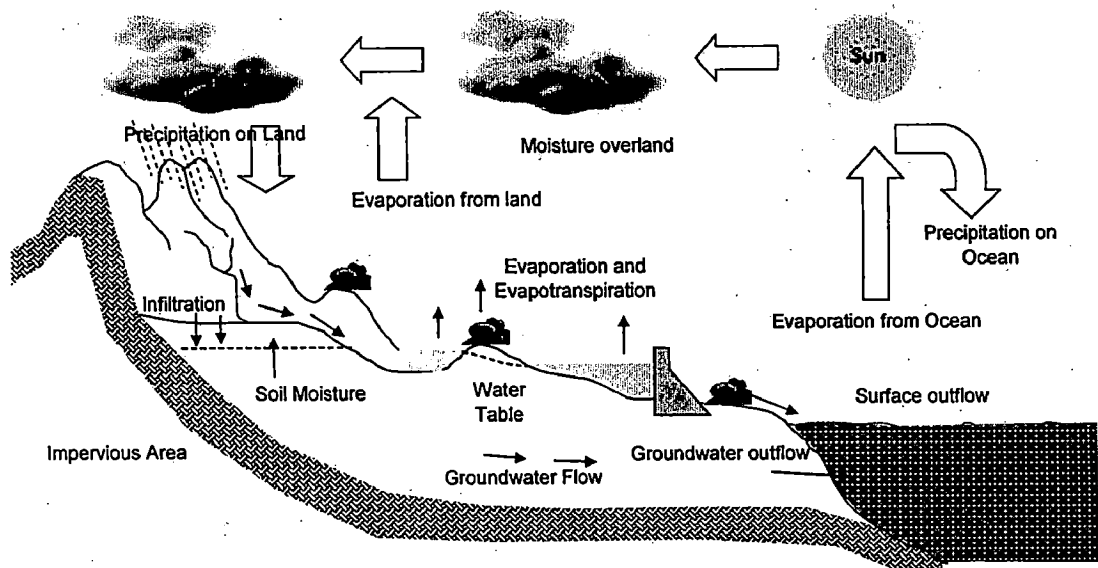


Figure 2.1 Hydrology Cycle

For short time intervals (hours), evapotranspiration and deep seepage can be generally ignored. For long time intervals (weeks), surface storage, surface detention, and interception are often ignored. In the absence of ponds, reservoirs or lakes the hydrologic equation can be further simplified.

The above equation has been widely used in rainfall-runoff modeling. The modeling of runoff-generation from rainfall began in the second half of the nineteenth century in response to three major engineering problems (Todini, 1988): urban sewer design, land reclamation drainage system design, and reservoir spillway design.

At first, many engineers applied empirical equations developed in one region to many other areas and situations (Todini, 1988). They assumed that the conditions were "close enough." The other popular technique was the "rational method" to predict peak flow rates (Todini, 1988). Developed for small watersheds, the rational method is based on land use and rainfall intensity. It was the first attempt to "rationally" predict runoff from rainfall. During the 1920's, the need arose to have an analogous procedure that predicts the peak flow rate for larger watersheds. A modification of the rational method was developed based on the concept of isochrones. Isochrones are areas with equal travel times. The modified rational method was used to solve many of the same types of problems as the original rational method, however it generally produced more realistic, accurate solutions (Todini, 1988).

2.2. UNIT HYDROGRAPH

In 1932, Sherman developed the unit hydrograph concept for determining the hydrograph of direct runoff from the hyetograph of effective rainfall, which has since been widely used in applied hydrology. The unit hydrograph (UH) of watershed can be defined as the hydrograph of direct runoff resulting from one unit (1 inch or 1 centimeter) of effective rainfall occurring uniformly over the watershed at a uniform rate during a unit period of time. This unit period is not necessarily equal to unity; it can be any finite number. This unit period of effective rainfall is the period for which the unit hydrograph is determined. For a specified watershed, the unit hydrograph changes with the change in this period. Thus, there can be as many unit hydrographs for a watershed as there are periods of effective rainfall.

Sherman (1932) introduced the unit hydrograph based on the principle of superposition. It was one of the first tools available to hydrologists to predict entire hydrographs instead of just peak discharges (Todini, 1988). The procedure to develop a unit hydrograph for a storm with a single peak is fairly simple. After the baseflow is removed from the total runoff hydrograph, the direct runoff hydrograph is obtained. The total runoff volume is then determined by integrating this direct runoff hydrograph. To obtain the unit hydrograph, each ordinate of the direct runoff hydrograph is divided by the runoff volume.

Theoretically, unit hydrographs developed from different storms should be identical, but they are not in practice. Therefore, to develop an average response, Ponce (1989) recommended developing unit hydrographs from at least five different storm events. Linsley et al. (1975) suggest that an average response may be determined by calculating the average peak flow rate and time to peak. Then sketch a hydrograph shape which contains 1 unit of runoff, passes through the average peak, and has a shape similar to the unit hydrographs developed from the individual storm events.

The unit hydrograph is the unit pulse response function of a linear hydrologic system (Chow et al., 1988). The unit hydrograph method is derived from the fundamentals of the linear system analysis. The unit hydrograph is based on the principle of superposition and the principle of time invariance. If the principle of superposition were not to hold then the runoff hydrograph for a complex storm could not be generated using a series of hydrographs, which in turn are generated using the unit hydrograph with a number of lagged rainfall-excess volumes. On the other hand, if the principle of time invariance were not to hold good then the predictions based on the past observations would never turn out to be true, because every other input would produce a different response as it would be undergoing a different transformation and hence these responses cannot be superimposed.

2.2.1. LIMITATION OF UNIT HYDROGRAPH

Unit hydrograph theory contains a number of assumptions that can limit its use. They are (Chow et al., 1988):

- The rainfall-excess has a constant intensity within the effective duration. When the unit hydrograph is developed using gauged data, the storms selected for analysis should have a short duration because they are the most likely to have a uniform intensity and produce a single-peaked hydrograph.
- The rainfall-excess is uniformly distributed throughout the entire drainage area. This assumption may pose difficulties for larger watersheds. For watersheds above a certain size, the assumption of uniform rainfall is no longer valid.
- The base time of the direct runoff hydrograph is constant based on a given duration of rainfall. This assumption implies that the unit hydrograph model cannot account for differences in the watershed response to different rainfall intensities.
- The ordinates of all direct runoff hydrographs with the same base time are proportional to the total amount of direct runoff represented by each hydrograph.
- The hydrograph resulting from rainfall-excess reflects the unique characteristics of the watershed. The unit hydrograph model cannot reflect variations in the watershed response due to changes in the season, land use or channel characteristics.

The unit hydrograph is assumed to be a constant response function of the watershed as long as there are no major changes in the land use. Traditional unit hydrograph models cannot account for differences in the watershed response due to seasonal conditions or rainfall intensities.

2.2.1.1. AREA

While many authors agree that the unit hydrograph is only applicable for a limited range of watershed sizes, they disagree about what the extent actually is. Sherman (1932) used the unit hydrograph theory on watersheds ranging from 1300 km² to 8000 km². Linsley et al. (1975) recommended that the unit hydrograph only be used on watersheds less than 5000 km², while Ponce (1989) suggested that it should only be applied on midsize catchments between 2.5 km² and 250 km². Because the unit hydrograph model

assumes that rainfall is uniform over an entire area, it is not applicable to large watersheds. Small catchments tend to reflect variations in the rainfall-excess more than large watersheds, because small catchments have less channel storage than large watersheds, thus the small catchments are less appropriate for unit hydrograph analysis (Huggins and Burney, 1982).

2.2.1.2. WATERSHED LINEARITY

One of the most significant limitations of the unit hydrograph theory is the assumption of linearity. In fact, the watershed is a highly nonlinear system (Huggins and Burney, 1982). Due to the assumption of linearity, the unit hydrograph method is not applicable for watersheds that have appreciable storage effects (Gray, 1973). In addition, the unit hydrograph theory may not be applicable to small watersheds because they tend to exhibit a nonlinear response more than larger areas (Huggins and Burney, 1982). In practice, the linearity assumption is useful because the equations are relatively simple and the results are acceptable for most engineering purposes (Bedient and Huber, 1992).

2.2.1.3. SUPERPOSITION

The unit hydrograph theory is based on the idea of superposition. The hydrograph ordinates for a complex storm event are the sum of the ordinates of the incremental hydrographs that are developed for each period of rainfall excess.

2.3. SPATIALLY DISTRIBUTED UNIT HYDROGRAPH

The "spatially distributed unit hydrograph" proposed by Maidment (1993) is similar to the geomorphic instantaneous unit hydrograph (Rodriguez-Iturbe and Valdes, 1979), except that it uses a Geomorphological Information System (GIS) to describe the connectivity of the links and the watershed flow network instead of probability arguments. Maidment calculated the flow distance from each cell to the watershed outlet. The travel time from each cell to the watershed outlet was calculated by dividing each flow length by a constant velocity. He developed a time-area curve based on the travel time from each grid cell. Maidment (1993) evaluated his methodology on a hypothetical watershed that consisted of 36 grid cells. His results were inconclusive; the time-area histogram did not result in the expected S-hydrograph shape. The poor results were blamed on the small size of the watershed.

Muzik (1995) applied Maidment's procedure to a 229 km² watershed in the Canadian Rockies. He estimated the flow velocity through each grid cell by combining the continuity equation and Manning's equation. The resulting time-area curve had the expected S-hydrograph shape. A unit hydrograph can be derived from the time-area curve by applying the standard S-curve technique (Chow et al., 1988).

Ajward (1996) applied the spatially distributed unit hydrograph to two large watersheds in the Canadian Rockies, comparing the predictions from the spatially distributed unit hydrograph with the observed hydrograph for eight rainfall events. He found that the model generally gave good predictions of the peak flow rate and the time to peak. He also found that the best predictions were produced when a unit hydrograph developed from a storm with a similar intensity to the test event was used. An "average" unit hydrograph always gave less accurate predictions of time to peak and peak flow rate than a unit hydrograph that was developed with an intensity that was close to the average intensity of the test event.

Development of spatially distributed unit hydrograph in a GIS involves computation of time to equilibrium and time-area diagram. The text below reviews the relevant literature on these aspects.

2.4. TIME TO EQUILIBRIUM

The relationship between the kinematic time to equilibrium, catchment characteristics, and rainfall properties has been analytically derived for well-defined simple geometries. For example, using the method of characteristics, the kinematic time to equilibrium was derived by Lighthill and Whitham (1955) and Henderson and Wooding (1964) for a rectangular plane sloping in a single direction. Using the same method, Agiraliloglu (1984, 1988) derived integral forms for t_e of converging and diverging planes. Wooding (1965a) developed analytical solutions for a hydraulic model of kinematic flow over a plane V-shaped catchment under uniform rainfall of finite duration and for a line****check**** stream outflow laterally supplied by the overland catchment discharge. The overland flow and channel flow were treated separately. A dimensionless time parameter λ was introduced as a measure of the ratio of stream response time (i.e. stream equilibrium time) to catchment response time (i.e. overland equilibrium time). Large

values of λ cause delay in the arrival time of flood peak and reduce its amplitude. For small values of λ , the stream outflow tends toward the catchment outflow (Woodward 1965b, 1966).

In reality, the absolute steady state is achieved only when the rainfall duration is infinite. For practical purposes, however, a virtual equilibrium condition often replaces the absolute equilibrium condition. Larson (1965), for example, selected the 'time to virtual equilibrium' to be the time when the discharge reaches 97% of steady-state discharge. However, an arbitrary 'time to virtual equilibrium' may be effectively used as the upper limit, although not in the exact sense for a rainfall duration which produces a partial equilibrium hydrograph. Machmeier and Larson (1968) derived a relationship for the time to virtual equilibrium t_{ve} , the time at which flow rate is 97% of equilibrium flow, for the case of a synthesized model watershed of 54.66 km² in size, having a channel system with defined physical characteristics. The procedure involved disaggregating the watershed into several units of overland plane and then routing the lateral inflow in the channel network. Their results indicated that t_{ve} varied inversely with the 0.23 power of rainfall rate, similar to those of Ben-Zvi (1984).

By taking t_{ve} to be the particle travel time from the watershed farthest point to the outlet, Golany and Larson (1971) tried to develop a general relationship for t_{ve} . The physical and geomorphological characteristics used previously by Machmeier and Larson (1968) were incorporated in a synthesized watershed model that routes the runoff on overland planes and in channel network. This model was used to estimate the constants in the t_{ve} equation.

Hjelmfelt (1978) provided a method to calculate the time of concentration t_c for constant rainfall intensity and transient infiltration. He pointed out that the outflow increases after reaching that time. He also inferred that as a general trend the varying infiltration during a storm has a significant effect on the time of concentration and on the shape of the runoff hydrograph.

Akan (1986) developed a mathematical model based on kinematic flow and the Green-Ampt infiltration equation to calculate the time of concentration t_c of overland flow on a rectangular plane surface. He expressed the non-dimensional t_c in terms of two dimensionless parameters. Akan (1988) attempted to determine the time of concentration

and the peak runoff discharge from an infiltrating converging basin. He used an approach similar to that of a rectangular plane and provided several charts for t_c and peak discharge for storms with duration equal to t_c . Based on this, the literature clearly lacks in the development of time to equilibrium formulation applicable to large watersheds. Numerical solutions are required when dealing with two-dimensional watersheds subjected to spatially distributed rainstorms.

Time to equilibrium for small and large watersheds is a very important parameter governing the linearity of the rainfall-runoff process. When the rainfall duration t_r exceeds the time to equilibrium t_c , the surface runoff discharge increases linearly with rainfall intensity in the sense of the rational formula. Accordingly, linear methods such as the unit hydrographs (UH) and instantaneous unit hydrographs (IUH) are applicable. On the other hand, when the rainfall duration is short compared with the time to equilibrium, partial equilibrium hydrographs are obtained for which the relationship between rainfall and surface runoff is non-linear. Surface runoff calculations based on linear techniques such as UH and IUH are not applicable and methods that account for the non-linearity of surface runoff must be used. In recent investigations (Julien and Moglen, 1990); Ogden and Julien, 1993), the concept of time to equilibrium was applied to impervious planes and to small semiarid watersheds. When considering the magnitude and variability of peak discharge owing to spatial and temporal variability in watershed and rainfall characteristics, there is similarity at different scales when plotting the runoff response versus the ratio of rainfall duration to time to equilibrium. To examine whether the similarity characteristics also extend to large watersheds, one must be capable of calculating the time to equilibrium for large watersheds.

2.5. TIME-AREA DIAGRAM

Time area (TA)-based rainfall-runoff analysis is widely known as a hydrologic watershed routing technique to derive hydrograph due to rainfall-excess hyetograph. In this technique, by ignoring storage effects, the watershed is divided into a number of subarea separated by isochrones; i.e. the isolines of equal travel time to the outlet. The Clark unit hydrograph (Clark, 1945) is based on the TA concept in which watershed storage effects are also taken into account. The TA technique is believed to be applicable up to midsize watershed (Ponce, 1989).

Similar to many other rainfall-runoff transformation techniques, the TA method shares the assumption of 'stationarity' with the unit hydrograph theory. This means that a unique time invariant transfer function is applied for watershed runoff hydrograph calculations regardless of the rainfall-excess input. Considering dynamics of the runoff system, however, the transfer function must respond to temporal change in rainfall-excess intensity. Rodriques-Iturbe and Valdes (1979) recognized that instantaneous unit hydrographs (IUH) vary both from storm to storm and during a storm. They added that such variability may account for the variability in the mean stream flow velocity. Rodriques-Iturbe et.al. (1979) suggested that the use of constant velocity at the peak discharge is justifiable for estimating peak and time to peak discharge. However, errors in estimating flow velocity may lead to large errors in discharge estimating when the flow velocity is smaller than 2 m/s.

Although 'stationarity' is a major constraint in original TA, the method has several advantages and potential. The temporal distribution of rainfall-excess may be accounted for in the runoff discharge calculations. The influence of the space and detailed drainage pattern of the watershed provided that isochrones are based on distributed watershed hydro-geomorphologic characteristics. Many hydrologists consider TA a lumped parameter model (Ponce, 1989).

CHAPTER 3

REMOTE SENSING AND GIS CONCEPT

3.1. REMOTE SENSING CONCEPT

Remote sensing is the process of collecting data about objects or landscape features without coming into direct physical contact with them. Most remotely sensed data are observed from orbital or sub-orbital platforms using instruments which measure electromagnetic radiation reflected or emitted from the terrain referred from Jensen, 1996 as given Figure 3.1.

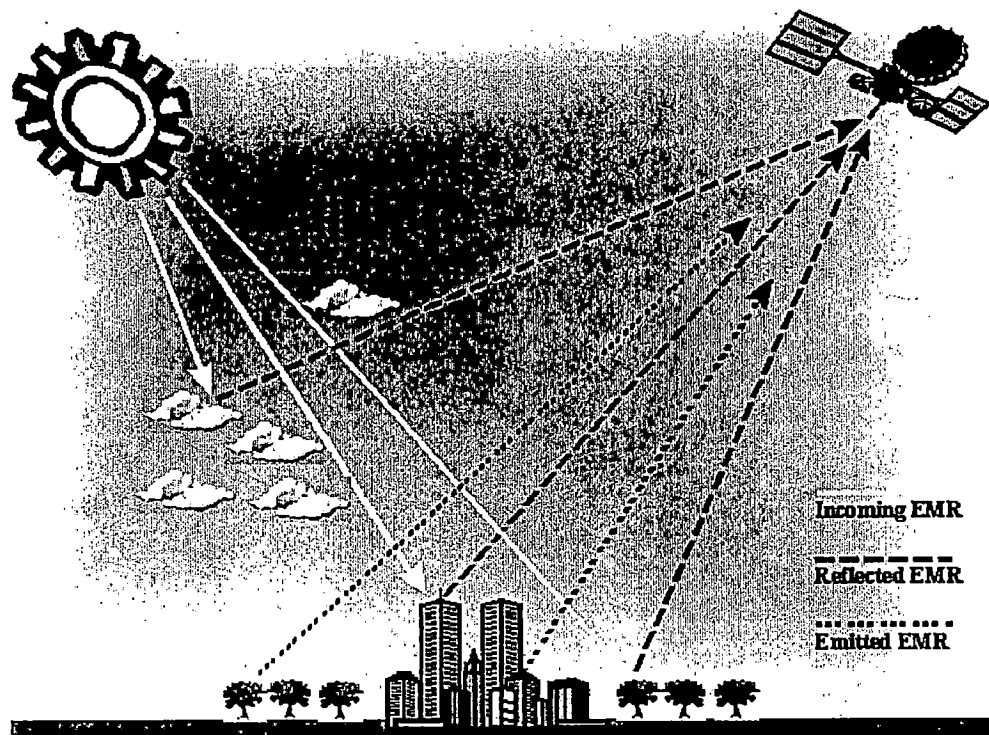


Figure 3.1 Schematic Representation of taking Remotely Sensed Data

Other sensors use other mediums such as magnetic fields, sound waves, etc. These methods work on the same principles as electromagnetic remote sensing, but comprise a small part of the total data produced from remote sensing. Remote sensing is a technique that can be used in a wide variety of disciplines, but is not a discipline or subject itself. The primary goal of remote sensing is not only the pursuit of knowledge, but also the

application of any knowledge gained. The digital image processing helps further this goal by allowing a user to manipulate and analyze the image data produced by these remote sensors in such a way as to reveal the information that may not be immediately recognizable in the original form.

3.2. THE REMOTE SENSING PROCESS

To understand the relationship of digital image processing to remotely sensed data, one should have a clear concept of the steps involved in the remote sensing process referred from Jensen, 1996. These steps are given in Figure 3.2.

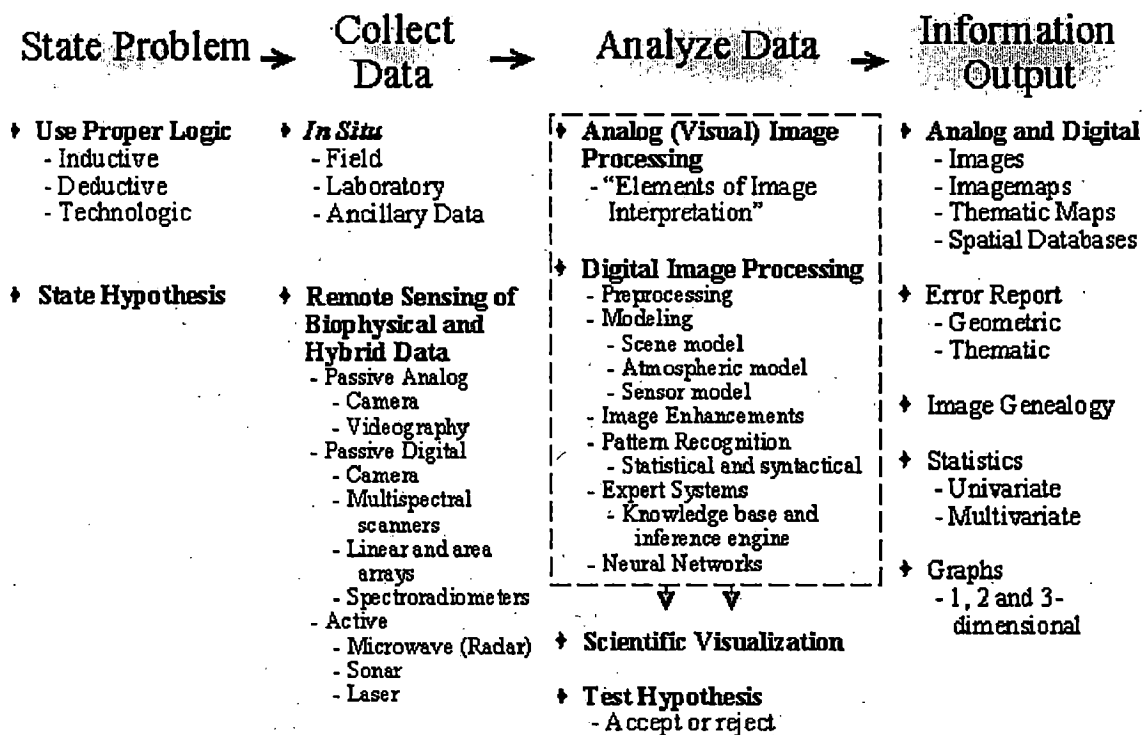


Figure 3.2 The Remote Sensing Process

3.3. IDENTIFYING THE PROBLEM

The first step in remote sensing, as in any other scientific study, is the definition of a problem. Due to its multidisciplinary nature, the problems that remote sensing can be applied to are numerous and diverse. In spite of this, the approaches to remote sensing can be categorized as being either scientific in nature or technological in nature. The

distinction is primarily a function of the motive behind solving the problem. Scientific approaches are driven primarily by "curiosity or whim" (Curran, 1987) while technological approaches are driven by human need. The methodology that is subsequently applied to the problem is usually dependent upon the origin of the individual's problem.

There are three basic types of logic that can be applied to a problem: inductive, deductive, and technologic. Scientific approaches use both inductive logic and deductive logic methodologies, while a technological approach uses a technologic logic methodology. The steps in each of these logic methodologies referred from Jensen, 1996) can be seen in Figure 3.3.

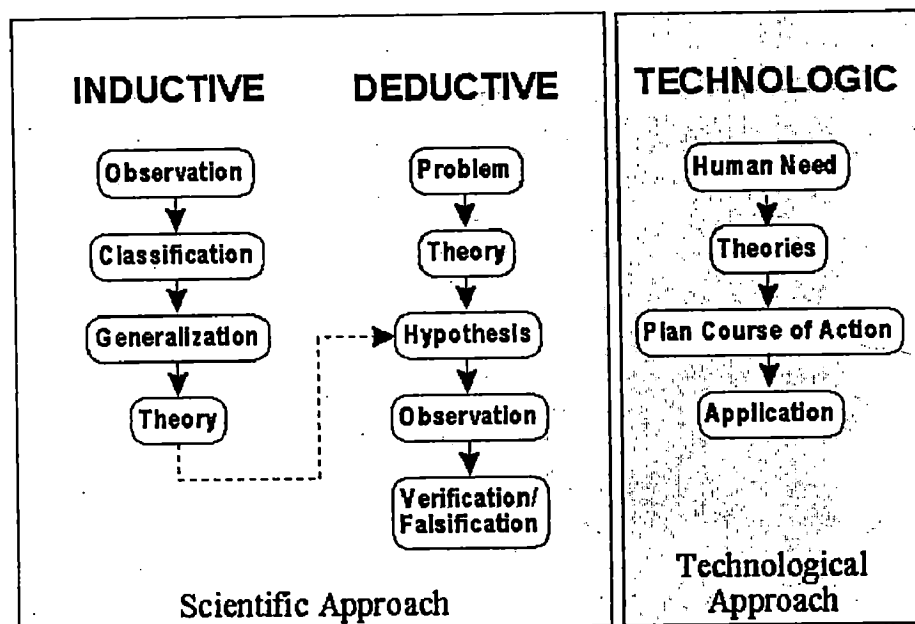


Figure 3.3 Methodologies in Remote Sensing

Inductive logic could be described as learning logic. The inductive methodology seeks to form tenable theories by making observations of phenomena, classifying these observations and making generalizations that form the basis of theories. Theories formed are often fed directly into a deductive methodology (see Figure 3.3) where hypotheses are developed for testing the theories.

The focus of deductive logic is the formulation of theories and the subsequent testing of hypotheses. Once a problem is identified, a researcher conjectures a theory to solve it. To determine the validity of any such theory, hypotheses are developed and

tested. The hypotheses are at the core of the deductive logic. Because of their importance, great care should be taken to formulate a hypothesis that is appropriate to the problem at hand. Two of the most common types of hypotheses are the factual and the inferential. A factual hypothesis clearly states a position that can be either verified or falsified. It is possible to verify this hypothesis as either truth or falsehood. An inferential hypothesis is one which can be falsified. Observations that fail to disprove the hypothesis do not necessarily prove its truthfulness. However, a failure to disprove the hypothesis generally results in the acceptance of the theory being tested with the knowledge that future observations may later reverse that decision.

A technological approach differs from both the inductive and deductive in both its origin and its goal. The basis of this approach is human need rather than scientific inquiry. The goal is the rectification of that need rather than simply an increase in knowledge. The focus of a technological methodology is the design of coherent plan which successfully blends "inputs from science, economics, aesthetics, law, logistics and other areas of human endeavor" (Curran, 1987).

3.4. DATA COLLECTION

Once the problem has been stated and the theories formed it is necessary to collect data, both in situ and remotely, in order to progress toward a solution. If data is to be useful, it must be collected properly. Whatever logic used, every problem will have different data requirements. While there may be situations which dictate either in-situ or remotely sensed data, many situations will require collecting both types of data.

3.4.1. IN-SITU DATA

Remotely sensed data is being used in numerous fields and for a wide variety of applications. Consequently, the collection of in-situ data may take the form of field sampling, laboratory sampling, or some combination of both. The techniques for these types of data collection should ideally be learned from the physical and natural science courses most related to the specific field of study such as chemistry, biology, forestry, soil science, hydrology, or meteorology. When in-situ data is to be used with remotely sensed data, it is important that the positions of these data are known in relation to the remotely sensed data. Due to ease of use and increasing affordability, global positioning system

(GPS) receivers are the ideal tool to be used to gather such positional data when needed. Using a GPS receiver, an x, y, and z coordinate can quickly be obtained to identify and locate individual samples in relation to remotely sensed data.

3.4.2. REMOTELY SENSED DATA

Although most remote sensors collect their data using the basic principles described above, the format and quality of the resultant data varies widely. These variations are dependent upon the resolution of the sensor. There are four types of resolution that affect the quality and nature of the data a sensor collects: radiometric, spatial, spectral and temporal. Radiometric resolution refers to the sensitivity of the sensor to incoming radiance (i.e., How much change in radiance must there be on the sensor before a change in recorded brightness value takes place?). This sensitivity to different signal levels will determine the total number of values that can be generated by the sensor (Jensen, 1996).

Spatial resolution is a measurement of the minimum distance between two objects that will allow them to be differentiated from one another in an image (Jensen, 1996). This is a function of sensor altitude, detector size, focal size and system configuration. For aerial photography the spatial resolution is usually measured in resolvable line pairs per millimeter on the image. For other sensors it is given as the dimensions, in meters, of the ground area which falls within the instantaneous field of view of a single detector within an array - or pixel size (Logicon, 1997).

Different remote sensing instruments record different segments, or bands, of the electromagnetic spectrum. The number and size of the bands which can be recorded by a sensor determine the instrument's spectral resolution. A sensor may be sensitive to a large portion of the electromagnetic spectrum but have poor spectral resolution if its sensitivity is contained in a small number of wide bands. Another sensor that was sensitive to the same portion of the electromagnetic spectrum but had many small bands would have greater spectral resolution. Like spatial resolution, the goal of finer spectral sampling is to enable the analyst, human or computer, to distinguish between scene elements. Figure 3.4 source: Jensen, 1996) illustrates this principle by showing the spectral reflectance curves, or spectral signatures, generated when two sensors are used on the same target. Both

sensors cover the same range of the electromagnetic spectrum (2 to 2.5 μm). The solid bars at the top of the graph represent the specific segments of electromagnetic energy that each sensor can detect and record. The first sensor (shown in red) has 17 bands in this range, while the second sensor (shown in blue) records the energy in only four bands. As can be seen, the reflectance curve of the first sensor has greater detail, which may be useful in distinguishing its target from other objects with similar compositions.

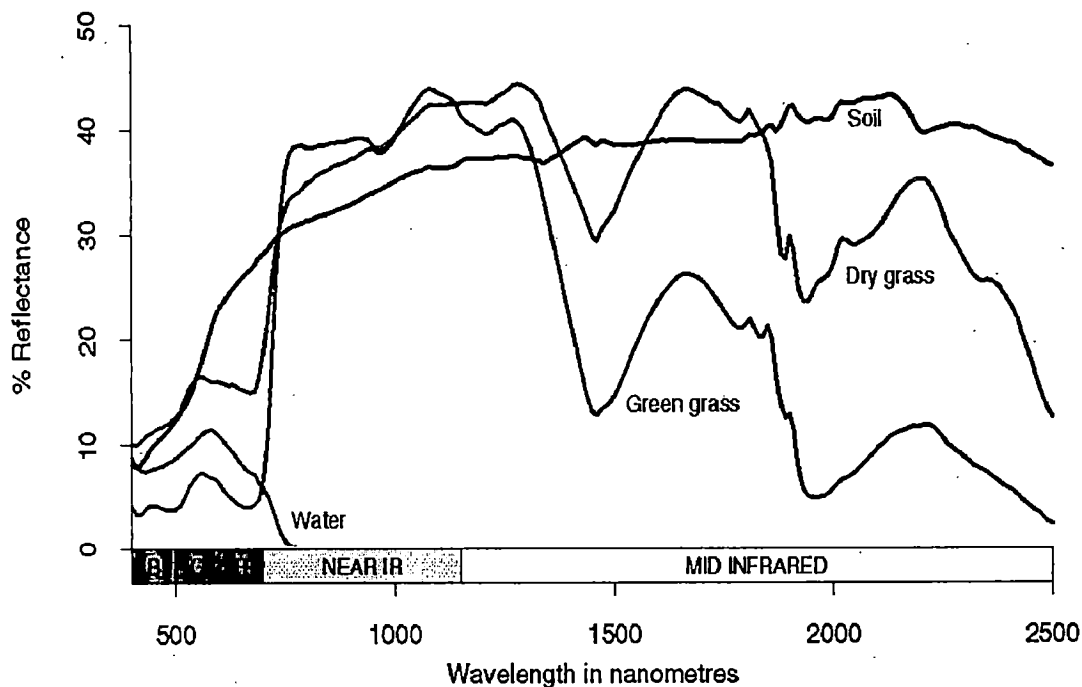


Figure 3.4 Reflectance curves produced when a target is sensed using a sensor with a higher spectral resolution (Red) vs. a lower spectral resolution (Blue)

Temporal resolution refers to the amount of time it takes for a sensor to return to a previously recorded location. This aspect of resolution becomes important when change detection is at the root of the research being done. Most orbital remote sensing platforms will pass over the same spot at regular time intervals that range from days to weeks depending on their orbit and spatial resolution. Data collected on multiple dates allows the scientist to chart changes of phenomena through time. Examples would include the growth of crops in various parts of the world, the expansion of urban areas, monitoring desertification, and, perhaps most common, the ever changing weather.

By increasing one or any combination of these resolutions, one increases the chance of obtaining remotely sensed data about target that contains accurate, realistic, and useful information. The downside to increased resolution is the need for increased storage space, more powerful data-processing tools (hardware and software), and more highly trained individuals to perform or guide analysis (Jensen, 1996). For these reasons, it is important to determine the minimum resolution requirements needed to accomplish a given task from the outset. This helps avoid (a) the time wasted in processing more data than needed and (b) the problem of too little data to allow completion of the task.

3.5. DATA ANALYSIS IN REMOTE SENSING

Remotely sensed data is analyzed using various image processing techniques and methods (Figure 3.2). These include either visual (or analog) processing techniques applied to hard copy data such as photographs or printouts and the application of digital image processing algorithms to the digital data (Jensen, 1996). One of the purposes of applying both analog and digital techniques to remotely sensed data is to enable the analyst see the data in several ways. This process, often termed scientific visualization, can be likened to an individual who finds an object but is unsure of its purpose or origin. Some individuals might then proceed to take the object apart and examine the individual components and how they relate one to another. All these steps, intimately familiar with the objects which has been found. That is the goal of image processing - to allow the researcher to examine their data from all possible angles, to place entire images in context with their surroundings, and to allow the relationships of individual scene elements to be discovered. Scientific visualization is this process of exploring data visually to gain an intimate knowledge of it and, hopefully, insight into it.

3.5.1. ANALOG IMAGE PROCESSING

Table 3.1 shows the most commonly used elements of image interpretation used in visual image analysis referred from Jensen (1996). The extent to which each of these elements is used depends on not only the area being studied but also the analyst knowledge of the study area.

The texture of an object is useful in distinguishing objects that may appear the same if judging solely on tone (i.e., water and tree canopy may have the same mean brightness values, but their texture is much different).

Table 3.1 The most commonly used elements of image interpretation used in visual image analysis

Elements of Image Interpretation	
Primary Elements	Black and White Tone
	Color
	Stereoscopic Parallax
Spatial Arrangement of Tone and Color	Size
	Shape
	Texture
	Pattern
Based on Analysis of Primary Elements	Height
	Shadow
Secondary Elements	Site
	Association

Analog image processing combined with the multi-concept of examining remotely sensed data in multiple bands of the electromagnetic spectrum (multispectral), on multiple dates (multitemporal), at multiple scales (multiscale) and in conjunction with other scientists (multidisciplinary), allows us to make a judgment not only as to what an object is but also its significance. Other tasks performed in analog image processing include the optical photogrammetric techniques allowing for precise measurement of the height, width, location, etc. of an object (Jensen, 1996).

Many of these tasks are summarized in Figure 3.5 (Jensen, 1996).

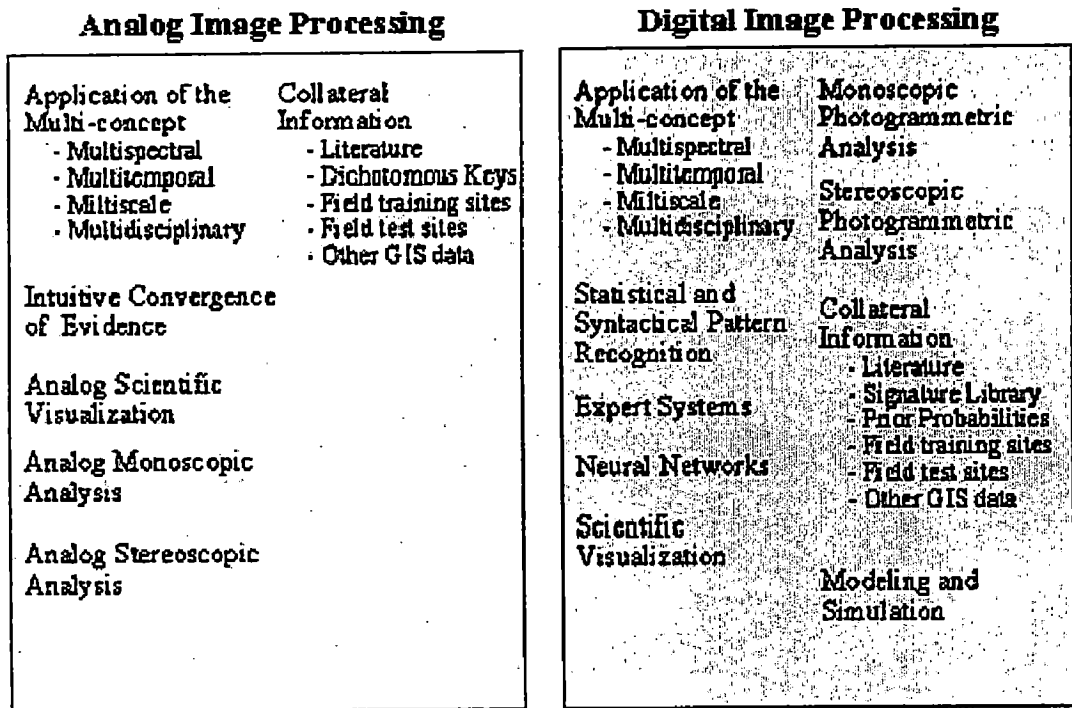


Figure 3.5 Basic Steps in Analog and Digital Image Processing

3.5.2. DIGITAL IMAGE PROCESSING

As the term implies, digital image processing is not only a step in the remote sensing process, but is itself a process which consists of several steps. The ultimate goal of this process is to extract information from an image that is not readily apparent. There are three general steps in processing a digital image; preprocessing, display and enhancement, and information extraction (Jensen, 1996).

3.5.2.1. PREPROCESSING

Before digital images can be analyzed, they usually require some degree of preprocessing. This may involve radiometric corrections which attempt to remove the effects of sensor errors and/or environmental factors. A common method of determining what errors have been introduced into an image is by modeling the scene at the time of data acquisition using ancillary data collected.

Geometric corrections are also very common prior to any image analysis. If any types of area, direction or distance measurements are to be made using an image, it must be rectified if they are to be accurate. Geometric rectification is a process by which points in an image are registered to corresponding points on a map or another image that has already been rectified. The goal of geometric rectification is to put image elements in their proper planimetric (x and y) positions.

3.5.2.2. INFORMATION ENHANCEMENT

There are numerous procedures that can be performed to enhance an image and these can be classified into two major categories: point operations and local operations. Point operations change the value of each individual pixel independent of all other pixels, while local operations change the value of individual pixels in the context of the values of neighboring pixels. Common enhancements include image reduction, image magnification, transect extraction, contrast adjustments (linear and non-linear), band rationing, spatial filtering, Fourier transformations, principle components analysis, and texture transformations (Jensen, 1996).

3.5.2.3. INFORMATION EXTRACTION

Unlike analog image processing, which uses all of the elements listed above (Table 3.1), digital image processing presently relies almost wholly on the primary elements of tone and color of image pixels. There has been some success with expert systems and neural networks which attempt to enable the computer to mimic the ways in which humans interpret images. Expert systems accomplish this through the compilation of a large database of human knowledge gained from analog image interpretation which the computer draws upon in its interpretations.

3.6. GEOGRAPHIC INFORMATION SYSTEM (GIS) CONCEPT

Like the field of geography, the term Geographic Information System (GIS) is hard to define. It represents the integration of many subject areas. Accordingly there is no absolutely agreed upon definition of GIS (de Mers, 1997). A broadly accepted definition of GIS is the one provided by the National Centre of Geographic Information and Analysis: *a GIS is a system of hardware, software and procedures to facilitate the*

management, manipulation, analysis, modeling, representation and display of georeferenced data to solve complex problems regarding planning and management of resources.

Geographic information systems have emerged in the last decade as an essential tool for urban and resource planning and management. Their capacity to store, retrieve, analyze, model and map large areas with huge volumes of spatial data has led to an extraordinary proliferation of applications.

Geographic information systems are now used for land use planning, utilities management, ecosystems modeling, landscape assessment and planning, transportation and infrastructure planning, market analysis, visual impact analysis, facilities management, tax assessment, real estate analysis and many other applications. Functions of GIS include: data entry, data display, data management, information retrieval and analysis.

A more comprehensive and easy way to define GIS is the one that looks at the disposition, in layers (Figure 3.6), of its data sets referred from Chang (2003). "Group of maps of the same portion of the territory, where a given location has the same coordinates in all the maps included in the system". This way, it is possible to analyze its thematic and spatial characteristics to obtain a better knowledge of this zone.

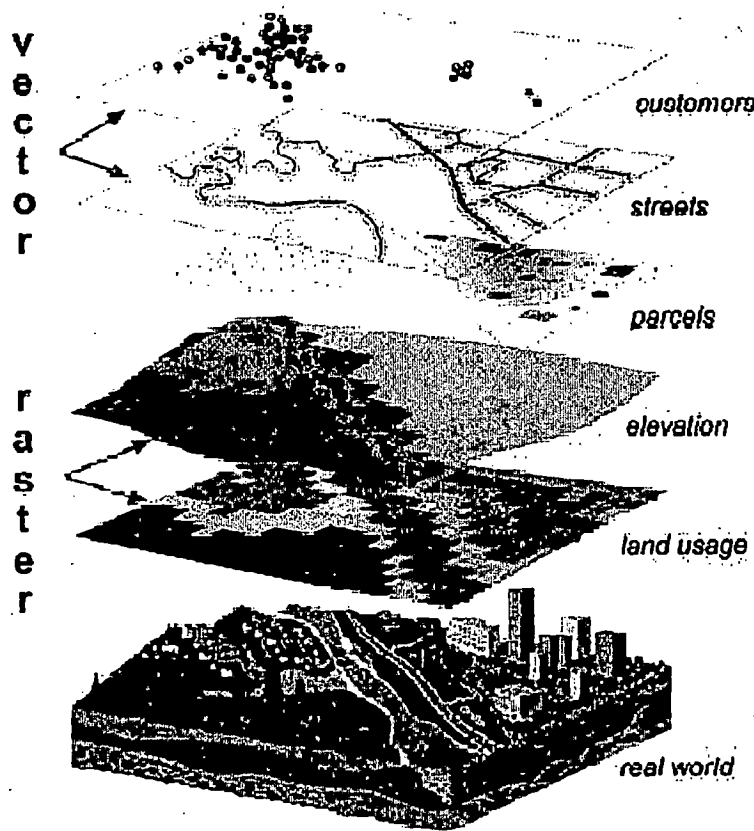


Figure 3.6 The Concepts of Layer

3.7. DATA STRUCTURE USED IN A GIS

3.7.1. VECTOR DATA STRUCTURE

Vector is a data structure, used to store spatial data. Vector data is comprised of lines or arcs, defined by beginning and end points, which meet at nodes. The locations of these nodes and the topological structure are usually stored explicitly. Features are defined by their boundaries only and curved lines are represented as a series of connecting arcs. Vector storage involves the storage of explicit topology, which raises overheads; however it only stores those points which define a feature, and all space outside these features is 'non-existent'.

There are different ways of organizing this double data base (spatial and thematic). Usually, vectorial systems are composed of two components: the one that manages spatial data and the one that manages thematic data. This is named as hybrid organization system,

as it links a relational data base for the attributes with a topological one for the spatial data.

In the vector based model, geospatial data is represented in the form of coordinates. In vector data, the basic units of spatial information are points, lines and polygons. Each of these units is composed simply as a series of one or more coordinate points. The basic units of spatial information referred from user's guide of ILWIS 2.1 are (Figure 3.7):

- POINT, a zero-dimensional abstraction of an object represented by a single X, Y coordinate. A point normally represents a geographic feature too small to be displayed as a line or area; for example, the location of a building location on a small-scale map, or the location of a service covers on a medium scale map.
- LINE, a set of ordered co-ordinates that represent the shape of geographic features too narrow to be displayed as an area at the given scale (contours, street centre lines, or streams), or linear features with no area (county boundary lines).
- POLYGON, a feature used to represent areas. A polygon is defined by the lines that make up its boundary and a point inside its boundary for identification. Polygons have attributes that describe the geographic feature they represent.

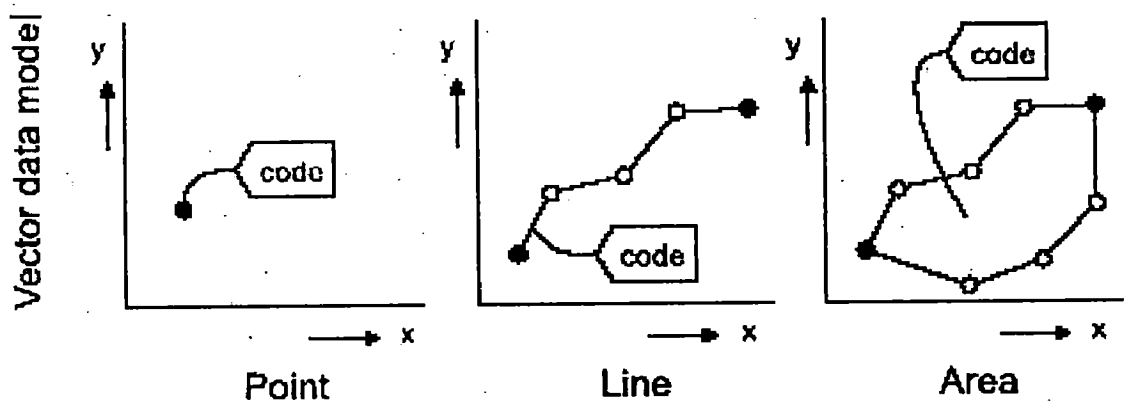


Figure 3.7 Vector Representations

3.7.2. RASTER DATA STRUCTURE

In a raster model, spatial data are organized in grid cells or pixels referred from user's guide of ILWIS 2.1 (see Figure 3.8). Pixels, a term derived from picture element,

are the basic units for which information is explicitly recorded. Each pixel is assigned only one value. The maps stored according to the raster model are called raster maps. Pixels in a raster map all have the same dimensions. It is enough to determine the pixel size and the parameters to transform between X and Y coordinates of a map and the pixel locations in the raster map (rows/lines and columns). The process to establish this relationship is called georeferencing. Through a georeference we know the relationship between a coordinate system and pixel locations in the image.

A point is described in the raster model by the position of a single pixel. The position of each cell is defined by a row and column number. A line and an area are described by a set of connected pixels having the same code. In the raster model there is no basic difference in how points, lines and areas are stored.

Through rasterization, vector data (points, lines or polygons) can be converted to the raster format. Apart from this source of raster maps, there are imported images, satellite images, scanned aerial photographs or imported raster maps from other sources.

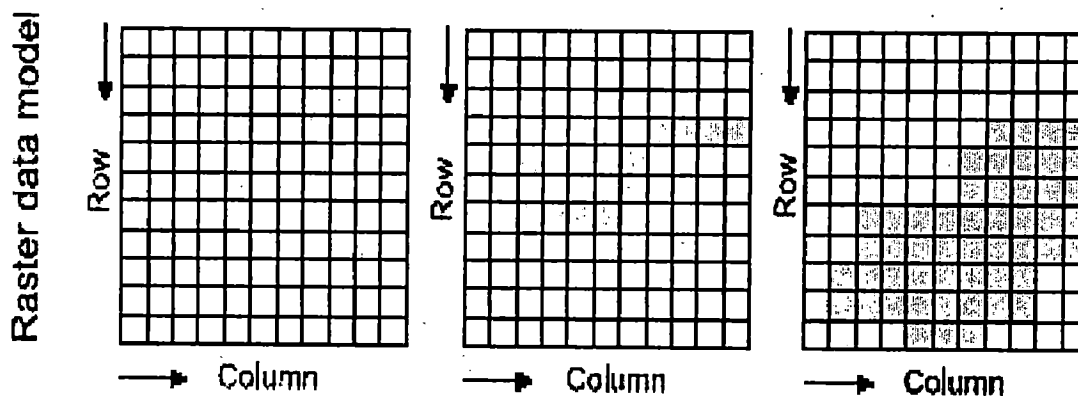


Figure 3.8 Raster Representations

3.8. COORDINATE SYSTEM AND GEOREFERENCE

The information on the X and Y coordinates of a vector map is stored in a service object called the coordinate system. A coordinate system is a service object for point, segment and polygon maps, and for georeferences (the latter are used for raster maps and will be treated in the next section).

A coordinate system defines the possible minimum and maximum X's and Y's that be used in a map, and in case of a coordinate system of type projection, also store

information on a map's projection, ellipsoid and/or datum. Normally locations on the earth's surface are shown in geographic coordinates.

The geographic coordinates of the earth are expressed in Latitudes and Longitudes referred from user's guide of ILWIS 2.1 (see Figure 3.9). Latitudes (parallels) are measured from the equator and may range from 0° to 90° N or from 0° to 90° S. Longitudes (meridians) are measured from the Greenwich meridian and may range from 0° to 180° E or from 0° to 180° W.

The shape of the earth is like a ball (spherical) or like a "horizontal rugby ball with flattened poles" (ellipsoidal). To represent areas from this sphere or ellipsoid into a plain surface, need a map projection. The earth's surface can even be better approached if a projection uses a datum. Practically every country in the world uses its own coordinate system, based on a certain projection. One of the most used projections is the so-called Universal Transverse Mercator (UTM).

The UTM is an international metric coordinate system, which covers the whole earth and divides it into 60 zones each covering 6° Longitude. Because of the small area covered by each zone, a high degree of accuracy is possible. The conversion from geographic to metric coordinate is done via a map projection. For example, point data obtained from GPS (Global Positioning Systems) may have been registered in geographic coordinates.

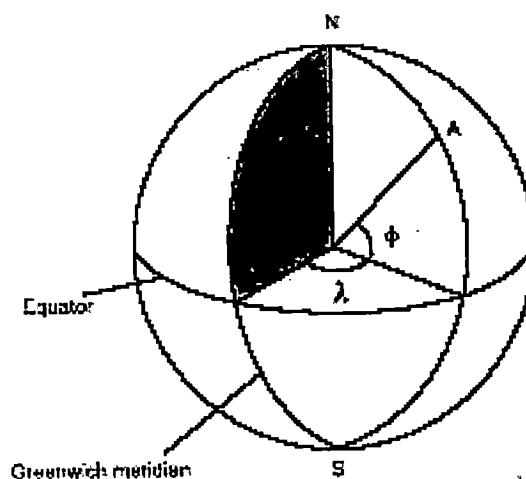


Figure 3.9 Geographic coordinate system: the location of A is determined by the Longitude (λ) and the Latitude (ϕ)

A georeference is a service object, which stores the relation between the rows and columns in raster map(s) and the ground-coordinates (X, Y). A georeference is needed for raster maps and uses a coordinate system. With several raster maps of the same area, and to overlay them, it is important that all maps have the same number of rows and columns, and the same pixel size. The pixels in both maps thus refer to the same position on the ground. Therefore all raster maps of the same area should have the same georeference.

Two types of georeferences for raster maps are:

- Georeference corners are used for raster maps made from rasterizing vector maps, and the resulting maps from operations on these maps. A georeference corners is used for raster maps that are oriented to the north.
- Georeference tiepoints are used for satellite images, scanned aerial photographs and other imported images, which may not be north-oriented.

3.9. DIGITAL ELEVATION MODEL (DEM)

3.9.1. DATA SOURCES

At present, there are five main sources of the elevation data: ground surveys, airborne photogrammetric data capture, existing cartographic surveys, airborne laser scanning, and stereoscopic or radar based satellite imagery. These DEM collection methods can be compared considering four aspects : (a) price, (b) accuracy, (c) sampling density, and (d) pre-processing requirement, referred from Hengl et al. (2003) (Table 3.2). Traditionally, the elevation data has been collected by land surveyors from ground surveys or by semi-automated digitizing using stereoplotters. This is the most accurate but also the most expensive data collection method.

Table 3.2 Typical elevation accuracy of different data sources used to derive DEMs.

Collection method	Main characteristics	Some examples of used systems	Typical DEM accuracy
Ground surveys	Highest accuracy; small sampling density; high cost.	DGPS systems Tacheometry Levelling systems	≤ 1 m 1 mm – 1 m ≈ 1 mm
Stereoscopic imagery	High sampling density; can be semi or fully automated; problems with vegetation.	Areal photography Satellite Imagery (SPOT, ASTER)	0.1 – 1 m 10 m (20 m)
Laser scanning	Laser scanner is placed in the airplane which is GPS navigated; the raw data require filtering and resampling before it can be used; it can penetrate tree foliage and record both surface of the vegetation cover and ground.	Airborne laserscanning (LIDAR)	$\approx 0.2 - 1.0$ m
Radar imagery	The lowest costs per km ² ; requires ground control data; complex processing.	Airborne SAR (Synthetic Aperture Radar) Apaceborne (ERS, SRTM)	$\approx 0.5 - 2$ m 10 m (25 m)

3.9.2. DATA STRUCTURES

In a GIS environment, a DEM is commonly modeled and visualized using two main data structures: rectangular grid or elevation matrix (GRID) and triangulated Irregular Network (TIN). The GRID DEM is typically stored as a raster map (or image), where each pixel carries the information on elevation or terrain parameter. The TIN DEM is based on the triangular elements with their vertices at the sample points. The advantage of TIN DEM compared to the GRID DEM is that it can incorporate structural features such as peaks, slope breaks and conic pits. Some consider these to be a more accurate structure for terrain parameterization especially when contour data is used. Although the gridded DEM data model is non adaptive and commonly over samples in low relief areas and under samples in high relief area, it is somewhat more attractive than the TIN DEM due to a simple data structure and high possibilities of GIS operation.

3.10. HYDROLOGICAL TERRAIN PARAMETERS

Hydrological or flow accumulation based terrain parameters are typically used to describe flow of material over a gridded surface, i.e. quantify flow intensity, accumulation potential or erosion potential. In the most raster GIS applications flow accumulation algorithms are implemented by directing the flow into the lowest neighboring cell. Imagining a tilted plane subdivided into square cells that is exposed to rain, one can determine the number of cells above each one cell that contribute water flowing through this cell, referred from Hengl et al. (2003) given as Figure 3.10. The lower the position of a cell is on this plane, the more area above will contribute water to it. Additionally, the form of the surface is important in directing the path of the accumulating flow. Peaks and ridge will tend to have diverging flow and low accumulation of water. This hypothetical property of water accumulation is typically quantified by estimating the contributing area and local slope.

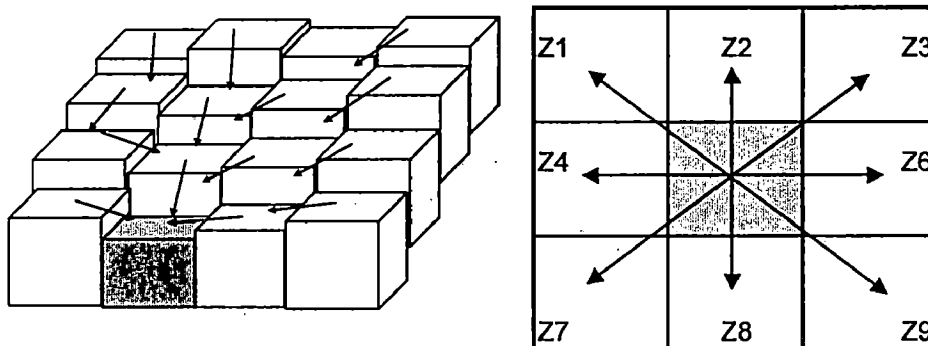


Figure 3.10 Schematic example of contributing cells at observed location (a) and effective contour lengths at cardinal and diagonal directions (L1 and L2) in a 3x3 window environment (b).

CHAPTER 4.

METHODOLOGY

The methodology followed in this study consists of two aspects (i) preparation of base map involving map acquisition, conversion into digital form, creating Digital Elevation Model (DEM) from contour map source and overlay operation and (ii) deriving maps for travel time and time area histogram for spatially and temporally variable rainfall intensities. Figure 4.1 illustrates methodology followed in this study.

4.1. MODELLING FRAMEWORK

In the context of numerical formulation, the watershed domain is discretized by a raster grid and proper tools are developed whereby spatial variations can be accounted for. The methodology consists of four steps. In the first step terrain based features are derived using a GIS software. It involves^s generation of digital database from toposheet data and other ancillary information, conversion into vector data and generation of raster terrain maps such as DEM, optimized DEM after burning existing drainage information for its enhancement, depressionless DEM, flow direction and flow accumulation. The second step involves computation of temporally variable rainfall-excess using ϕ -index method. The third step involves classification of satellite image to generate landuse map for deriving map of roughness coefficient to determine differential and total cumulative travel time to outlet maps as well as time series of isochrones maps corresponding to rainfall-excess intensities. The fourth step involves TA convolution and routing through two conceptual linear reservoirs to account for catchment storage effects on the resulting runoff hydrograph. Details on mathematical formulations involved and steps are presented in the following text.

4.2. MODELLING STEPS

In the first step following procedures are executed for deriving terrain based maps:

1. The DEM is generated from the digitized elevation contours of the watershed using ILWIS 3.2 with interpolation functions in a raster spatial data model at a finer resolution of 10-m pixel size. The generated DEM was aggregated at 90-m pixel size to reduce computational requirements.
2. The generated DEM was further optimized by burning the observed digitized drainage to facilitate closer compliance of DEM generated flow directions with observed drains. The optimized DEM contains depressions and flat areas where flow direction is not defined. Attributed such artifacts to mistake in the input data, unsuitable interpolation techniques or the interaction grid spacing with contour spacing and valley orientation. The artificial depressions and flat areas were removed using FILL operation in ILWIS 3.2.
3. A flow direction map based on eight direction D8 approach (O'Callaghan and Mark, 1984) has been developed, which produces steepest slope direction by operating on the DEM using FLOW DIRECTION operation in ILWIS 3.2.
4. Flow accumulation map representing cumulative count of the number of pixels draining through any given pixel in the catchment into outlets using FLOW ACCUMULATION operation in ILWIS 3.2 has been developed.

The second step is to prepare time series of rainfall-excess intensity maps in the watershed with estimated based on the temporally variable rainfall-excess using ϕ -index method. The third step prepares differential and cumulative maps of travel time corresponding to a given map of rainfall-excess intensity in the following manner:

1. The map of equilibrium discharge (Q_e) in first prepared. This is done for any pixel by accumulating the rainfall-excess intensity multiplied by the pixel area over the flow drainage area of that pixel known from the accumulation map.
2. Differential kinematic wave travel time over any pixel is calculated based on the piece wise form of eq. (4.14) described later. The input maps for this part include flow

direction, bed slope, equilibrium discharge and roughness coefficient. The roughness map prepared by reclassifying vegetation, and land use maps according to suggested tables in the literature (Woolhiser, 1975).

3. Accumulating the above differential map along flow paths to the outlet produces cumulative travel time maps. This map indicates the spatial distribution of the time required for a kinematic wave to travel from any pixel to the outlet.
4. For a cumulative travel time map, isochrones of equal travel times are derived and the areas bounded by adjacent isochrones determined.

All the four points listed under third steps must be repeated N times, where N is the number of rainfall-excess intensity maps. This is equal to the number of rainfall-excess intensities.

In the fourth step, N incremental hydrographs corresponding to N isochrone maps are determined by convolution, where discharge is computed based on the integrated excess intensity over the areas bounded by appropriate isochrones. These incremental hydrographs, delayed by their corresponding excess intensity time, are then superimposed to yield the total hydrograph. The resultant total hydrograph is further routed through two conceptual linear reservoirs in series to account for the catchment-induced storage effects (Ponce, 1989), one for overland regions and other for channel regions. The storage coefficients of these reservoirs are assumed to be same for simplicity reasons.

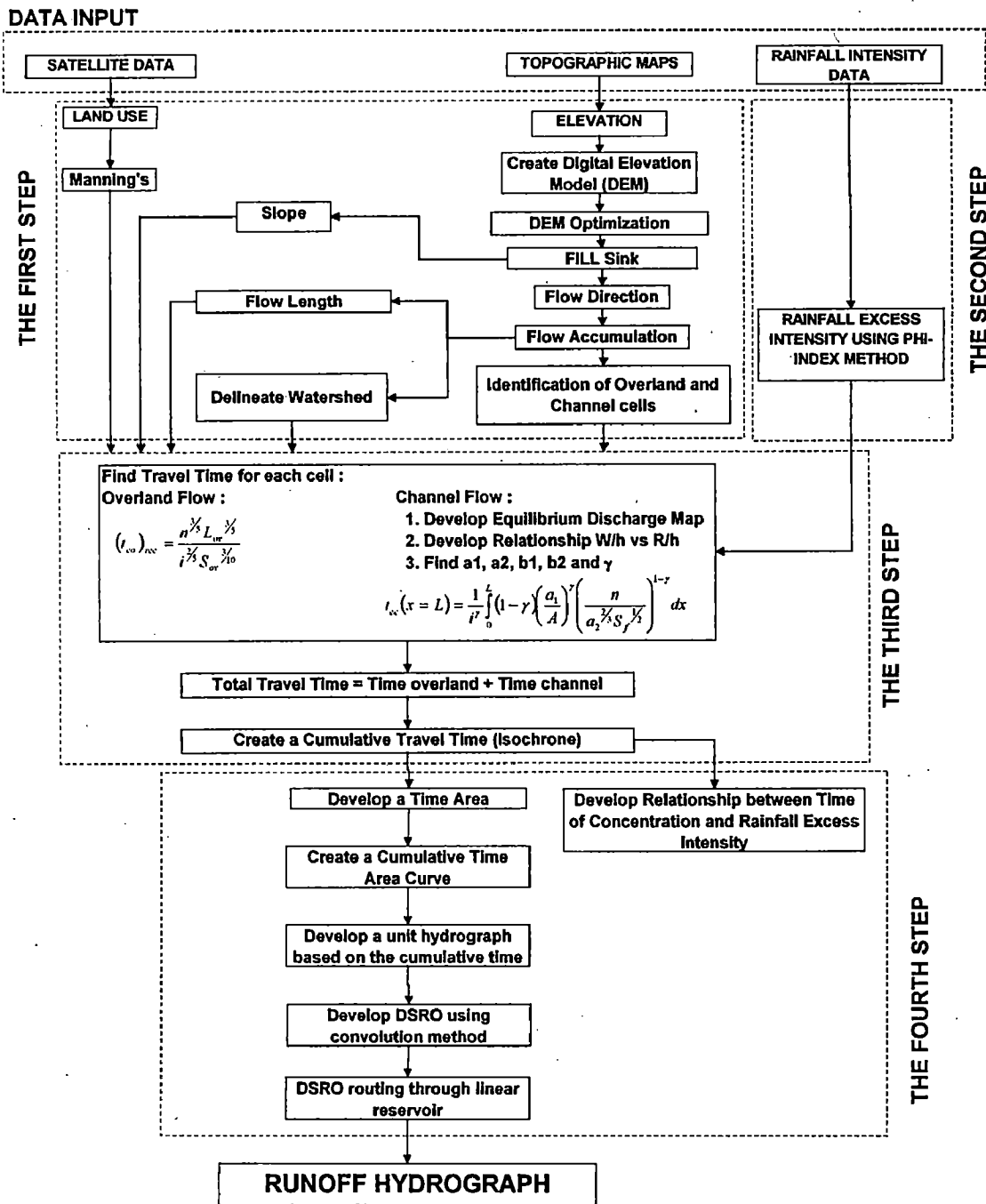


Figure 4.1 Flow Chart of Methodology

4.3. TRAVEL TIME

4.3.1. ANALYTICAL FORMULATION

Surface runoff over a watershed is generally assumed to occur in two distinct phases, namely overland flow and channel flow. Although it is difficult to separate these two phases clearly, overland flow is generally slower owing to shallow flow depths, whereas channel flow is usually confined to a limited width boundary with faster flood wave celerity. The computation of travel time or time to equilibrium is generally done for overland as well as channel flow using simplified form of St. Venant equations (Chow et al., 1988). The present study utilizes kinematic wave approximation for computation of time to equilibrium as the kinematic wave approximation is appropriate for most overland flow conditions (Woolhiser, 1975). For a basin to reach steady state at the time to equilibrium, the wave originating from the hydraulically most remote point in the basin must reach the basin outlet by traveling through both the overland and channel flow phases. The wave travel time is first formulated in a general form and then separately computed for these two phases.

On an impervious watershed, due to rain falling with constant intensity, a wave originates from a point at a distance $x = X_1$ and travels to $x = X_2$, in either overland or channel flow phase, the wave travel time t_w may be written as

$$t_w = \int_{x_1}^{x_2} \frac{dx}{c} \quad \dots \dots \dots (4-1)$$

where x is the distance measured along the flow path and c is the wave celerity. The celerity of the wave depends upon an expression for resistance as well as the wave type. In general, the wave celerity is expressed as (Chow et al., 1988),

$$c = \frac{\partial Q}{\partial A_x} = \frac{\partial Q}{\partial h} \frac{dh}{dA_x} \quad \dots \dots \dots (4-2)$$

where Q is the discharge, h is the flow depth, and A_x is the flow cross-section area.

The relationship between flow depth h , flow velocity V , and unit discharge q for a general resistance law can be written as

$$V = \alpha h^{\beta-1}; \quad q = \alpha h^{\beta} \quad \dots \dots \dots (4-3)$$

where α and β are resistance parameters. Based on flow cross-section, the flow area A_x and the hydraulic radius R can be determined as functions of flow depth h , either precisely through geometrical relationships or approximately through rating curves. In equation form, assume

$$A_x = a_1 h^{b_1} ; R = a_2 h^{b_2} \quad \dots \dots \dots (4-4)$$

where $a_1, a_2, b_1,$ and b_2 are constants for a given cross-section. Substituting the discharge $Q = A_x V$ from equations (4-3) and (4-4) in the wave celerity equation (4-2) yields

$$c = \frac{\beta + b_1 - 1}{b_1} \alpha h^{\beta-1} \quad \dots \dots \dots (4-5)$$

At this stage, we must evaluate flow depth at the equilibrium state. As a wave originates from the hydraulically most remote point P_r in the basin and it travels downstream along a certain kinematic path x , each flow through cross-section reaches equilibrium just as the wave from P_r passes through it. Each cross-section along flow path x is assumed to have a certain drainage area (upslope area). The equilibrium discharge passing through a given cross-section p would be the spatially integrated rainfall rate over the drainage area associated with that cross-section. This can be mathematically expressed by

$$Q_e(x_p, y_p) = \int_0^{A(x_p, y_p)} i(x, y) dA \quad \dots \dots \dots (4-6)$$

where $Q_e(x_p, y_p)$ is the equilibrium discharge passing through cross-section p , (x_p, y_p) are the rectangular coordinates of cross-section p , $A(x_p, y_p)$ is the total drainage area at p , $i(x, y)$ is rainfall intensity at coordinates (x, y) , and (x, y) are rectangular coordinates of any point draining to p . The steady-state discharge for a uniform rainfall, for instance, would simply be equal to the rainfall rate times the drainage area. The equilibrium flow depth is computed based on $Q_e = A_x(h_e)V(h_e)$ using equations (4-3) and (4-4) as follows:

$$h_e = \left(\frac{Q_e}{a_1 \alpha} \right)^{\frac{1}{\beta + b_1 - 1}} \quad \dots \dots \dots (4-7)$$

By substituting h_e in the wave celerity equation (4-5) and then back into the wave travel time equation (4-1) one obtains

$$t_w = \int_{x_1}^{x_2} \frac{dx}{\alpha \left(\frac{\beta + b_1 - 1}{b_1} \right) \left(\frac{Q_e}{a_1 \alpha} \right)^{\frac{\beta-1}{\beta+b_1-1}}} \dots \dots \dots (4-8)$$

Let

$$\gamma = \frac{\beta-1}{\beta+b_1-1} \dots \dots \dots (4-9)$$

which yields

$$t_w = \int_{x_1}^{x_2} \frac{\gamma b_1}{(\beta-1) \alpha^{1-\gamma} \left(\frac{a_1}{Q_e} \right)^\gamma} dx \dots \dots \dots (4-10)$$

Equation (4-10) is the general wave travel time relationship which accounts for basin characteristics, including slope, roughness, drainage area density, flow width, and flow cross-section, as well as rainfall properties reflected in spatial distribution of rainfall rate. When the flow is turbulent over the major portion of a watershed, the Manning resistance equation can be applied. Alternate formulations for laminar flow are possible (e.g. Woolhiser, 1975). The flow velocity in SI units is obtained from

$$V = \frac{1}{n} R^{2/3} S_f^{1/2} = \frac{1}{n} (a_2 h^{b_2})^{2/3} S_f^{1/2} \dots \dots \dots (4-11)$$

where S_f is friction slope; and α , β , and γ are expressed by

$$\alpha = \frac{1}{n} a_2^{2/3} S_f^{1/2}; \quad \beta = \frac{2}{3} b_2 + 1; \quad \gamma = \frac{2b_2}{2b_2 + 3b_1} \dots \dots \dots (4-12)$$

Consequently, t_w for the Manning resistance equation transforms into

$$t_w = \int_{x_1}^{x_2} (1-\gamma) \left(\frac{a_1}{Q_e} \right)^\gamma \left(\frac{n}{a_2^{2/3} S_f^{1/2}} \right)^{1-\gamma} dx \dots \dots \dots (4-13)$$

Here, it is noted that the equation retains its generality with respect to the spatial variability in rainfall. When the friction slope is replaced by the bed slope S_0 for the kinematic wave approximation, the derived time is called kinematic time to equilibrium. If the wave travel time is computed for $X_1 = 0$ and $X_2 = L$, where L is the total length along the hydraulically longest flow, then t_w represents the kinematic equilibrium time for the portion of the basin draining along length L :

$$t_e = \int_0^L (1-\gamma) \left(\frac{a_1}{Q_e} \right)^\gamma \left(\frac{n}{a_2^{2/3} S_f^{1/2}} \right)^{1-\gamma} dx \quad \dots \dots \dots (4-14)$$

or if the rainfall intensity i is uniformly distributed in space:

$$t_e = \frac{1}{i^\gamma} \int_0^L (1-\gamma) \left(\frac{a_1}{A} \right)^\gamma \left(\frac{n}{a_2^{2/3} S_f^{1/2}} \right)^{1-\gamma} dx \quad \dots \dots \dots (4-15)$$

The total time to equilibrium t_e can be separated into two phases: the travel time for overland flow t_{eo} and for channel flow t_{ec} . Explicitly:

$$t_e = t_{eo} + t_{ec} \quad \dots \dots \dots (4-16)$$

Equation (4-16) is used for analyzing the overland flow and channel flow phases separately. It should be noted that the channel flow phase considers the cumulative runoff from the upstream overland flow phase.

4.3.2. OVERLAND FLOW

The parameter values corresponding to the flow over an overland plane are as follows: $a_1 = W$; $b_1 = 1$; $a_2 = 1$; $b_2 = 1$; $\gamma = 2/5$; $L = L_{ov}$; $S_o = S_{ov}$; where W is the local overland plane width and L_{ov} is the total length of the overland plane starting from the hydraulically most remote point. The bed slope S_{ov} would then be the local overland plane bed slope. Therefore, the kinematic time to equilibrium for turbulent overland flow from equation (4-14) becomes

$$t_{eo} = \frac{3}{5} \int_0^{L_{ov}} n^{3/5} \left(\frac{W}{Q_e} \right)^{2/5} \frac{1}{S_{ov}^{3/10}} dx \quad \dots \dots \dots (4-17)$$

If variations of width W , drainage area A , surface roughness n , bed slope S_o , and rainfall intensity i along the hydraulically longest flow path are known, the overland flow travel time can be estimated by simplifying the above equation. In the case of a uniform rectangular plane under uniform rainfall intensity i , the equilibrium discharge of rectangular plane $(Q_e)_{rec}$ is given by

$$(Q_e)_{rec} = iA(x) = ixW \quad \dots \dots \dots (4-18)$$

Solving (4-17) yields the following well-known formula:

$$(t_{eo})_{rec} = \frac{n^{3/5} L_{ov}^{3/5}}{i^{2/5} S_{ov}^{3/10}} \dots \dots \dots (4-19)$$

Saghafian (1992) tested equation (4-15) for converging and diverging planes and reported good agreement with the experimental data of Schaake, 1965), Dickinson et al. (1967) and Woolhiser (1969). The calculated values of time to equilibrium matched those reported by Agiralioglu (1984, 1988).

4.3.3. CHANNEL FLOW

Once a kinematic wave enters the channel network, it travels faster depending upon flow depth and channel cross-section geometry. Certain relationships for $A_x(h,x)$, $R(h,x)$, $S_o(x)$, and $Q_e(x)$, or alternatively $i(x,y)$ and $A(x)$, must be obtained to allow the calculation of the travel time integral. If the channel system consists of several segments with uniform cross-section, then the integral performed piecewise. For the j-th channel segment of uniform cross-section and constant roughness from $X_1 = L_{j-1}$ to $X_2 = L_j$, the travel time from equation (4-14) by

$$t_{ec,j} = (1 - \gamma_j) (a_{1,j})^{\gamma_j} \left(\frac{n_j}{a_{2,j}^{2/3}} \right)^{1-\gamma_j} \int_{L_{j-1}}^{L_j} \frac{dx}{Q_e^{\gamma_j} S_o^{(1-\gamma_j)/2}} \dots \dots \dots (4-20)$$

where $t_{ec,j}$ is the travel time through the j-th channel. The substitution for Q_e requires knowledge of spatial variability of rainfall and also that of drainage area along the channel path.

4.4. TIME AREA DIAGRAM

The time area diagram is a plot of time of travel and the portion of the watershed (henceforth referred as sub area) that is having that particular time of travel. The time of travel of the rainfall occurring in any location (source) of the sub area of the watershed will be the same for all the locations in the same sub area of the watershed. The cumulative time of travel for all the locations of the watershed is computed and then the watershed is divided into sub areas of equal time of travel by isochrones. Thus isochrones may be defined as the contours, which connect all the locations having the same time of travel. The isochrones cannot cross each other, cannot enclose each other and must begin and terminate at the watershed boundaries (Dooge, 1959).

The time area used in the lag and route method in which the rainfall-excess is lagged by the amount of the time interval of the isochrones that divide the watershed into zones of equal intervals of the time of travel. However it is to be noted that the time area method only accounts for the translational transformation of the inflow and that the storage effects of the watershed are left unconsidered. Not considering the storage effects leads to the lack of attenuation in the hydrograph, which would then show a higher peak of discharge. This storage effect can be accounted for by routing the hydrograph developed from the time area diagram through a linear reservoir with an appropriate storage coefficient that properly approximates the watershed characteristics.

Velocity is a vector quantity specified by magnitude and direction referred from Chow et al., (1988) represented by a Figure 4.2a. The travel time in the channel cell is calculated by equation (4-20). The overland flow travel time for cells defined as overland flow cells is calculated by equation (4-19). The grid flow travel times where the value in each cell is the time taken for water from that cell to flow to the watershed outlet can be created by combining the grid of overland flow travel time and the channel flow travel time.

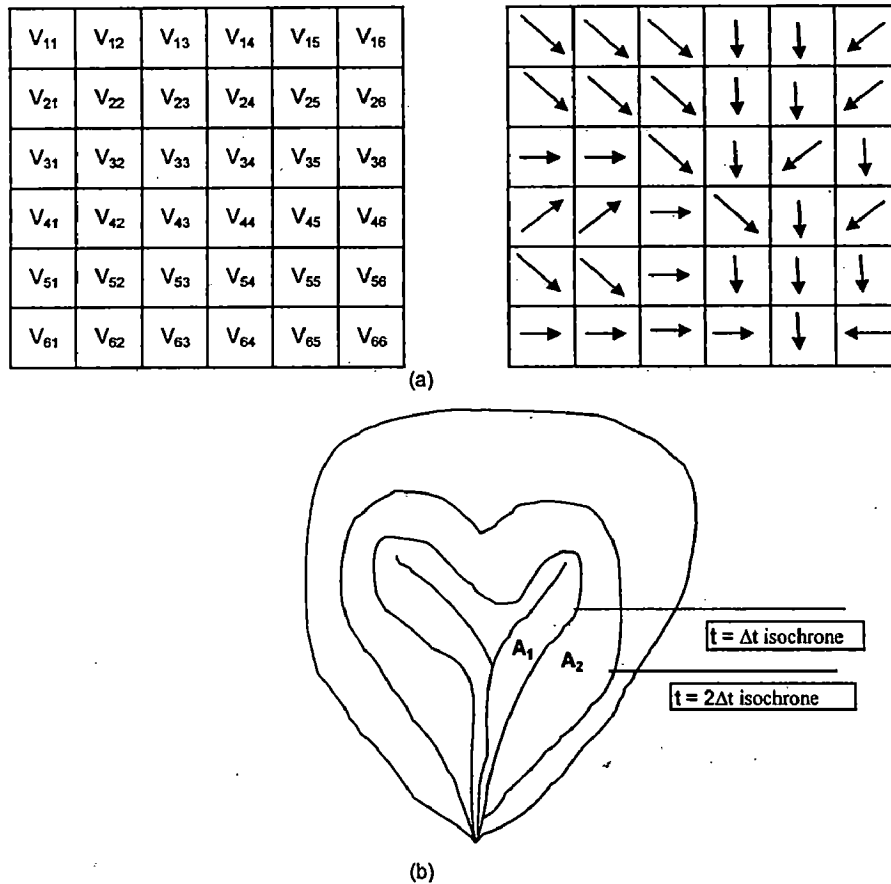


Figure 4.2 Watershed time-area relationships

The cells may then be classified into zones i , $i = 1, 2, 3, \dots$, whose travel time t falls into time intervals Δt , that is, the zone 1 has travel time $0 \leq t < \Delta t$, the zone 2 has travel time $\Delta t \leq t < 2\Delta t$, and so on. The line bounding the outer limit of the cells in zone i is the isochrone of travel time $t = i\Delta t$ to the watershed outlet. The total area of cells in zone i is A_i . In this way, the isochrone map of watershed is created as shown in Figure 4.2b. The isochrone which has maximum time of flow to the outlet is the time of concentration of the watershed, t_c , also sometimes called the time to equilibrium.

The time area diagram is a graph of cumulative drainage area flowing to the outlet within a specified time of travel. It is constructed by summing the incremental areas A_i as shown in Figure 4.3a (referred from Chow et al., 1988). Thus at time points $t = 0, \Delta t, 2\Delta t, \dots, i\Delta t$, the cumulative area draining to the outlet $A(i\Delta t)$ is given by (Maidment, 1993),

$$A(i\Delta t) = \sum_{k=1}^i A_k \quad \dots \dots \dots (4-21)$$

Conversely, the incremental areas can be given by (Maidment, 1993),

$$A_i = A[i\Delta t] - A[(i-1)\Delta t] \quad \dots \dots \dots (4-22)$$

It is important to note that incremental time area diagram (Figure 4.3b) is a discrete time function having a single value over each time interval Δt , while the cumulative time area diagram (Figure 4.3b) is a continuous time function whose sampled value is given at regular time point by equation (4-21). Thus if the time flow grid into isochrones separated by a different time step Δt is classified, the appearance of the incremental time-area histogram will be altered but the cumulative time-area diagram will simply be the same continuous curve sampled with a different time step.

4.5. UNIT HYDROGRAPH

The concept of a spatially distributed unit hydrograph, proposed by Maidment, (1993) is based on the fact that the unit hydrograph ordinate at the time $i\Delta t$ is given by the slope of the watershed time-area diagram over the interval $((i-1)\Delta t, i\Delta t)$. The validity of the above can be proved by considering the S-hydrograph method. An S-hydrograph, defined as the runoff at the outlet of a watershed resulting from a continuous effective rainfall occurring at rate, i.e. over the watershed, is given by

$$Q_s(i\Delta t) = i_e A(i\Delta t) \quad \dots \dots \dots (4-23)$$

where $A(i\Delta t)$ is the watershed area contributing to the flow $Q_s(i\Delta t)$ at the outlet at time $i\Delta t$. The direct runoff hydrograph discharge at time $i\Delta t$, resulting from a pulse of effective rainfall $P_e = i_e \Delta t$, is equal to the different between the S-hydrograph value at time $i\Delta t$ and its value lagged by time Δt , i.e.

$$Q_D(i\Delta t) = i_e A(i\Delta t) - i_e A[(i-1)\Delta t] \quad \dots \dots \dots (4-24)$$

The unit hydrograph ordinates are $U(i\Delta t) = Q_D(i\Delta t)/P_e$, and thus

$$U(i\Delta t) = \frac{A(i\Delta t) - A[(i-1)\Delta t]}{\Delta t} \quad \dots \dots \dots (4-25)$$

Or by

$$U_{ii} = U(i\Delta t) = \frac{A_i}{\Delta t} \dots \dots \dots (4-26)$$

Thus the unit hydrograph can be constructed by standard S-hydrograph method (Chow et al., 1988), i.e. the time area curve is lagged by one hour and subtracted from original curve. The discharge values obtained, adjusted for unit input, yield the one hour distributed unit hydrograph. The typical distributed unit hydrograph is presented in Figure 4.3c.

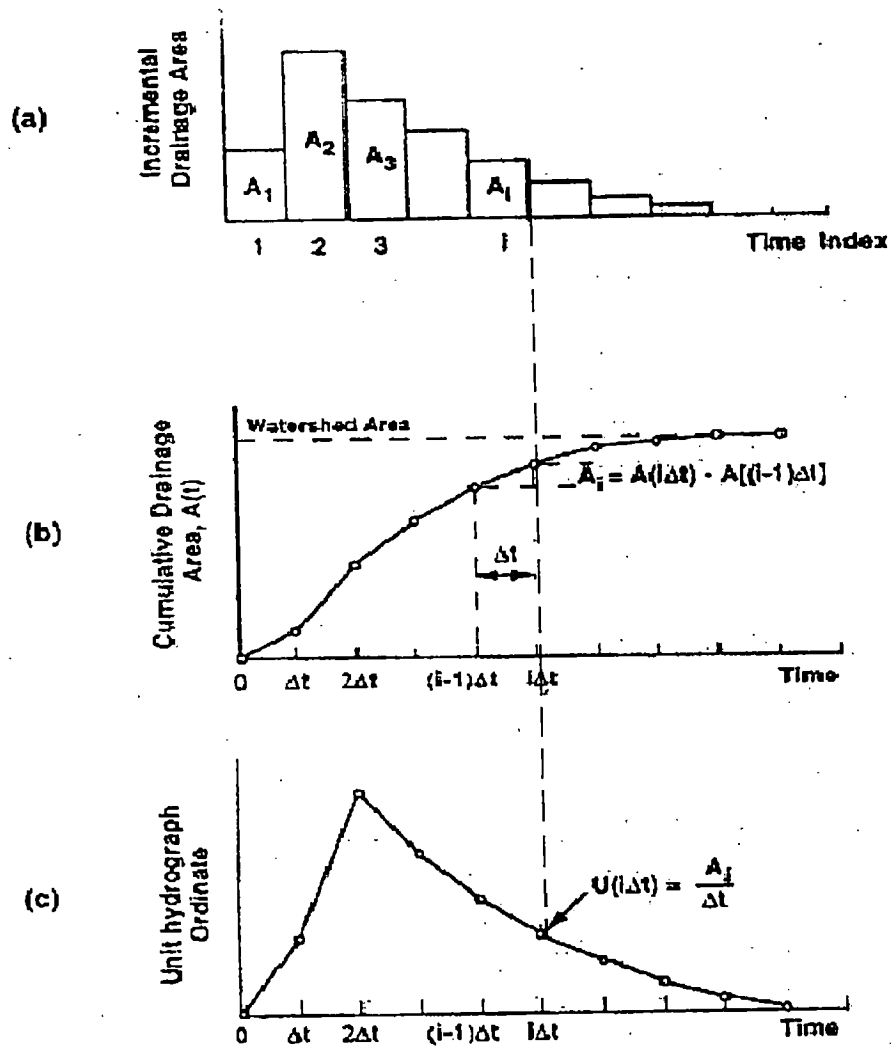


Figure 4.3 The time-area diagram and the unit hydrograph :
 (a) incremental drainage area; (b) the cumulative time-area diagram;
 (c) unit hydrograph found as the slope of the time-area diagram.

4.6. DIRECT RUNOFF HYDROGRAPH

The portion of the rainfall, which produces direct runoff, is called the rainfall-excess. The values are symbolized by Q_1, Q_2, \dots, Q_i , where Q is the rainfall-excess in mm and the corresponding direct runoff values are given by q_1, q_2, \dots, q_n , where q is a discharge rate at the watershed outlet measured in cumec. Given the rainfall-excess hyetograph for a watershed, the direct runoff hydrograph is computed for the first time interval as (Maidment, 1993):

$$q_1 = Q U_1 \quad \dots \dots \dots (4-27)$$

By substitution of $U_1 = A_1/\Delta t$ modifies above equation as follows (Maidment, 1993)

$$q = \frac{Q_1 A_1}{\Delta t} \quad \dots \dots \dots (4-28)$$

Thus, if an effective rainfall of intensity $Q_1/\Delta t$ begins falling on the watershed at time 0, after time t area A_1 is contributing to flow at the outlet so the direct runoff rate is $(Q_1/\Delta t)A_1$ at that time. After time $t = 2\Delta t$, there are two rainfall pulses to contend with Q_1 and Q_2 , and direct runoff is computed by (Maidment, 1993):

$$q_2 = Q_2 U_1 + Q_1 U_2 = \frac{1}{\Delta t} [Q_2 A_1 + Q_1 A_2] \quad \dots \dots \dots (4-29)$$

which include the immediate impact at the outlet of Q_2 flowing from area A_1 plus the delayed effect of Q_1 flowing from area A_2 . In normal unit hydrograph calculations, the rainfall-excess is assumed uniformly distributed over the watershed in space so that any particular rainfall increment Q_j refers to the average rainfall in time interval $[(j-1)\Delta t, j\Delta t]$ on all areas $A_1, A_2, \dots, \text{etc.}$

With GIS grid capabilities for rainfall mapping, this uniform spatial rainfall distribution is no longer necessary so that two subscripts are needed to characterize rainfall, Q_{ij} , where Q_{ij} is the average rainfall-excess over all cells in isochrone zone i during time interval j . Direct runoff at time $t=n.\Delta t$ is given by summing the runoff contributions from each of the applicable isochrone zones suitably lagged in time (Maidment, 1993):

$$Q_n = \sum_{i=1}^n \frac{P_{eij} A_i}{\Delta t} \dots \dots \dots (4-30)$$

4.7. LINEAR RESERVOIR ROUTING

The linear reservoir routing is widely used method of hydrologic catchment routing to account for catchment diffusion effects. The method is based on the connection of one or several linear reservoir in series. For N such reservoirs, the outflow from the first would be taken as inflow to the second, the outflow from the second as inflow to the third, and so on, until the outflow from the (N-1)th reservoir is taken as inflow to the Nth reservoir. The outflow from the Nth reservoir is taken as the outflow from the cascade of linear reservoirs.

Each reservoir in the series provides a certain amount of diffusion and associated lag. For a given set of parameters $\Delta t/K$ and N, the outflow from the last reservoir is a function of the inflow to the first reservoir. In this way, a one parameter linear reservoir method ($\Delta t/K$) is extended to a two parameter catchment routing method. The routing equation for the method of cascade linear reservoir is given as:

$$Q_{j+1}^{n+1} = C_0 Q_j^{n+1} + C_1 Q_j^n + C_2 Q_{j+1}^n \dots \dots \dots (4-31)$$

in which Q represents discharge, whether inflow or outflow and j and n are space and time indexes, respectively referred from Ponce, (1989) given as Figure 4.4.

The routing coefficients C_0 , C_1 and C_2 are a function of the dimensionless ratio $\Delta t/K$. This ratio is properly a Courant number ($C=\Delta t/K$). In terms of Courant number, the coefficients are expressed as :

$$C_0 = \frac{C}{2-C} \dots \dots \dots (4-32)$$

$$C_1 = C_0 \dots \dots \dots (4-33)$$

$$C_2 = \frac{2-C}{2+C} \dots \dots \dots (4-34)$$

For application to catchment routing, it is convenient to define the average inflow as follows :

$$\bar{Q}_j = \frac{Q_j^n + Q_j^{n+1}}{2} \dots\dots\dots (4-35)$$

Substituting equation gives:

$$Q_{j+1}^{n+1} = 2C_1 \bar{Q}_j + C_2 Q_{j+1}^n \dots\dots\dots (4-36)$$

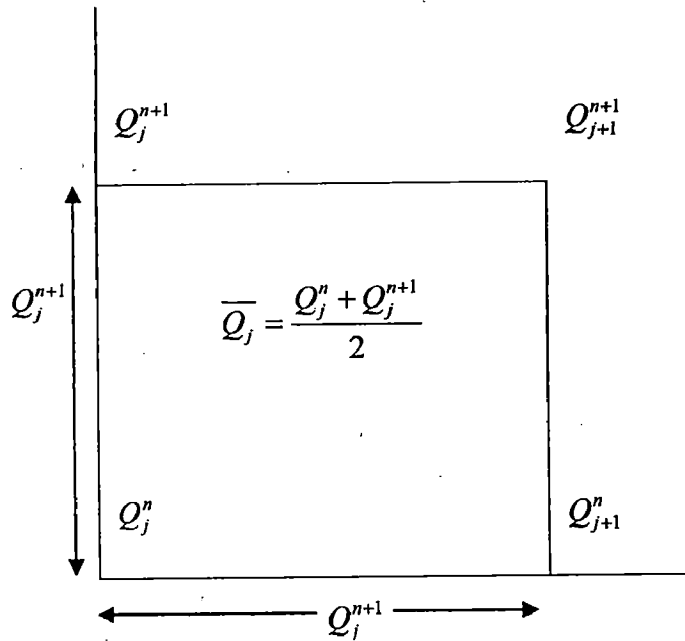


Figure 4.4 Space time discretization in the method of cascade of linear reservoir

CHAPTER 5

THE STUDY AREA AND DATA AVAILABILITY

5.1. THE TEMUR BASIN

The Temur sub-basin is located in the latitude range of 22°45' to 22°55' East and longitude 79°45' to 80°0' North. The Temur river originates in the Vindhychal mountain range at an elevation of 550 m above mean sea level (msl) in the district Sehore of Madhya Pradesh State. It is a tributary of Narmada river. In the present study the catchment area of 518.67 sq.km up to bridge no. 249 gauge-discharge site has been considered. Physical data of Temur river are given as: average slope of river equal to 3.027 m/km, length of basin equal to 56.51 km, and width of basin equal to 26.89 km. The index map of the Temur basin up to bridge no. 249 is presented in Figure 5.1.

Topographically, the Temur basin can be divided into two distinct zones, i.e., upper part and lower part. The upper part having elevations ranging from 660 m to 400 m is predominantly covered by deciduous forest (dense and open) covering about 35% area of the Temur basin. The northern part of the catchment is having mild slopes. The general response of this upper part of basin to rain appears to be quick.

The lower part of the basin consisting of flat bottomed valley narrowing towards the outlet and having elevations ranging from about 300 m to 400 m is predominantly cultivable area (30% from Temur basin) and land with or without scrub (40% from Temur basin). The soils are generally deep in this part and have flat slopes. The places where agricultural activity is carried out have banded fields in which water is impounded during the monsoon period. Agricultural activity is carried out in relatively large areas in the western part and in small pockets elsewhere in which the main crops are wheat and gram. The response of this area to input rainfall is likely to be quiet slow.

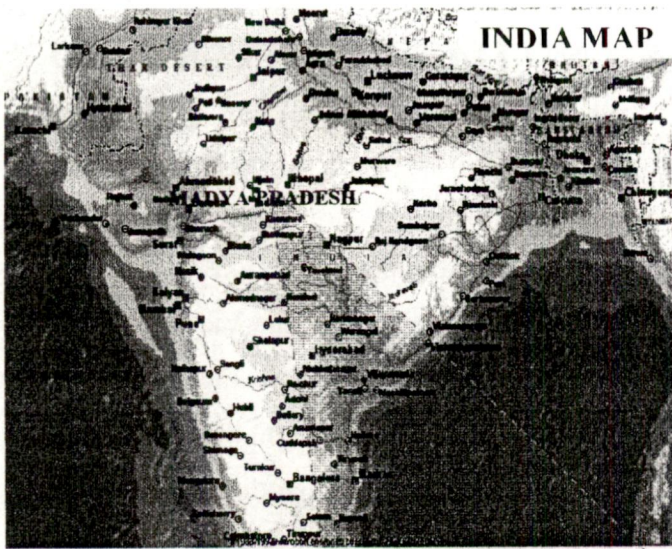


Figure 5.1 Study Area of Temur Watershed



5.2. DATA AVAILABILITY

The base map of the Temur sub-basin was prepared using the Survey of India toposheets (No. 55 N/9, 10, 13 and 14) at the scale of 1 : 50,000. Remote sensing data in digital format was available at NIH, Roorkee for the year 1996/1997 (given as Figure 5.2). For this study IRS LISS III data of Path/Row 100/56 of 10 October 1996, 26 November 1996, and 7 February 1997 were used for the classification of landuse. The pattern of reflectance was used to classify the landuse types.

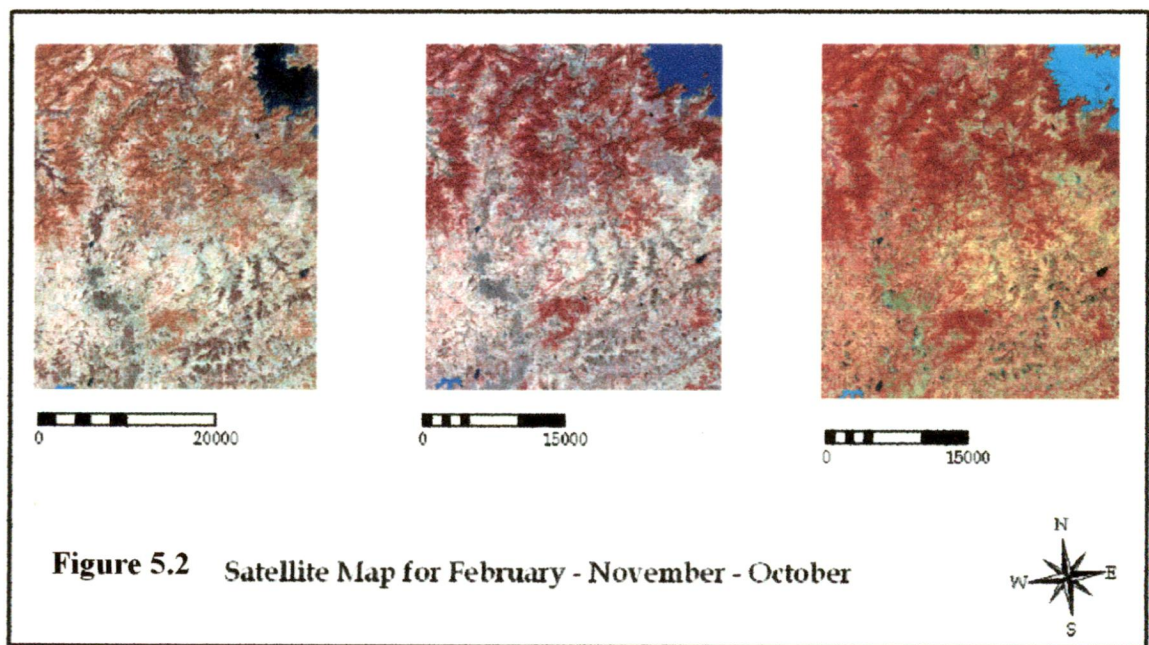


Figure 5.2 Satellite Map for February - November - October

Hourly rainfall data for the years 1961-1965 was available. The rainfall events of 5.09.1962, 30.08.1965, 14.08.1964, 7.09.1965, 20.07.1964, 23.7.1962 and 24.08.1961 were considered for the simulation of runoff hydrographs. The spatially averaged rainfall values for the events considered and the corresponding discharge at bridge no. 249 are presented in Table 5.1. The discharge values presented in Table 5.2 are direct runoff hydrograph. The base flow values are deducted from the total runoff hydrograph using the method outlined in Chow et al. (1988).

TABLE 5.1**SPATIALLY AVERAGED RAINFALL DATA FOR THE EVENTS CONSIDERED FOR THE SIMULATION**

TIME	EVENT 5.9.62 1	EVENT 30.8.65 2	EVENT 14.8.64 3	EVENT 7.9.65 4	EVENT 20.7.64 5	EVENT 23.7.62 6	EVENT 24.8.61 7
1	0.30	0.27	0.17	0.13	0.33	0.17	0.33
2	0.49	0.33	0.27	0.20	0.46	0.29	0.50
3	0.11	0.52	0.14	0.69	1.08	0.13	0.35
4	0.50	0.00	0.26	0.23	0.56	0.14	0.32
5	0.00	0.20	0.41	0.02	0.38	0.68	0.62
6	0.13	1.51	0.43	0.02	0.09	0.36	0.38
7	0.13	0.45	0.44		0.03	0.05	0.09
8		0.26	0.13			0.06	0.01
9			0.15			0.37	0.00
10			0.11			0.05	0.00
11			0.08			0.21	0.00
12						0.15	0.04
13						0.07	0.07
14							0.43
15							0.56
16							1.10
17							0.46
18							0.17
19							0.16
20							0.27
21							0.19

TABLE 5.2

THE OBSERVED DISCHARGE DATA (MINUS BASEFLOW) AT BRIDGE NO. 249 FOR THE EVENTS

TIME	EVENT 5.9.62	EVENT 30.8.65	EVENT 14.8.64	EVENT 7.9.65	EVENT 20.7.64	EVENT 23.7.62	EVENT 24.8.61
	1	2	3	4	5	6	7
0	0.00	0.00	0.00	0.00	0.00	0.00	0.00
1	1.70	1.82	0.00	1.10	13.65	0.00	0.00
2	5.66	3.92	0.00	2.80	24.78	0.00	0.00
3	12.74	7.16	2.83	14.90	58.46	0.71	1.50
4	28.32	12.09	11.32	33.90	128.75	2.83	2.20
5	120.35	26.09	15.29	55.90	167.53	6.37	4.00
6	135.92	38.67	22.65	59.50	187.32	11.33	6.00
7	128.84	50.12	31.15	55.90	206.94	19.82	8.00
8	93.44	58.16	45.30	48.20	214.93	28.32	9.52
9	80.02	29.52	107.60	41.80	197.54	44.60	8.10
10	68.02	27.79	124.59	31.20	165.90	67.96	8.10
11	59.02	23.53	122.66	26.90	128.58	174.86	5.98
12	50.97	17.99	116.10	22.40	91.47	181.23	4.56
13	44.17	13.29	95.71	17.40	64.07	169.90	4.56
14	36.81	12.28	76.45	13.00	48.10	152.91	4.56
15	28.88	8.72	70.79	9.60	42.13	131.67	4.56
16	22.65	8.55	62.29	6.70	30.31	110.44	4.56
17	16.14	6.97	49.83	4.10	27.64	87.78	4.56
18	11.33	6.52	42.47	2.10	20.81	67.96	13.77
19	8.91	5.24	34.54	0.80	19.66	58.33	21.09
20	5.66	4.36	28.31	0.00	17.28	48.14	83.66
21	4.81	3.49	24.92		14.45	39.08	185.99
22	2.83	2.47	22.65		10.92	31.15	182.96
23	1.70	1.75	17.55		9.75	25.91	172.00
24	0.00	1.02	14.16		7.29	19.82	158.50
25		0.00	10.19		6.04	16.99	145.00
26			8.49		3.65	14.16	128.00
27			4.53		2.79	11.89	114.40
28			2.83		0.00	11.32	174.00
29			1.41			9.91	235.99
30			0.00			7.08	380.00
31						5.38	430.39
32						0.00	374.09
33							351.45
34							385.43
35							427.90
36							385.43
37							374.09
38							340.10
39							291.98
40							234.00
41							184.38
42							148.27
43							127.99
44							106.39
45							88.00
46							74.00
47							65.00
48							58.00
49							52.00
50							47.00
51							41.00
52							36.00
53							31.00
54							26.00
55							22.00
56							18.00
57							16.00
58							13.00
59							11.00
60							8.00
61							6.00
62							4.00
63							3.00
64							0.00

CHAPTER 6

DATA PROCESSING

The GIS software used in this study is ILWIS (Integrated Land and Water Information System) (ITC, 1997). It is a Geographic Information System (GIS) with Image Processing capabilities. ILWIS has been developed by the International Institute for Aerospace Survey and Earth Sciences (ITC), Enschede, The Netherlands.

As a GIS and Remote Sensing package, ILWIS allows inputting, managing, analyzing and presenting geographical data on the spatial and temporal patterns and processes on the earth surface. Geographic Information Systems are nowadays indispensable in many different fields of applications to assist in the decision making process. Most decisions are influenced by some facts of geography.

6.1 SPATIAL DATA INPUT

6.1.1 SCANNING

Analysis and modeling in a GIS requires input of relevant data. The data may be broadly classified into two categories: spatial data representing geographic features (points, lines and areas) and attribute data (descriptive information). Data input should be done with utmost care, as the results of analyses heavily depend on the quality of the input data. In ILWIS data can be entered by:

- Digitizing, if you want to use data from analog (paper) maps;
- Keyboard entry, for entering tabular data;
- Scanning, if you want to use paper prints of satellite images, aerial photographs, maps and pictures;
- Importing existing data files from other sources.

In the present study scanned topographic maps in 1:50,000 scale were used to derive spatial information such as contours, drainage, spot height etc. Temur watershed is covered under Survey of India Toposheets 55N/9, 55N/10, 55N/13 and 55N/14.

6.1.2 COORDINATE SYSTEM AND GEOREFERENCE

A coordinate system define in coordinates (x,y) that be used in maps and thus stores information on the kind of coordinates which are used in maps. A georeference is needed for raster maps and uses a coordinate system. A georeference is a service object, which store the relation between the rows and columns in raster maps. Description of the coordinate system and georeferences used are (🌐TEMURP and 🌐TEMUR55n9) given as Figure 6.1.

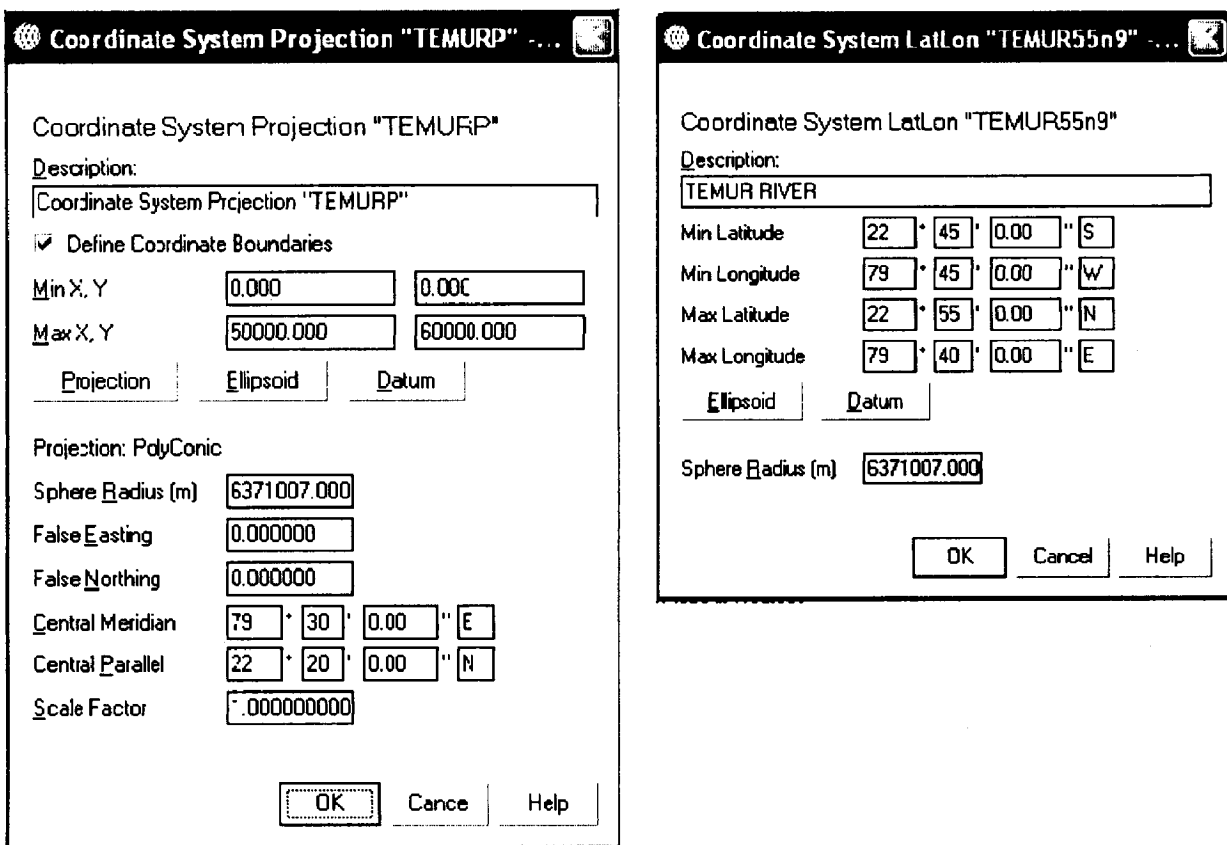



Figure 6.1 Georeference and Coordinate System of Temur Watershed

6.1.3 DIGITIZING POINT MAP

Service objects such as a domain and a coordinate system, are needed to create a point map. A list of classes, or the value ranges and the precision used to codify elements in a map, are defined in a domain. The domain contains all possible names or values that may occur in a map. The domain type identifier is selected for this point map, because each point in the map is identified by a unique number.

In ILWIS the point editor command box shows the position of the digitizer cursor and consists of the following commands:


- Button 0: Add Point: For digitizing a new point.
- Button 1: Move Point: Allows you to move a point.
- Button 2: Change Window: For changing the window displayed on the screen.
- Button 3: Edit Point: For editing the label of a point.

This study point map is created for high spot elevation of Temur watershed (HIGHSP).

6.1.4 DIGITIZING SEGMENT MAP

For digitize a line by holding down the cursor button and simultaneously moving the cursor on the line (digitizing in stream mode). The line coordinates are recorded at regular time intervals. The disadvantage is that many points are needed to define the segment. Many of these points do not improve the accuracy of the line and are considered redundant.

Digitization of a line can also be done by pressing the cursor button only when a point in the segment needs to be digitized (digitizing in point mode). In this way coordinates are only recorded if the button is pressed. The number of points used to store a segment depends on the complexity of the line, and on the accuracy of the person digitizing.

A segment map is created for contour line of Temur watershed (CONTOURP) given as Figure 6.2.

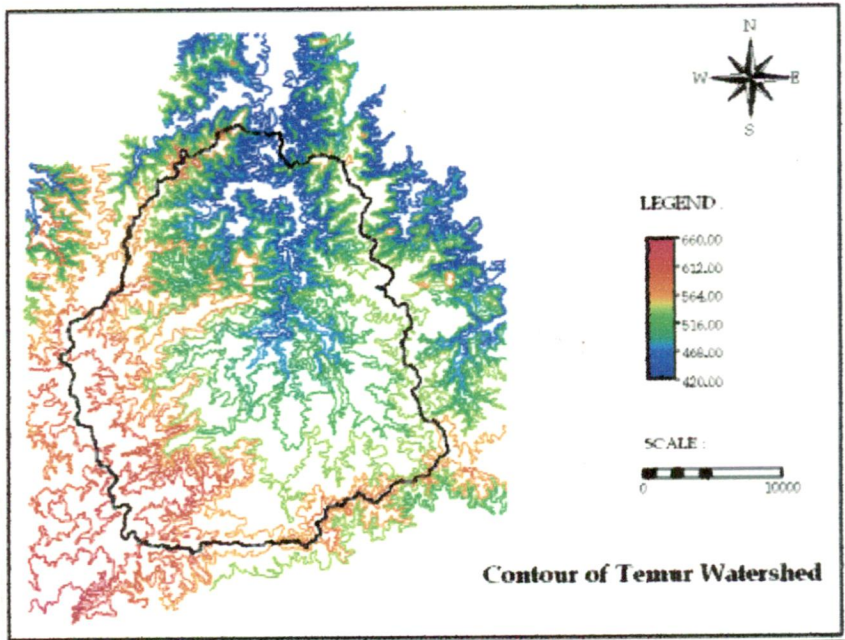


Figure 6.2 Contour Line of Temur Watershed

6.1.5 VECTOR TO RASTER CONVERSION

Most of the analysis and overlay operation are easily and efficiently implemented in the raster model, all maps encoded in vector structure are converted into raster structure (rasterization) (CONTP) given as Figure 6.3.

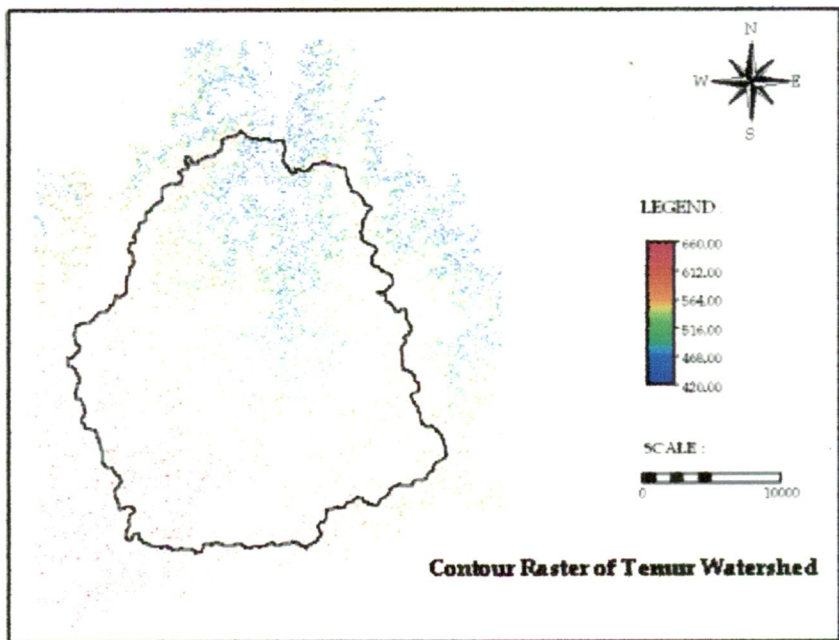


Figure 6.3 Raster Contour of Temur Watershed

6.2 CREATING DIGITAL ELEVATION MODEL (DEM)

The creation of digital elevation model (DEM) with pixel size 10-m from a segment map (contour map) is done with the contour interpolation operation in ILWIS 3.2 (DEM10). The generated DEM was further aggregated at 90-m pixel size to reduce computational requirements (DEM90). The aggregated DEM at 90-m pixel resolution was further conditioned by optimization for drainage, filling of sinks and flat areas for maintaining continuity of flow to catchment outlet.

6.2.1 DEM OPTIMATIZATION

The DEM optimization operation enhances a Digital Elevation Model (DEM) to better comply with observed drainage pattern by 'burning' existing drainage features into Digital Elevation Model (DEM); a subsequent Flow direction operation will thus better follow the existing drainage pattern. The DEM optimization operation offers the following possibilities:

- Gradual drop of (drainage) segments in the output DEM, over a certain distance to the (drainage) segments.
- Gradual raise of (watershed-divide) segments on the output DEM, over a certain distance to the (watershed-divide) segments.
- Additional sharp drop or raise of segments on top of the gradual drop or raise.
- Simple drop or raise of polygons in the output DEM.

Figure 6.4, referred from user's guide ILWIS 3.2, below showing cross sections through the terrain.

- The dotted line shows the original height value(s) in the input DEM, the blue line shows the position of a drainage.
- The Buffer distance is shown in pink, the influence of Smooth drop in greenish and the influence of Sharp drop in red.

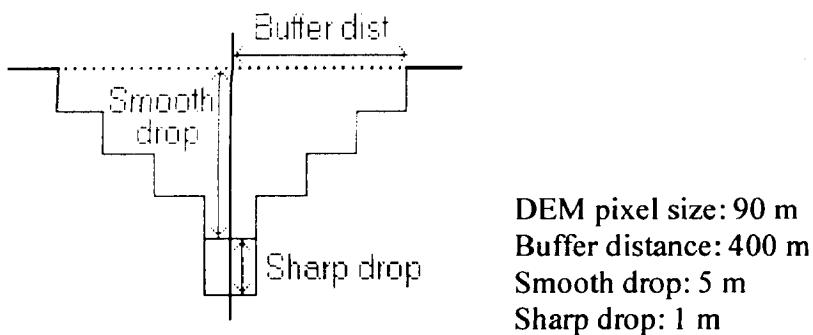


Figure 6.4 Effect of Buffer distance, Smooth drop and Sharp drop on a DEM, using a single drainage segment as example.

- Buffer distance:** Buffer distance determines the width at either side of a segment where height values should be adapted.
- Smooth drop:** Smooth drop determines the height with which segments and their surroundings (as specified by the Buffer distance) should be gradually dropped (positive value) or raised (negative value) in the terrain.
- Sharp drop:** Sharp drop determines the height with which segments themselves should be dropped (positive value) or raised (negative value) in the terrain.

6.2.2 FILL SINK

The Fill sinks operation will 'remove' the following from a Digital Elevation Model (DEM):

- Depressions that consist of a single pixel, i.e. any pixel with a smaller height value than all of its 8 neighbouring pixels,
- Depressions that consist of multiple pixels, i.e. any group of adjacent pixels where the pixels that have smaller height values than all pixels that surround such a depression.

Figures 6.5a – 6.5e, referred from user's guide ILWIS 3.2, below show the complete process of using fill sinks, flow direction and flow accumulation. Figure 6.5e, shows the result of using Flow direction and flow accumulation directly on the input map,

without using the Fill sinks operation. DEM map of Temur watershed given as Figure 6.9a.

Figure 6.5a
Input map for Fill sinks.

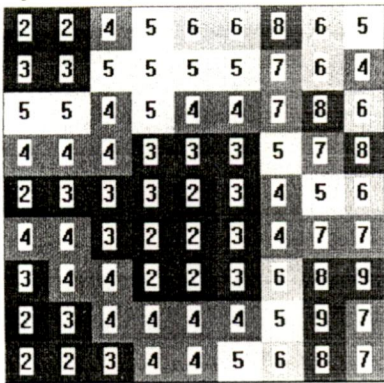


Figure 6.5b
Output map of Fill sinks.

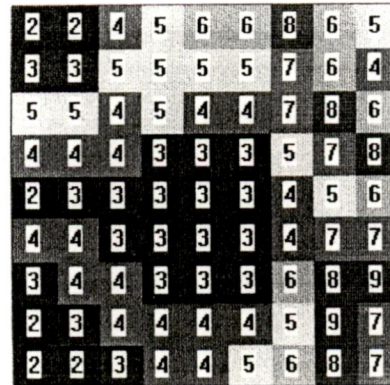


Figure 6.5c
Result of Flow direction.

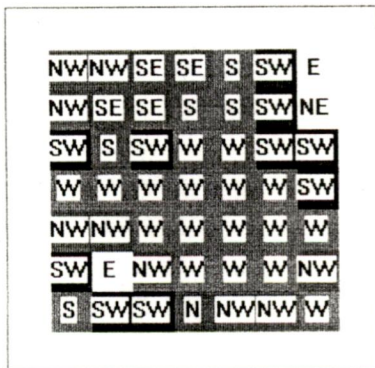


Figure 6.5d
Result of Flow accumulation.

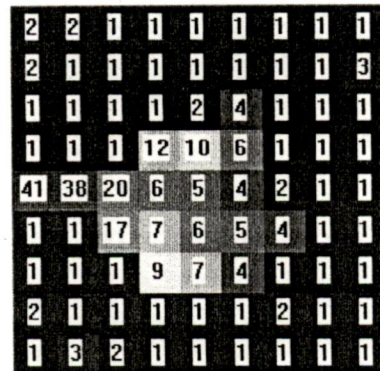
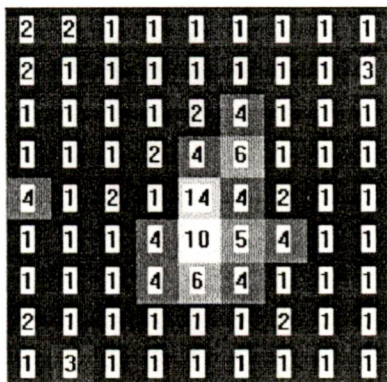


Figure 6.5e
Result of Flow accumulation when
Fill sinks is not used.

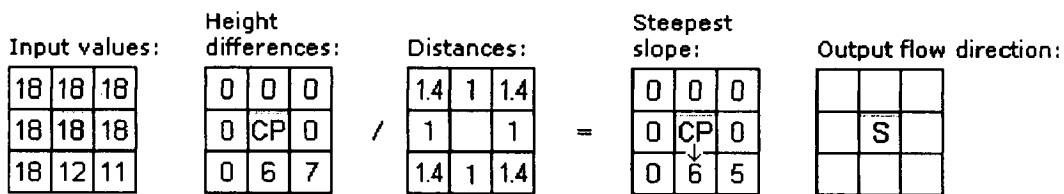


6.2.3 FLOW DIRECTION

In a (sink-free) Digital Elevation Model (DEM), the Flow direction operation determines into which neighboring pixel any water in a central pixel will flow. Flow direction is calculated for every central pixel of input blocks of 3x3 pixels, each time comparing the value of the central pixel with the value of its 8 neighbours. There are two calculation methods in flow direction i.e. steepest slope and lowest height method. Calculation method on steepest slope and lowest height method that referred from user's guide ILWIS 3.2 are show in Figure 6.6 and 6.7. The output map contains flow directions as N (to the North), NE (to the North East), etc.

Steepest slope method:

- For each block of 3x3 input pixels, the operation calculates the height difference between the central pixel (CP) and each of the 8 neighbour pixels.
- If, for a neighbour, the height difference is positive (i.e. central pixel has larger value than the specific neighbour), then for corner neighbours, height differences are divided by (distance) 1.4, and for horizontal neighbours, height differences are divided by (distance) 1. This determines the steepness between the central pixel and its neighbours.
- Then, the (position of the) neighbour with the largest 'steepness' value is the output flow direction for the current central pixel.



(a)

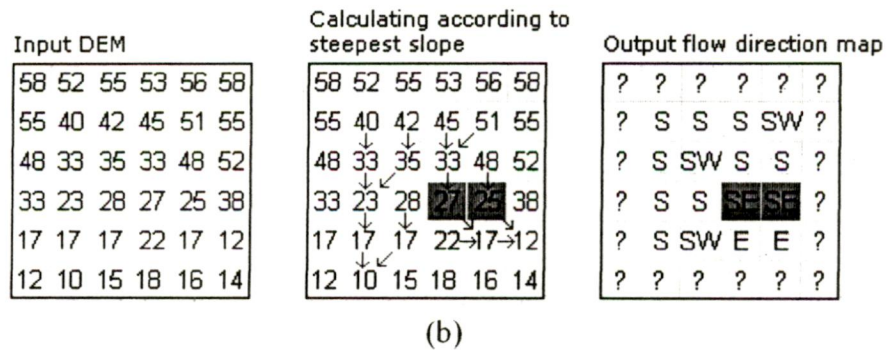


Figure 6.6 Calculation method of steepest slope method

Lowest height method:

- For each block of 3x3 input pixels, the operation calculates the height difference between the central pixel (CP) and each of the 8 neighbour pixels;
- From all neighbours with a positive height difference, (i.e. central pixel has larger value than a specific neighbour), (the position of) the neighbour with largest positive height difference is the output flow direction for the current central pixel.

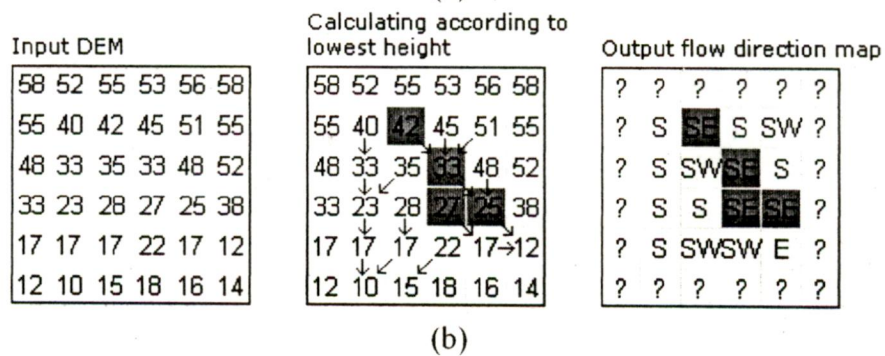
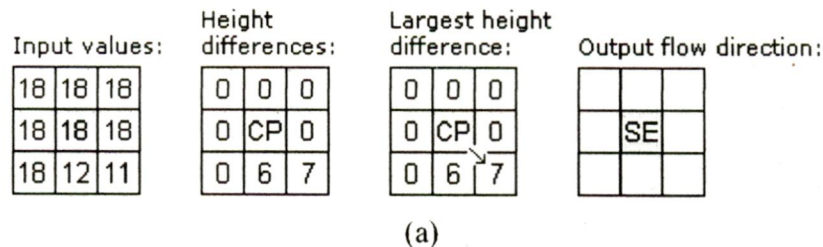


Figure 6.7 Calculation method of lowest height method

Flow direction map of Temur watershed based on calculation using steepest slope method is given as Figure 6.9b.

6.2.4 FLOW ACCUMULATION

The flow accumulation operation performs a cumulative count of the number of pixels that naturally drain into outlets. The operation is generally used to find the drainage pattern of a terrain from a DEM as input. The operation uses the output map of the flow direction operation. The output of this operation gives cumulative hydrologic flow values that represent the number of input pixels which contribute any water to any outlets, the outlets of the largest streams, rivers etc. will have the largest values. Calculation method of flow accumulation, referred from user's guide ILWIS 3.2, given as Figure 6.8.

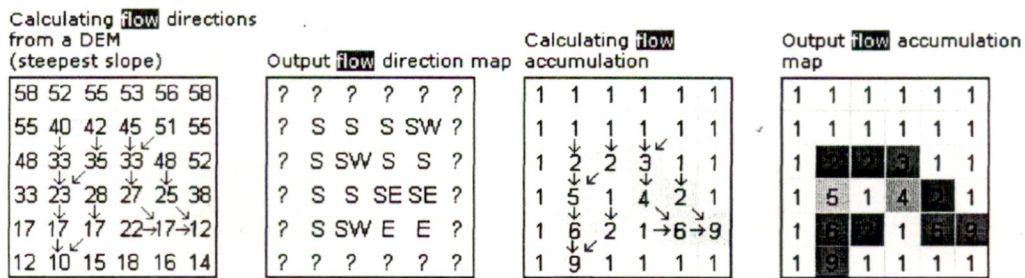


Figure 6.8 Calculation method of flow accumulation

Flow accumulation map (FlowAccum) of Temur watershed is given as Figure 6.9c.

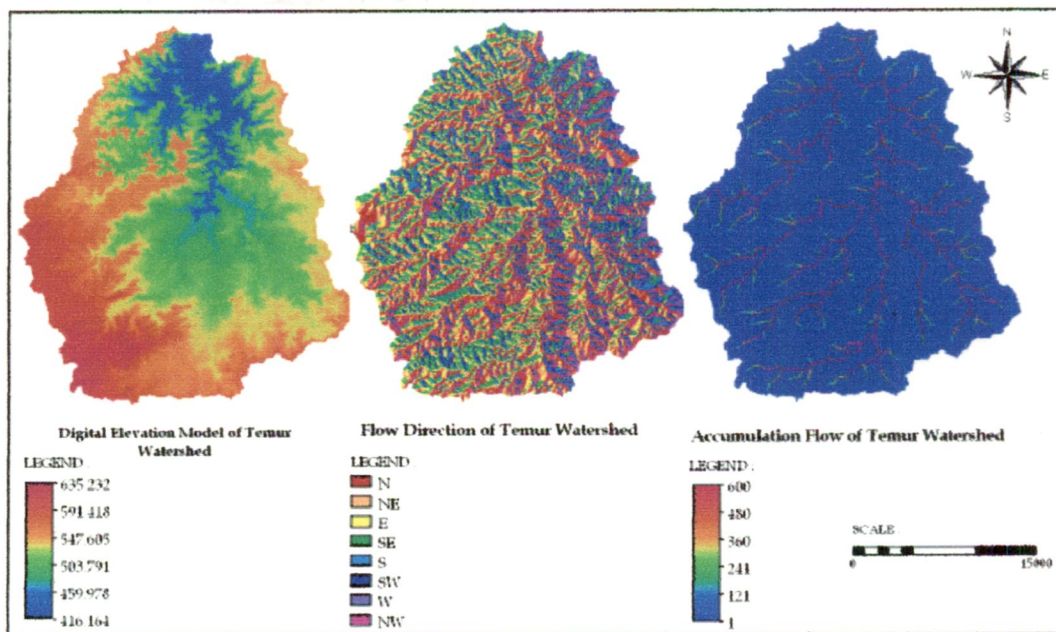


Figure 6.9 DEM map (a), flow direction map (b) and accumulation flow map (c) of Temur Watershed.

6.3 CHANNEL DELINEATION

The watershed channels were delineated based on the upstream contributing area of each cell. The area required to develop a channel depends on regional and watershed characteristics such as climatic conditions, soil properties, surface cover, and slope characteristics (Martz and Garbrecht, 1992, Jain and Kothiyari, 2000). Any cells that were not determined to be part of the stream network were assumed to be controlled by overland flow. Cells that did not have any other cells flowing into them were considered to be ridge cells. Many researchers have delineated stream networks based on the upstream area (Martz and Garbrecht, 1992; Jenson and Domingue, 1988; Mark, 1984).

For this watershed, a channel flow threshold with 20 cells was chosen. Figure 6.10 shows the stream network that result from the channel flow threshold of 20 cells. There was good agreement between the stream network derived using the GIS and the upstream area technique as depicted in Figure 6.10.

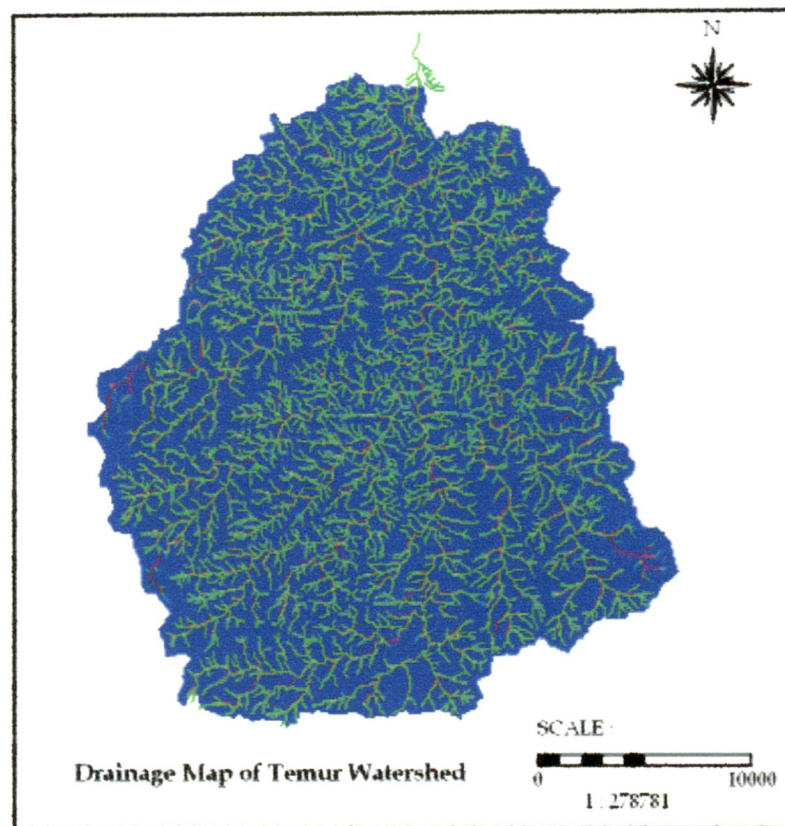


Figure 6.10 Temur basin DEM-based stream network (red) and digitized stream network (green).

6.4 CREATING SLOPE MAP

For creating a slope map from digital elevation model (DEM), the slope angle or slope percentage can be calculate in x and y direction using DEM, given formula :

$$\text{Slope} = 100 * \text{HYP}(\text{Dx}, \text{Dy}) / \text{pixsize}(\text{DEM50})$$

In this formula, HYP (hypotenuse) is an interval map calculation function to calculate the position root of the sum of square Dx plus square Dy (Pythagoras rule), Dx is horizontal gradient map, and Dy the vertical gradient map. In this formula, the numerator is divided by pixel size, using the internal function pixsize (map). Since the gradient is expressed in meters difference per pixel, the result should be in meters differences per meter. Slope map of Temur watershed given as Figure 6.11.

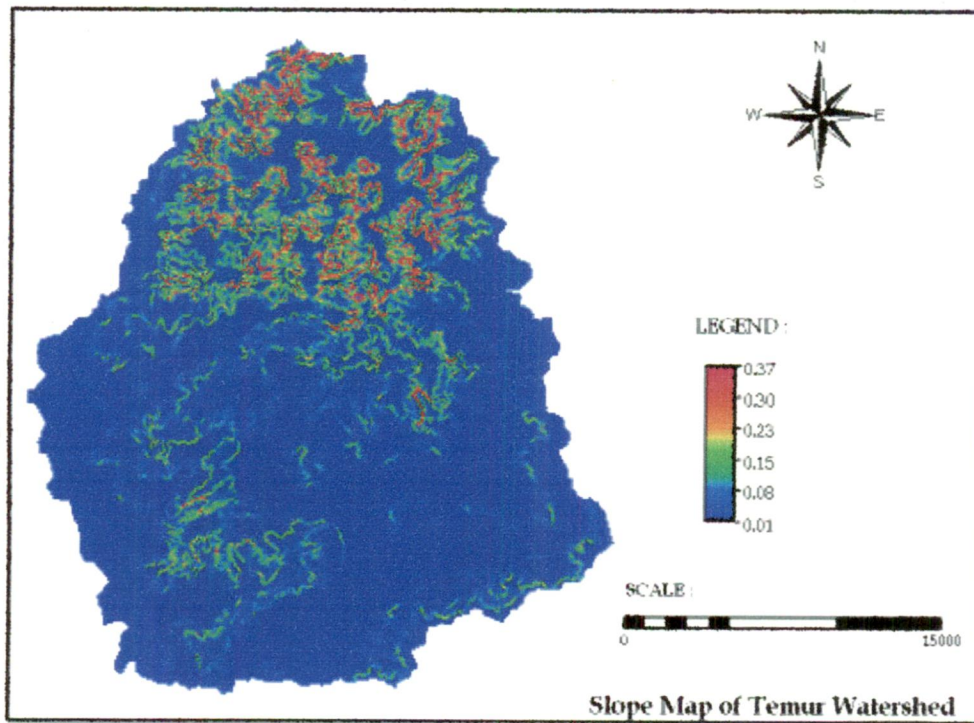


Figure 6.11 Slope Map of Temur Watershed

6.5 IMAGE CLASSIFICATION

To generate landuse map of the study watershed, digital data of LISS-III sensor of IRS system was utilized. Digital image classification can be performed by two broad methods viz. unsupervised classification method and supervised classification method. In

present study supervised classification method was followed. In supervised classification, a sample set has to be created in which the relevant spectral data of input bands (map list), for identified cover classes (domain codes) are selected to act as signatures for identified landuses. This is usually done in conjunction with ground truth information (either from field or from some published information), as well as the cover classes to be used.

The classes plotted in distinct colors in the feature space, which enables a judgement of whether the classes really be spectrally distinguished and whether each class corresponds to only one spectral cluster. The Classify operation performs a multi-spectral image classification according to training pixels in a sample set. Several methods are available to classify the image, however, in present study minimum distance classification algorithm is used. The minimum distance to mean algorithm comprises of following steps:

For each feature vector, the distances towards class means are calculated.

- The shortest Euclidian distance to a class mean is found;
- If this shortest distance to a class mean is smaller than the user-defined threshold, then this class name is assigned to the output pixel.
- Else the undefined value is assigned.

A scatter plot of different sample signatures collected in different spectral bands is depicted in Figure 6.12 for 7 February 1997 data. It can be seen from these plots that all the signatures collected are well separated from each other. The classified land use map is given as Figure 6.13.

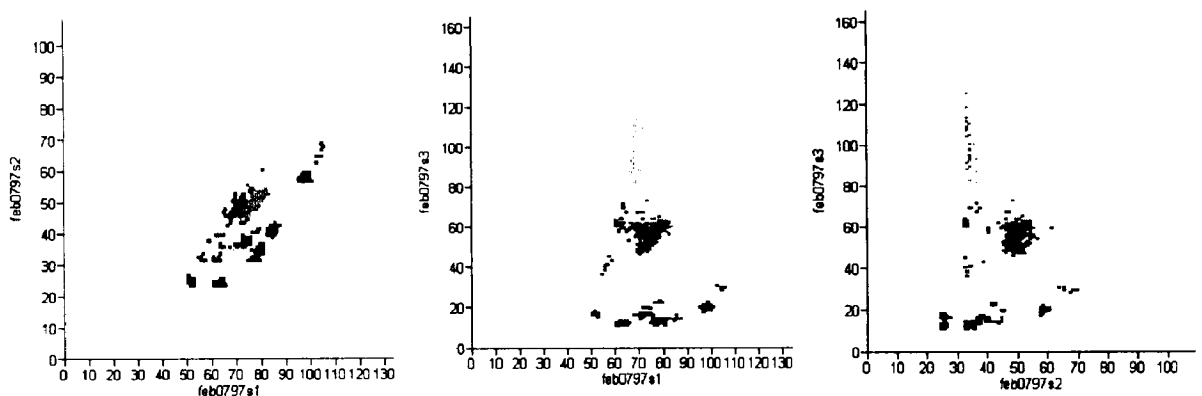


Figure 6.12 Sampling Corresponding to Remote Sensing Map

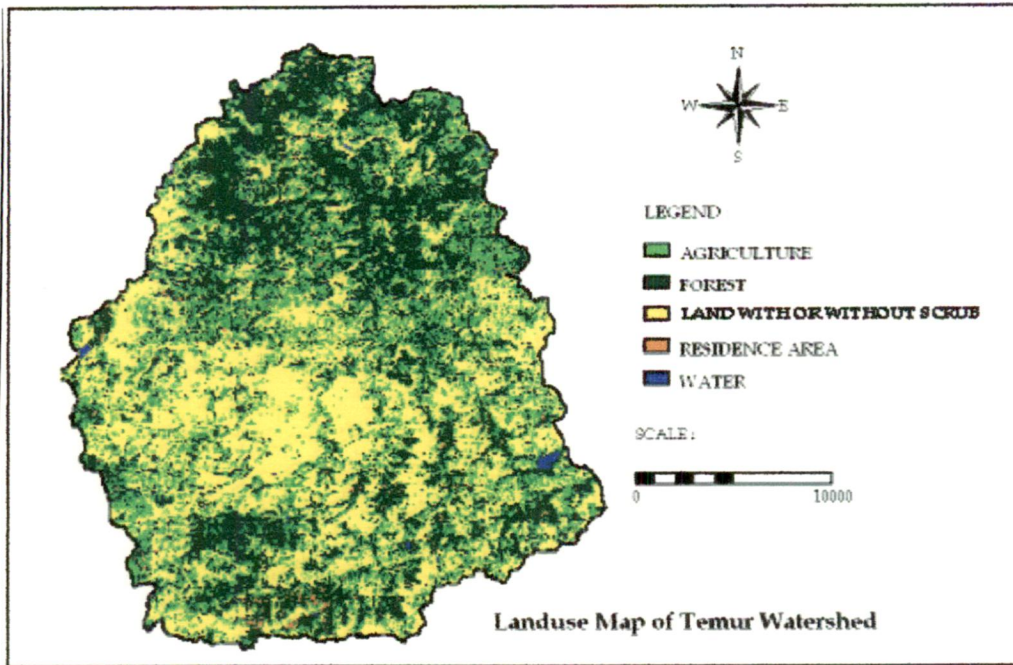


Figure 6.13 Classified Land use map of Temur basin

CHAPTER 7

ANALYSIS AND DISCUSSION OF RESULTS

As outlined in Chapter 4, the computations were performed as per Figure 4.1 and the details of analysis and interpretation of results obtained are presented here.

7.1 DETERMINATION OF TRAVEL TIME

In the context of numerical formulation, the watershed domain is discretized by a raster grid and proper tools are developed whereby spatial variations inside the integral in equation (4-14) can be accounted for.

7.1.1 DETERMINATION OF EXCESS RAINFALL

Time series of rainfall excess intensities for various events is calculated using phi index method. Details of these calculations are given as APPENDIX A-1 for all 7 storm events.

7.1.2 DIFFERENTIAL MAPS OF TRAVEL TIME

Differential kinematic wave travel time over any pixel is calculated based on the piecewise form of equation (4-14). The input map for this part include flow direction (FlowDirection), bed slope (Slope), equilibrium discharge (Qemap), and roughness coefficient (MANNINGmap). The map of Mannings n was generated utilizing land use map described earlier (Figure 7.2) by assigning values for Manning's n to a particular landuse class from literature (Woolhiser, 1975 and Engman, 1986). Manning map of Temur watershed given as Figure 7.1. For computing differential maps of travel time corresponding to a given excess rainfall intensity a map of equilibrium discharge (Qemap) is first prepared. This is done, for any pixel, by accumulating the excess intensity multiplied by the pixel area over the flow drainage area of that pixel known from the accumulation map (FlowAccum). Equilibrium discharge map for rainfall intensity of 0.2 cm/hr is given as Figure 7.2 as illustration.

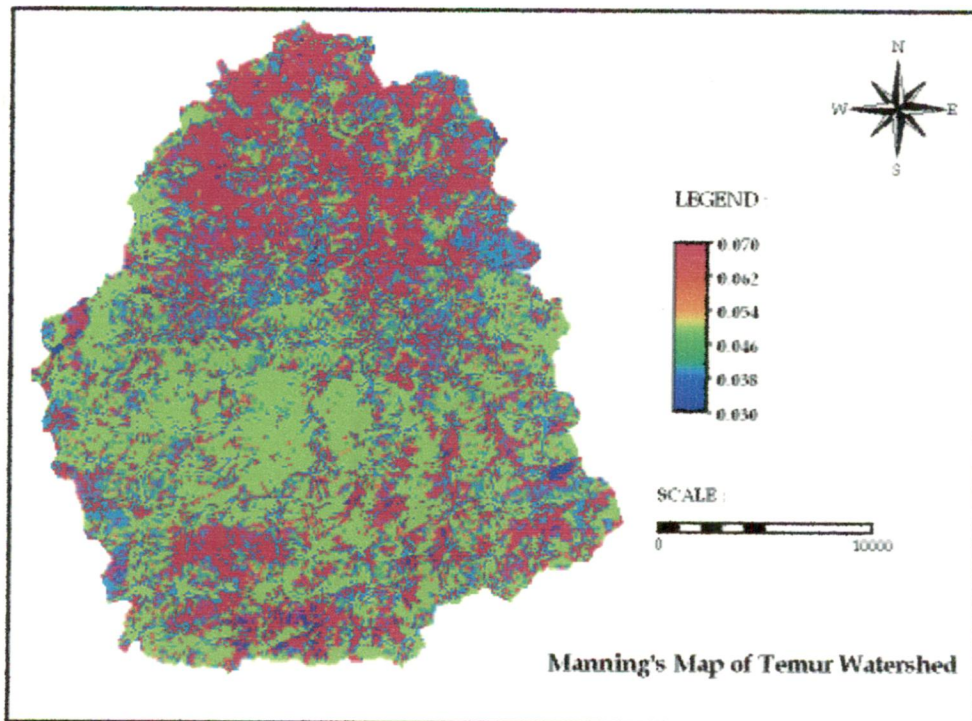


Figure 7.1 Manning's Map

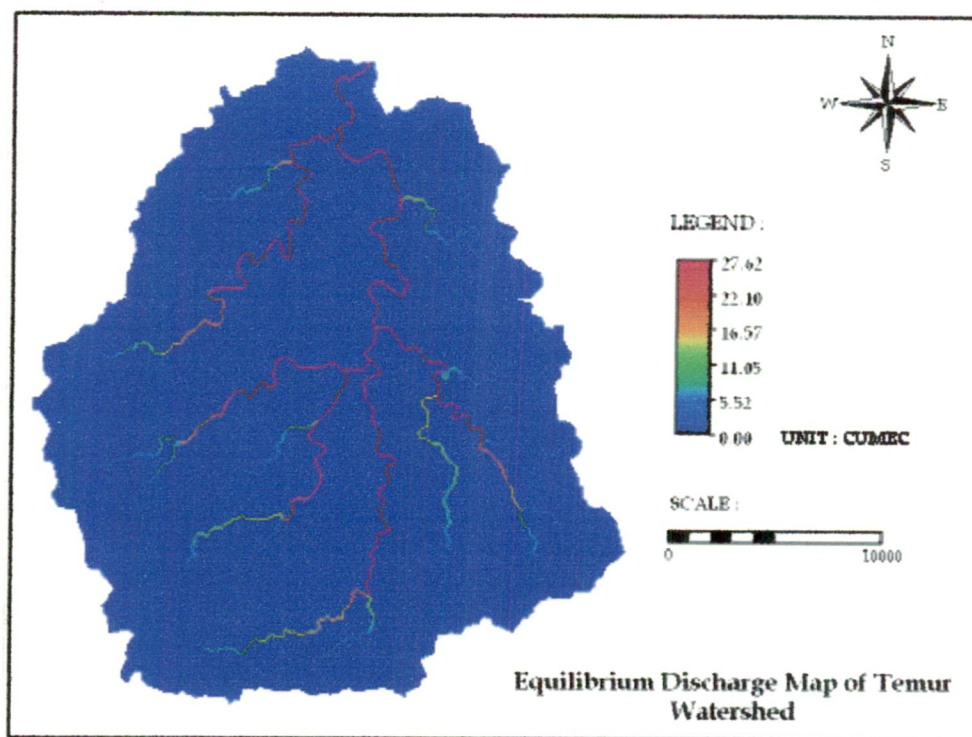


Figure 7.2 Equilibrium discharge Map

7.1.2.1 OVERLAND FLOW

Overland flow travel time ($\text{TIME}_{\text{overland}}$) was calculated using equation (4-19) for all rainfall excess blocks. Overland time travel every pixel for rainfall excess intensity 0.20 cm/hr given Figure 7.4b.

7.1.2.2 CHANNEL FLOW

Channel flow travel times were computed using equation (4-20) for all rainfall excess blocks. A_x and R were expressed as functions of flow depth h , using regression curve due to non availability of cross section data for Temur river. For the present analysis, the river section is assumed as rectangular channel (for such a case: $a_1=W$, $b_1=1$ and $A_x=W.h$). The width of channel was assumed as width of descritized cell width (= 90 m). Regression curve developed for relationship between R/h and W/h is given as Figure 7.3. Fitted regression equation is given below,

$$R/h=0.4752(W/h)^{0.249} \text{ with } R^2=0.9875 \quad \dots \dots \dots (7-1)$$

Substitution to equation $R=a_2h^{b_2}$ and $W=90$ m (pixel size 90-m), gives values of $a_2=1.0246$, $b_2=0.8949$ and $\gamma=0.4059$ for use in equation (4.12). Channel time travel ($\text{TIME}_{\text{channel}}$) for every channel pixel for rainfall excess intensity 0.20 cm/hr is given in Figure 7.4a.

Total travel time which is summation of overland flow travel time and channel flow travel time ($\text{TIME}_{\text{total}} = \text{TIME}_{\text{overland}} + \text{TIME}_{\text{channel}}$), is given in Figure 7.4c for excess rainfall intensity of 0.20 cm/hr as illustration.

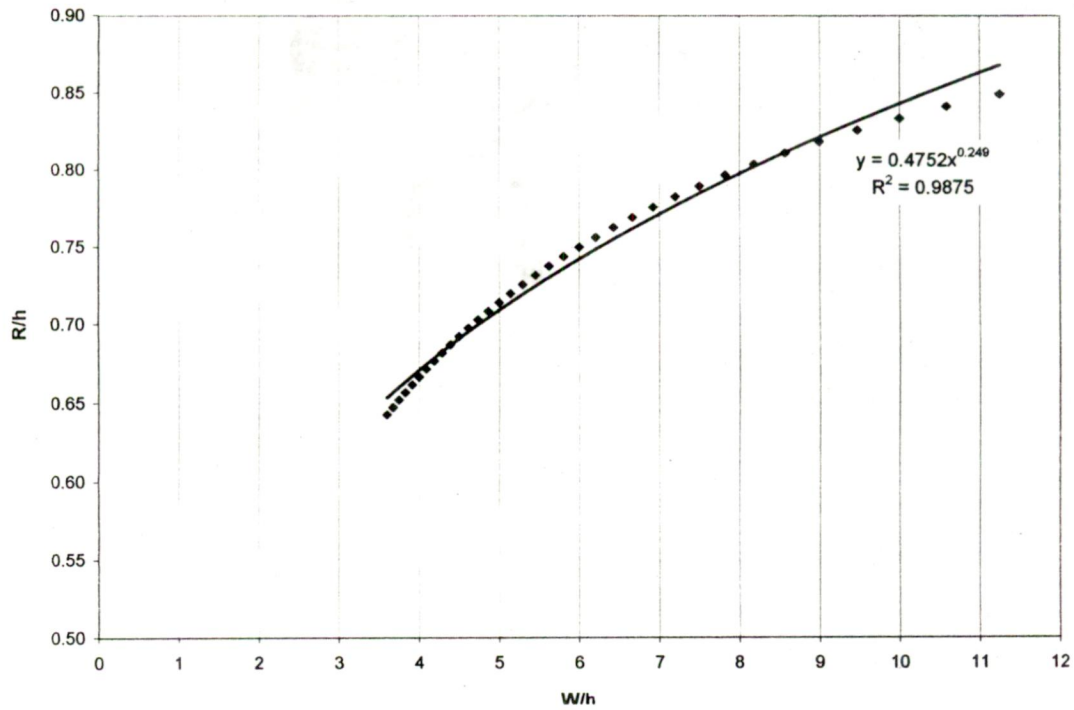


Figure 7.3 Relationship between R/h and W/h

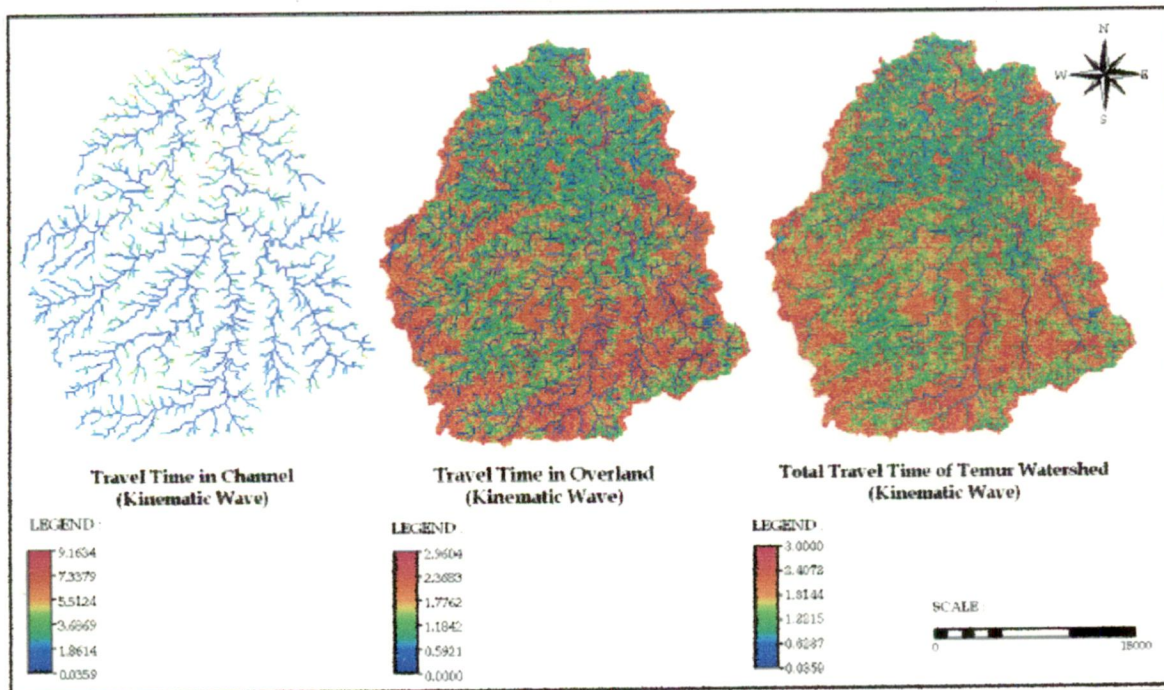


Figure 7.4 Maps of Travel time in channel (a), in overland (b) and total travel time (c), unit in minute.

7.1.3 CUMULATIVE TRAVEL TIME MAP

Accumulating of the total differential travel time map along flow paths to the outlet produces cumulative travel time map. This map indicates the spatial distribution of the required for a kinematic wave to travel from any pixels to the outlet. For a cumulative travel time map, isochrones of equal travel times are derived using map slicing operation and the areas bounded by adjacent isochrones are determined. Isochrone map for rainfall excess intensity of 0.20 cm/hr is given as Figure 7.5.

Such isochrone maps for all 30 rainfall intensities were computed to derive variable rainfall intensity dependent time-area histograms.

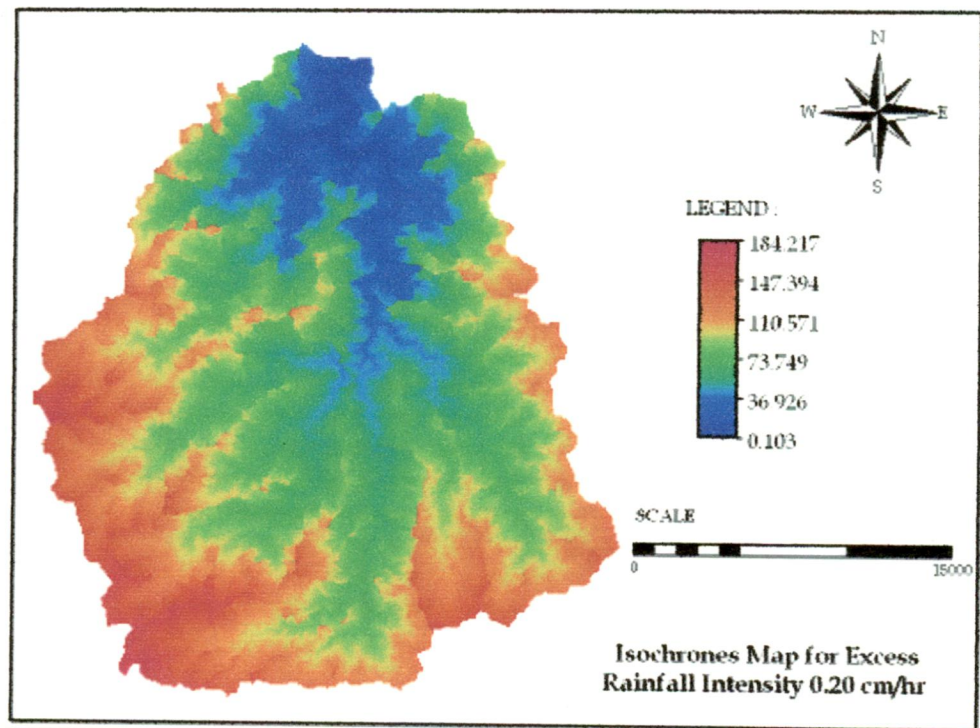


Figure 7.5 Isochrone map ($i = 0.20$ cm/hr), unit in minute

7.1.4 DEVELOPMENT OF RELATIONSHIP BETWEEN TIME OF CONCENTRATION AND RAINFALL EXCESS INTENSITIES

The relationship for the time of concentration for Temur watershed based on the maximum travel time values corresponding to different rainfall excess intensities (E), the following regression was fitted to the data (Figure 7.6) :

$$T_c = 96.02E^{-0.4076} \quad \dots \dots \dots (7-2)$$

With $R^2=0.9994$, T_c is in minutes and E is in mm/hr. The absolute value ($=0.4076$) of exponent for E is little bigger than 0.4 due to the effect of non-wide channel network in Temur watershed. The multiplicand ($=96.02$) represent watershed hydro-goemorphologic index conglomerating spatially distributed characteristics such as surface roughness, slope, flow length, flow accumulation, drainage pattern and channel geometry. This relationship could be utilized in deriving time area hyetograph (TAH) associated with any other value of excess intensity (say E_2), by scaling the time axis with the ratio of $(E_2/E_1)^{-0.4}$ without doing elaborate computations of travel time for each rainfall excess block if the excess rainfall is assumed as constant in space.

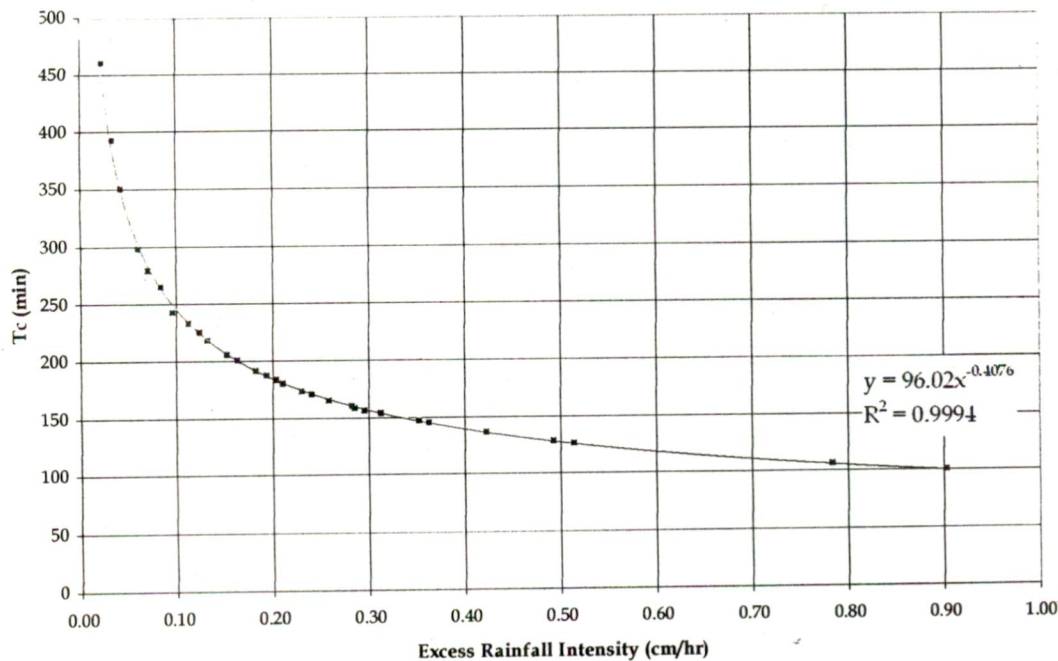


Figure 7.6 Variation of time of concentration with rainfall excess intensity

7.2 SENSITIVITY ANALYSIS

In order to evaluate the effect of roughness coefficient on time of concentration, a sensitivity analysis was performed. This was done by altering base values of Manning's coefficient by ± 10 and $\pm 20\%$. Altered values of Manning's n are presented in Table 7.1. Resultant changes in time of concentration due to alteration values of Manning's n are shown in Figure 7.7.

Table 7.1 Manning's coefficient for Temur Watershed

Land Classify	Manning Coeff. For Landuse				
	-20%	-10%	0%	+10%	+20%
Agriculture	0.032	0.036	0.040	0.044	0.048
Forest	0.056	0.063	0.070	0.077	0.084
Land with and without scrub	0.040	0.045	0.050	0.055	0.060
Residence Area	0.024	0.027	0.030	0.033	0.036
Water	0.008	0.009	0.010	0.011	0.012

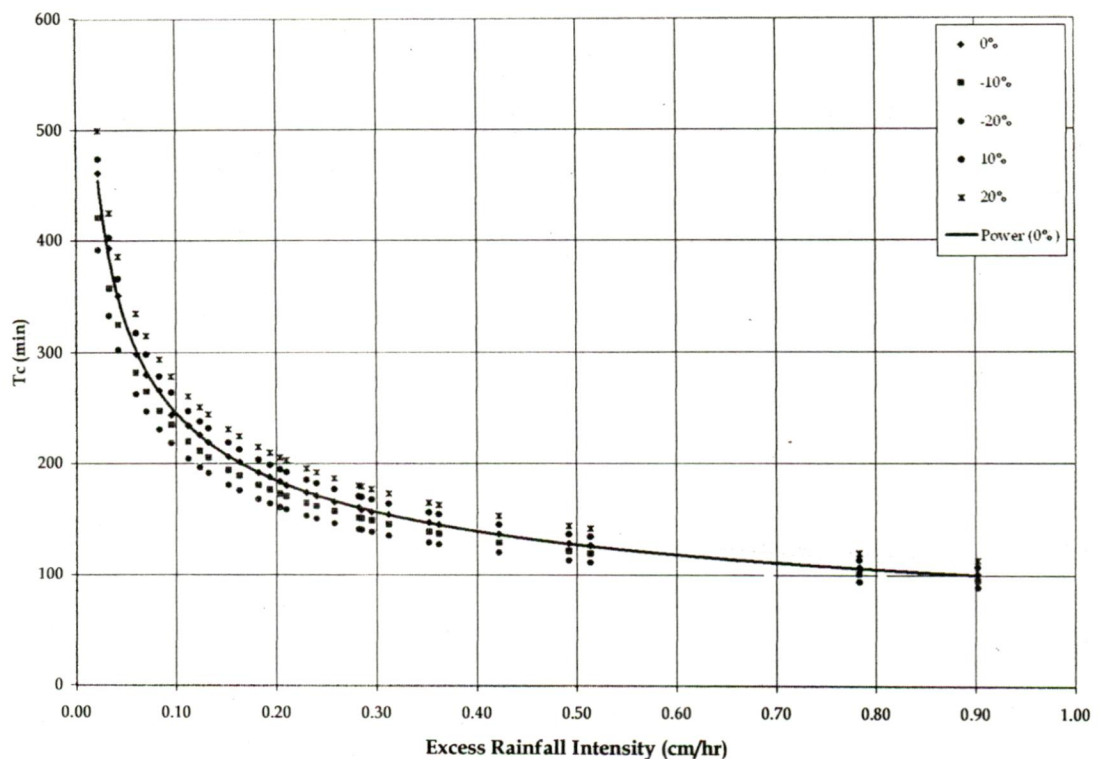


Figure 7.7 Respond of time concentration because Manning's coefficient change

As can be seen from Figure 7.7 that decrease of 10% in Manning's coefficient results in decrease in time of concentration from 3.60 to 9.00% with average value of 5.87% and with decrease of 20% in value of Manning's coefficient, time of concentration decrease from 10.23 to 15.26% with average value of 12.35%. Similarly with increase of 10% in value of Manning's coefficient, time of concentration increase from 2.47 to 8.55% with average value of 5.99% and with increase of 20% in value of Manning's coefficient, time of concentration increase from 8.08 to 14.49% with average value of 11.79%. The results obtained shows that increase or decrease in time of concentration is also influenced by rainfall intensity.

7.3 TIME AREA DIAGRAM

The computed travel times for the 90-m grid cells were summed up starting from watershed outlet to upstream cells using hydrological flow paths determine previously using 8 direction pour point model. Resultant map, termed as cumulative travel time map represent the map of travel time from each pixel to the watershed out following proper hydrological paths. For a cumulative travel time map, isochrones of equal travel time are derived for every rainfall excess intensity before (Figure 7.5) and the areas bounded by adjacent isochrones are determined using slicing tools in ILWIS 3.2 (Figure 7.8). The histogram of the area of cells falling within one-hour travel time increments are compiled, as well as their cumulative distribution, which is the time-area curve. This was done repetitively for all rainfall excess intensity blocks. Figure 7.9 shows the time-area curves from different rainfall intensities over the watershed.

The channel responds gradually to rain falling on the nearby areas and the channel itself. As time progresses, rain falling on remote overland segments contribute to the channels and traverses along the channels to the outlet. At the time to equilibrium the whole basin is responding and the entire storage capacity is used and the inflow is equal to the outflow. Moreover, as the rainfall intensity increases the slope of the S-hydrograph increases, and the time to equilibrium decreases.

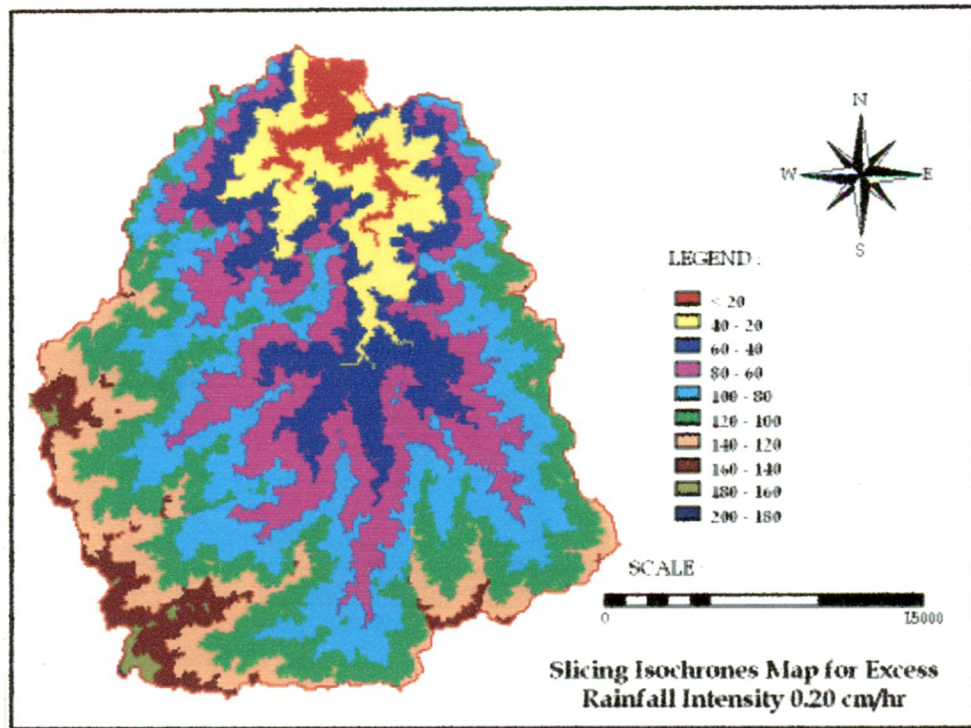


Figure 7.8 Slicing Isochrone map interval 20 min ($I=0.20$ cm/hr), unit in minute

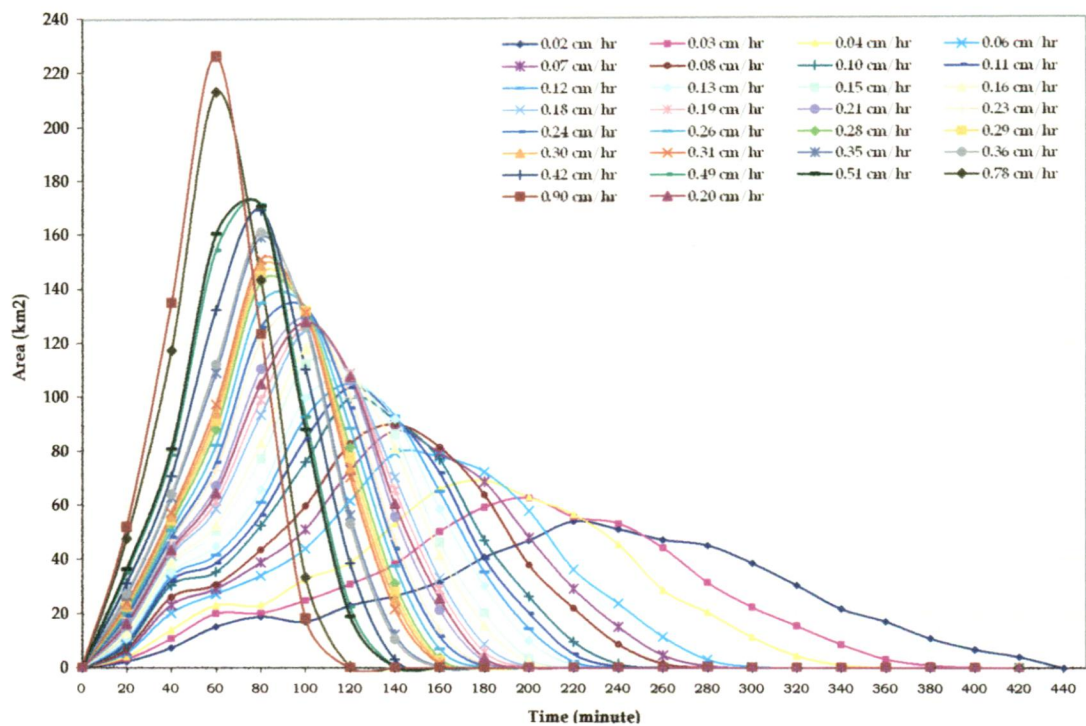


Figure 7.9 Time area diagram for every rainfall excess intensity

7.4 SPATIAL UNIT HYDROGRAPH

The S-hydrograph of time-area curve is lagged by $\Delta t=1$ hr and subtracted from the original curve, and the resulting values are divided by Δt , to yield the 1-hr spatial unit hydrograph. Graph of S-hydrograph for different excess rainfall intensities are shown in APPENDIX A-2. APPENDIX A-3 shows the 1-hr spatial unit hydrographs for different rainfall excess intensities.

7.5 UNIT HYDROGRAPH SIMULATION

Rainfall excess hyetograph is convoluted with the corresponding 1-hr spatial unit hydrographs to obtain the simulated hydrograph shown in APPENDIX A-4 and graph is shown in APPENDIX A-5. The superposition of outputs is retained in computing the direct surface runoff hydrograph by convolution method.

The DSRO hydrographs were simulated using convolution method due to seven storm events. Peak discharge and time to peak of runoff hydrographs from result of simulation using this method are presented in Table 7.21. As can be seen from Table 7.2, the computed hydrographs are having very high peak and very early time to peak. In some events the computed hydrographs show two or more peaks. This is probably manifestation of not considering catchment storage effects which seems to dominate the observed flood hydrographs.

Table 7.2 Peak discharge and time to peak of runoff hydrograph using convolution method

Storm No.	Peak Discharge (cumec)	Time to peak from the beginning of storm (hr)
5.09.1962	295.85	3
	329.67	5
30.08.1965	240.70	7
14.08.1964	391.96	7
7.09.1965	283.90	4
20.07.1964	898.36	3

23.7.1962	431.77	7
	148.47	11
24.08.1961	485.17	4
	537.03	7
	653.20	17

To account for catchment storage effects in computed runoff hydrographs, the resultant of DSRO hydrographs computed above were routed through two conceptual linear reservoirs in series (Ponce, 1989). The value of storage coefficient K was determined by optimization such that the computed hydrograph and observed hydrographs match reasonably. Resultant computed total runoff hydrographs using this method are given as Figure 7.12 – 7.18. Apparently this has resulted in different value of K for every storm event (Table 7.3) signifying effect of storm pattern and intensity on storage characteristics.

Table 7.3 Different value of K for 7 storm events

Storm No.	K value
5.09.1962	2.60
30.08.1965	2.25
14.08.1964	3.40
7.09.1965	2.70
20.07.1964	3.00
23.7.1962	2.20
24.08.1961	2.80

To study the effect of rainfall intensity on catchment storage effects, the 1-hour maximum excess rainfall intensity versus storage coefficient plot was made and given as Figure 7.10. As can be seen from Fig. 7.10, the Storage coefficients (K) in general decrease with increase in value of rainfall excess. Which implies that rainfall intensity plays a significant role in influencing catchment storage induced diffusion on resultant

runoff hydrograph. However, more from more catchments and storms need to be analyzed to further confirm these results.

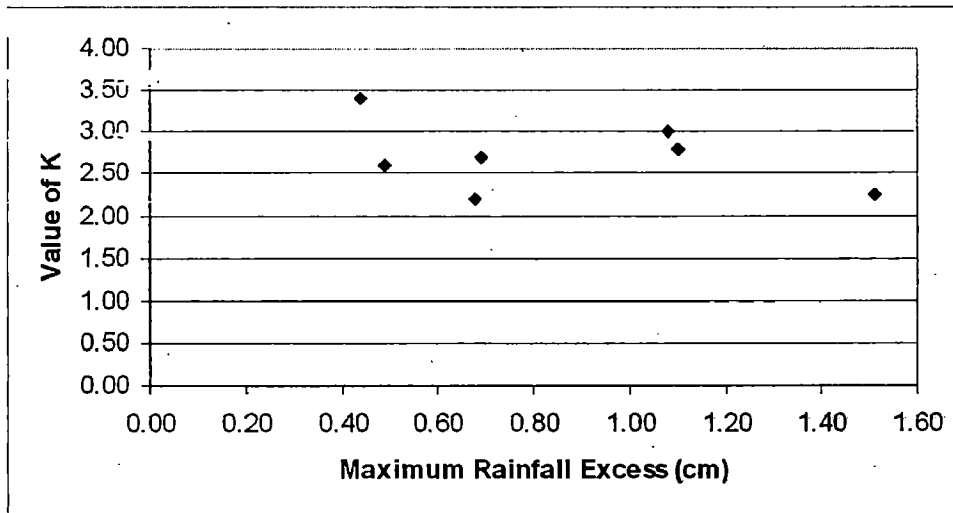


Figure 7.10 Storage coefficient (K) vs Maximum Rainfall Excess

7.6 MODEL PERFORMANCE EVALUATION

The performance of proposed method in simulating hydrographs were evaluated based on a visual comparison, an evaluation of the peak flow rate, the time to peak prediction, the coefficient of determination (equation 6-2) and Nash & Sutcliffe efficiency (equation 6-3). If the R^2 value equals 0, the model efficiency statistic may be interpreted that the model prediction is as accurate as using an average of the observed data. An R^2 value of 1 indicates a perfect fit between the computed and observed hydrographs.

$$R^2 = \frac{\left[\frac{\sum_{i=1}^n (Q_i - \bar{Q}) \left(Q_i - \hat{Q} \right)}{\left(\sum_{i=1}^n (Q_i - \bar{Q})^2 \right)^{0.5} \left(\sum_{i=1}^n \left(Q_i - \hat{Q} \right)^2 \right)^{0.5}} \right]^2}{\dots \dots \dots (6-2)}$$

$$E = 1 - \frac{\sum (Q_i - \hat{Q}_i)^2}{\sum (Q_i - \bar{Q}_i)^2} \dots \dots \dots (6-3)$$

where :

Q_i = observed data series

\hat{Q}_i = computed series

The per cent errors between observed and computed peak discharge, time to peak discharge and values for R^2 and E are given in Table 7.4 for all storm events.

Table 7.4 Error statistics between observed and computed hydrograph series.

EVENT	Peak flow (cumecs)			Time to peak (hour)			R^2	E
	Observed	Computed	% Error	Observed	Computed	% Error		
5.09.1962	135.920	133.868	1.510	6	6	0.00	0.918	0.902
30.08.1965	58.160	59.523	2.343	8	7	12.50	0.939	0.855
14.08.1964	124.590	124.119	0.378	10	10	0.00	0.933	0.926
7.09.1965	59.500	59.998	0.837	6	6	0.00	0.991	0.990
20.07.1964	214.930	213.881	0.488	8	7	12.50	0.971	0.969
23.7.1962	181.230	181.253	0.013	8	8	0.00	0.960	0.951
24.08.1961	185.990	313.703	68.667	8	7	12.50	0.740	0.730
	430.39	334.90	22.187	17	19	11.76		

In the storm event dated 5.09.1962, it was observed that the computed flow was above the observed flow up to the 5th hour, after 5th hour to peak was matching as compared to the observed flow hydrograph (Figure 7.11). The peak of the computed hydrograph was at 6th hour from the beginning of the storm whereas the observed peak was at the 6th hour from the beginning of the storm. The recession limb of the computed hydrograph was higher than the recession limb of the observed hydrograph until 12th hour and after 12th hour to 25th hour was lower than the recession limb of the observed hydrograph of the storm. The error of observed peak flow discharge with the computed peak flow discharge was 1.510%. Dimensionless coefficient (R^2) is 0.918 and Nash & Sutcliffe efficient (E) is 0.902, indicating good agreement between the observed and computed series.

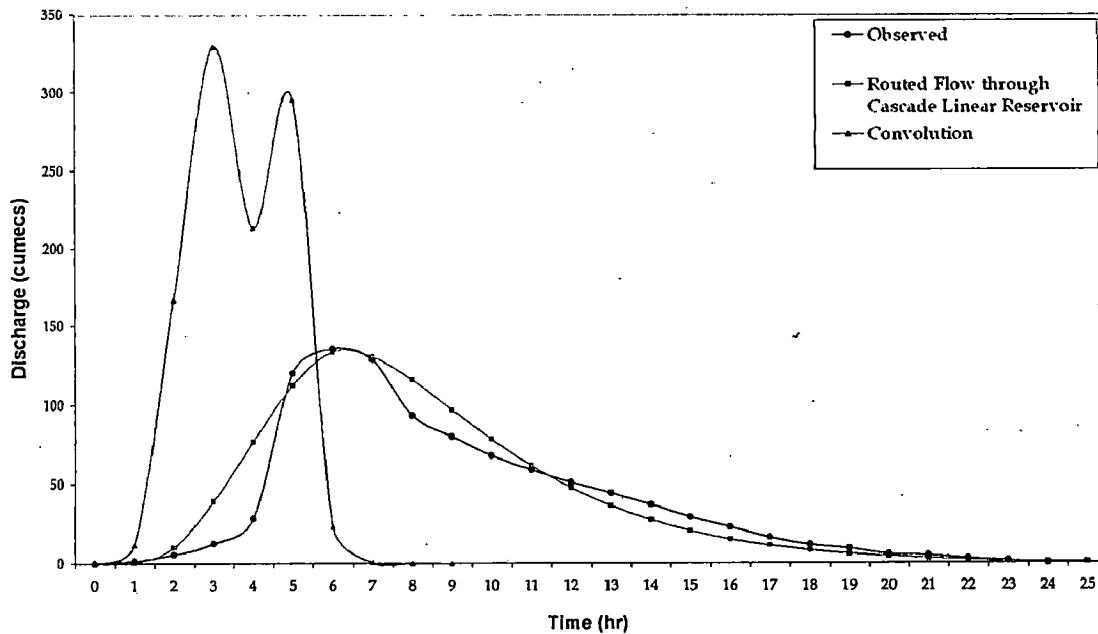


Figure 7.11 Runoff Hydrograph for Event 5.09.1962

In the storm event dated 30.08.1965, it was observed that the observed flow was not matching with the computed flow right from the beginning of the storm to its end (Figure 7.12). The peak of computed hydrograph was at the 7th hour from the beginning of the storm whereas the observed peak was at the 8th hour from the beginning of the storm. The error of observed peak flow discharge with the computed peak flow discharge was 2.343%. Dimensionless coefficient (R^2) is 0.939 and Nash & Sutcliffe efficient (E) is 0.855, for dimensionless coefficient is in good agreement however value of Nash & Sutcliffe efficient is lower compared to other events indicating fair match matching between observed and computed runoff hydrographs.

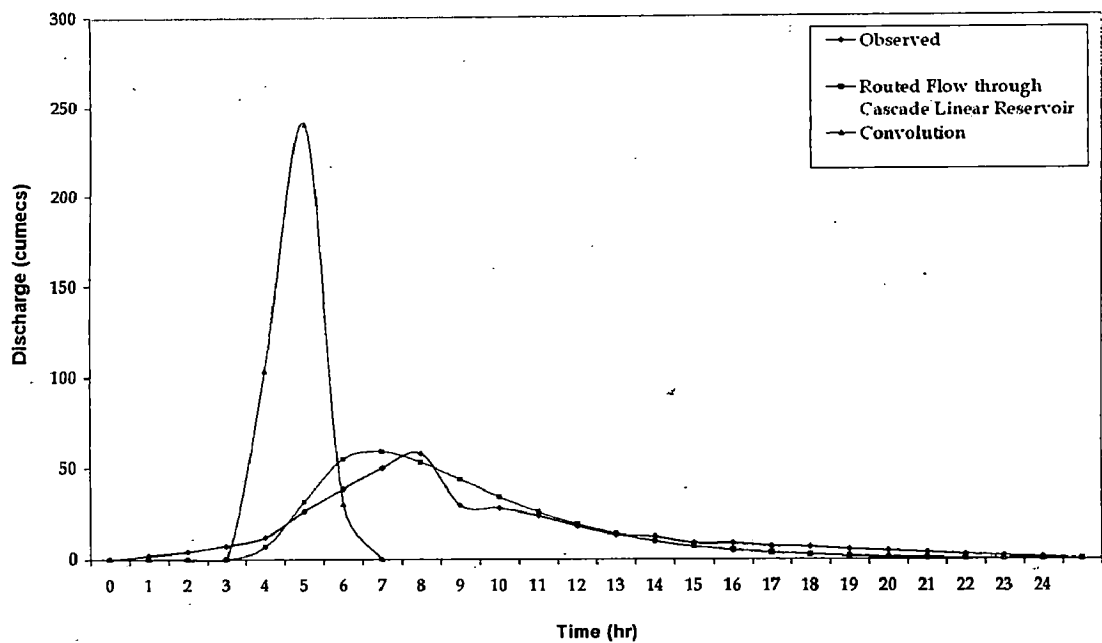


Figure 7.12 Runoff Hydrograph for Event 30.08.1965

In the storm event dated 14.08.1964, it was observed that the computed flow was above the observed flow up to the 10th hour from the beginning of the storm. The value of computed peak flow was little less than the observed peak flow (Figure 7.13). The peak of the computed hydrograph as well as observed peak was at the 10th hour from the beginning of the storm. The recession limb of the simulated hydrograph was matching with the recession limb of the observed hydrograph after the 34th hour from the beginning of the storm. The error of observed peak flow discharge with the computed peak flow discharge was 0.378%. Dimensionless coefficient (R^2) is 0.933 and Nash & Sutcliffe efficient (E) is 0.926, very good agreement between the observed and computed series.

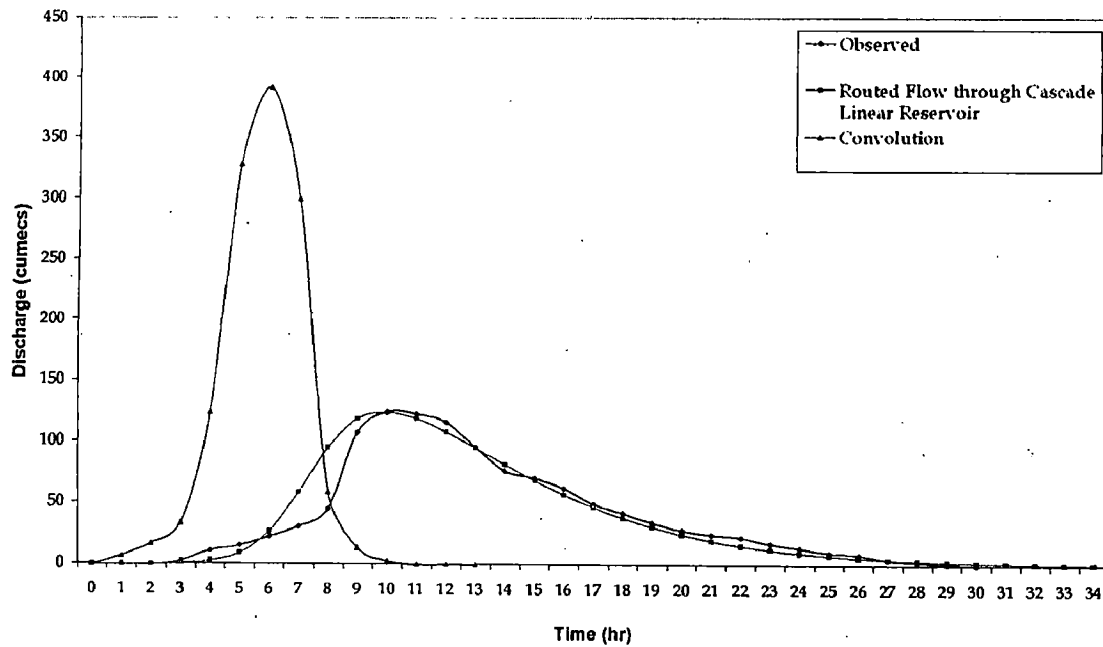


Figure 7.13 Runoff Hydrograph for Event 14.08.1964

In the storm event dated 7.09.1965, it was observed that the observed flow was little above the computed flow up to the 4th hour from the beginning of the storm. The value of computed peak flow was less than the observed peak flow (Figure 7.14). The peak of the computed hydrograph as well as observed peak was at the 6th hour from the beginning of the storm. The recession limb of the computed hydrograph was perfectly matching with the recession limb of the observed hydrograph after the 24th hour from the beginning of the storm. The error of observed peak flow discharge with the computed peak flow discharge was 0.837%. Dimensionless coefficient (R^2) is 0.991 and Nash & Sutcliffe efficient (E) is 0.990, indicating excellent agreement between the observed and computed series.

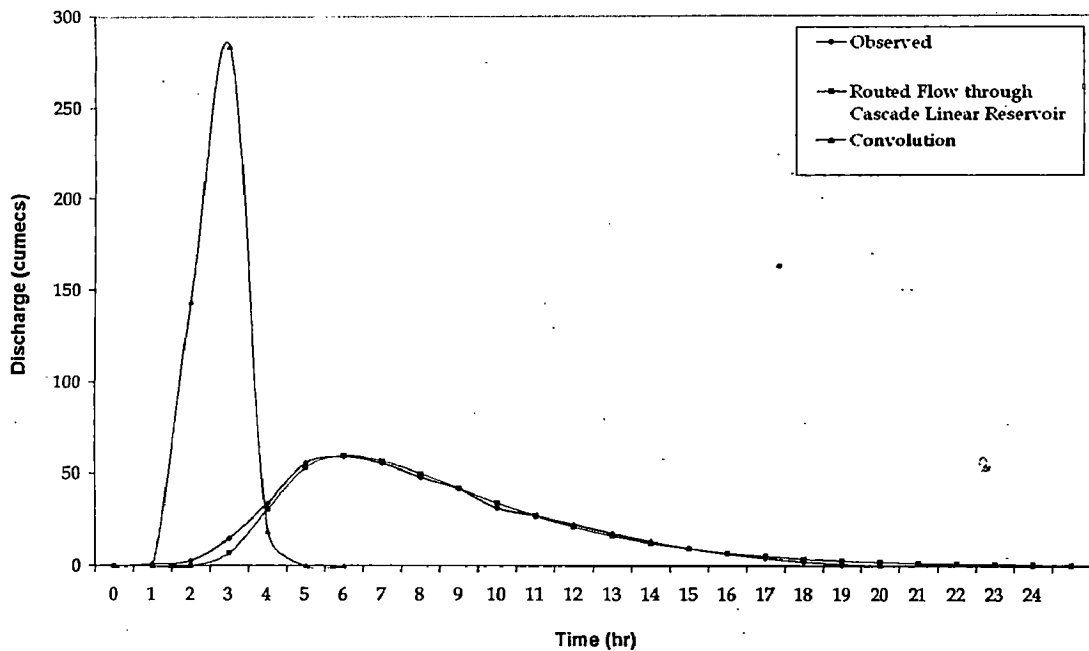


Figure 7.14 Runoff Hydrograph for Event 7.09.1965

In the storm event dated 20.07.1964, it was observed that the observed flow was below the computed flow from the beginning of the storm to 3th hour, was matching from 3th hour to 5th hour and was not matching at the peak of storm (Figure 7.15). The peak of computed hydrograph was at the 7th hour from the beginning of the storm whereas the observed peak was at the 8th hour from the beginning of the storm. The recession limb of the computed hydrograph was little higher than the recession limb of the observed hydrograph until 19th hour and after 19th hour to 28th hour was perfectly matching with the observed hydrograph of the storm. The error of observed peak flow discharge with the computed peak flow discharge was 0.488%. Dimensionless coefficient (R^2) is 0.971 and Nash & Sutcliffe efficient (E) is 0.969, indicating excellent agreement between the observed and computed series.

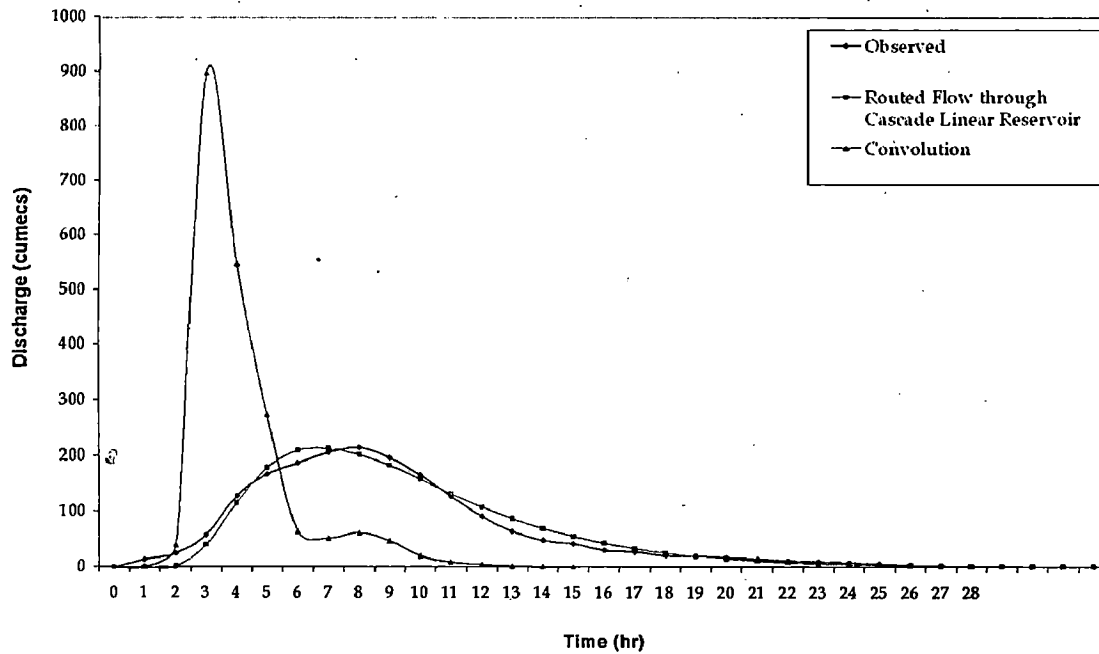


Figure 7.15 Runoff Hydrograph for Event 20.07.1964

In the storm event dated 23.7.1962, it was observed that the computed flow was not matching with the observed flow up to the peak of the storm. The value of computed peak flow was matching with the observed peak flow (Figure 7.16). The peak of the computed hydrograph was at the 8th hour from the beginning of the storm whereas the observed peak was at the 8th hour from the beginning storm. The recession limb of the computed hydrograph was little higher than the recession limb the observed hydrograph upto the 14th hour from the beginning of the storm. After 14th hour up to 26th hour from the beginning of the storm are matching. The error of observed peak flow discharge with the computed peak flow discharge was 0.013%. Dimensionless coefficient (R^2) is 0.960 and Nash & Sutcliffe efficient (E) is 0.951, indicating very good agreement between the observed and computed series.

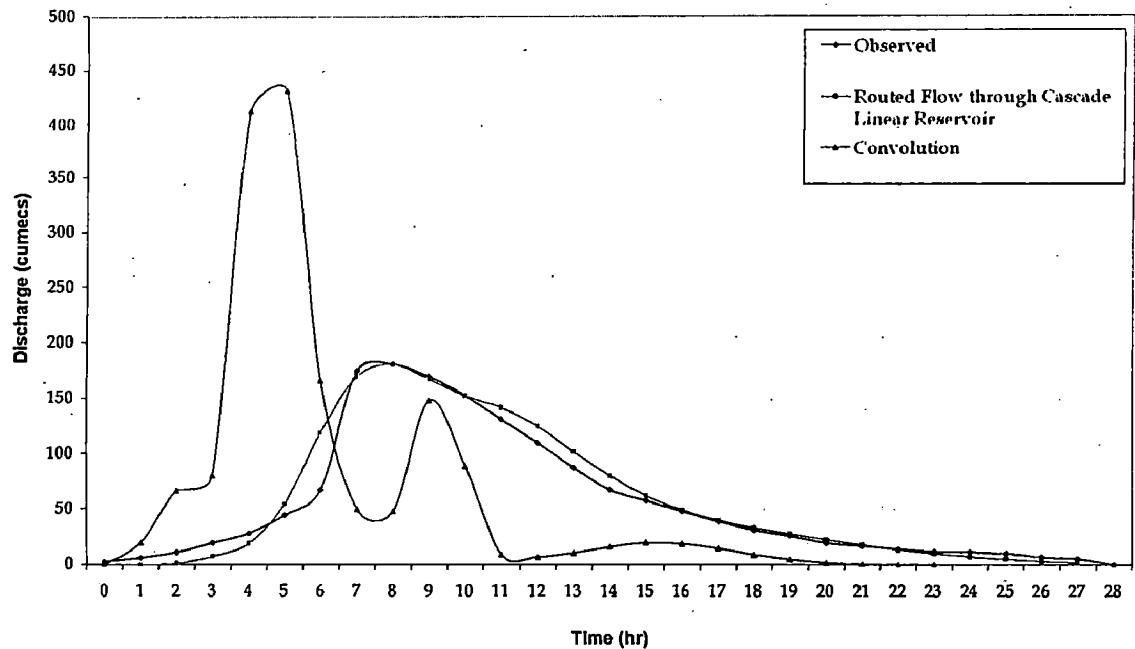


Figure 7.16 Runoff Hydrograph for Event 23.7.1962

In the storm event dated 24.08.1961, it was observed that the computed flow was not matching with the observed flow right from the beginning of the till to its end. The value computed peak flow was much higher than the observed peak flow at the first peak of the storm and at the second of the peak of the storm was not matching (Figure 7.17). The first peak of the computed hydrograph was at the 7th hour from the beginning of the storm whereas the observed peak was at the 8th hour from the beginning of the storm. The second peak of the computed hydrograph was at the 19th hour from the beginning of the storm whereas the observed peak was at the 17th hour from the beginning of the storm. The recession limb of the observed hydrograph was higher than the recession limb of the computed hydrograph up to the 50th from the beginning of storm. The error of observed first peak flow discharge with the computed peak flow discharge was 68.667% and the error of observed second peak flow discharge with the computed peak flow discharge was 22.187%. Dimensionless coefficient (R^2) is 0.740 and Nash & Sutcliffe efficient (E) is 0.730, indicating poorest agreement between the observed and computed series compared to all other storm events analyzed.

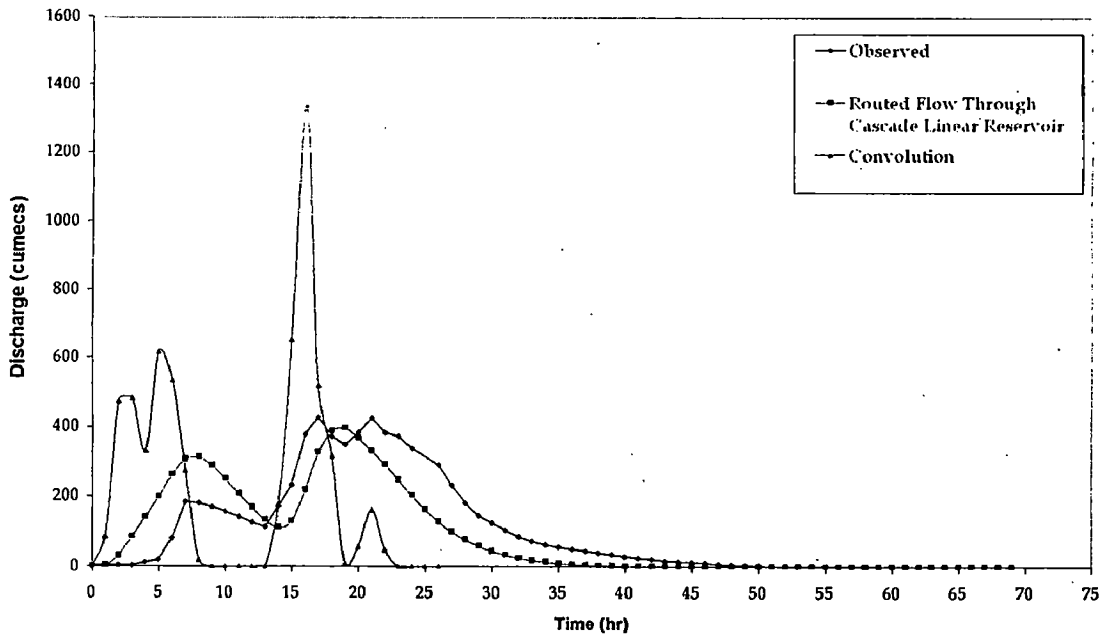


Figure 7.17 Runoff Hydrograph for Event 24.08.1961

Overall the matching of the observed hydrograph with the computed hydrograph was observed to be fair in the case of storm event dated 30.08.1965, good for storm event dated 5.09.1962, very good for storm event dated 14.08.1964 and 24.08.1961, excellent for storm event dated 7.09.1965 & 20.07.1964. However performance of the proposed method was rated as poor on storm event dated 24.08.1961. Excluding storm event dated 24.08.1961, the percentages of error in peak discharge varies from 0.01% to 2.343%; in time to peak discharge varies from 0 to 12.5%; R^2 varies from 0.918 to 0.991 and Nash & Sutcliffe efficient (E) from 0.855 to 0.990. For storm event dated 24.08.1961, the percentages of error in peak discharge 22.187 and 68.667%; in time to peak discharge 11.76 and 12.5%; R^2 0.740 and Nash & Sutcliffe efficient (E) 0.730 which may be attributed to uncertainty in observations or complex nature of storm event. Overall the proposed method is rated as very good for Temur catchment which exert substantial amount of storage induced diffusion effects on runoff hydrographs due to flatter topography in middle to southern part of the catchment.

CHAPTER 8

CONCLUSIONS

Based on the present investigation, the following conclusions can be drawn:

1. Remote sensing techniques are useful in deriving spatial information of a catchment such as landuse and subsequent information such as Manning's n.
2. Present study derives spatially distributed unit hydrograph using the isochrones varying in time with rainfall intensity, overcoming the stationary constraint of unit hydrograph concept.
3. The derived relationship between time of concentration and excess rainfall intensity can be utilized to derive time area hyetograph (TAH) associated with any other value of excess intensity (E2), by scaling the time axis with the ratio of $(E2/E1)^{-0.4}$ without performing elaborate computations of travel time for each rainfall excess block if the excess rainfall is assumed as constant in space. The multiplicand (=96.02) represents watershed hydro-geomorphologic index conglomerating spatially distributed characteristics such as surface roughness, slope, flow length, flow accumulation, drainage pattern and channel geometry.
4. With decrease of 10% in value of Manning's coefficient results in decrease in value of average time of concentration by 5.87% and decrease of 20% in value of Manning's coefficient, value of average time of concentration decrease by 12.35%. Similarly with increase of 10% in value of Manning's coefficient, increase in value of average time of concentration 5.99% and with increase of 20% in value of Manning's coefficient, value of average time of concentration 11.79%. The results obtained show that increase or decrease in time of concentration is also influenced by rainfall intensity.
5. Introduction of two reservoirs in series to account for catchment induced storage effects on runoff hydrograph has significantly improved the model computed results indicating use of simple kinematic wave derived travel time histogram for derivation

of unit hydrograph is not sufficient for mid-sized catchment exhibiting storage induced diffusion.

6. The storage coefficients (K) in general decrease with increase in value of rainfall excess. It implies that rainfall intensity plays a significant role in influencing the catchment storage induced diffusion on resultant runoff hydrograph.
7. The matching of the observed hydrograph with the computed hydrograph was observed to be fair in the case of storm event dated 30.08.1965, good for storm event dated 5.09.1962, very good for storm event dated 14.08.1964 and 24.08.1961, excellent for storm event dated 7.09.1965 & 20.07.1964. However performance of the proposed method was rated as poor on storm event dated 24.08.1961 which may be attributed to uncertainty in observations and complex nature of this storm event. Excluding storm event dated 24.08.1961, the percentages of error in peak discharge varies from 0.01% to 2.343%; in time to peak discharge varies from 0 to 12.5%; R^2 varies from 0.918 to 0.991 and Nash-Sutcliffe efficiency (E) from 0.855 to 0.990.
8. The overall very high values of R^2 and Nash-Sutcliffe efficiency for all but one event indicate suitability of the proposed method for Temur catchment which exert substantial amount of storage-induced diffusion effects on runoff hydrographs due to flatter topography in the middle to southern part of the catchment.

REFERENCES

1. Agiralioglu, N., (1984). Effect of catchment geometry on time of concentration. Proc. 3rd Int. Conf. on Urban Storm Drainage, Grteborg, Sweden, Vol. 1, pp. 177-184.
2. Agiralioglu, N., (1988). Estimation of the time of concentration for diverging surfaces. J. Hydrol. Sei., Vol. 33(2), pp. 173-179.
3. Ajward, M.H., (1996). A spatially distributed unit hydrograph model using a geographical information system. Ph.D. diss. Civil Engineering Dept., University of Calgary, Calgary.
4. Akan, A.O., (1986). Time of concentration of overland flow. J. Irrig. Drain. Eng. ASCE, Vol. 112(4), pp. 283-292.
5. Akan, A.O., (1988). Overland flow on pervious, converging surface. Nord. Hydrol., Vol. 19, pp. 153-164.
6. Bedient, P.B. and Huber, W.C. (1992). Hydrology and Floodplain Analysis. 2nd edition. Addison-Wesley Publishing Company, New York.
7. Ben-Zvi, A., (1984). Runoff peaks from two-dimensional laboratory watersheds. J. Hydrol., Vol. 69, pp. 115-139.
8. Chang, Kang-tsung (2002). Geographic Information Systems. Tata McGraw Hill Book Company, New Delhi.
9. Chow, V.T., Maidment, D.R. and Mays, L.W., (1988). Applied Hydrology, Mc Graw Hill Book Company, New York.
10. Clark, C.O., (1945). Storage and the unit hydrograph. Trans. Am. Soc. Civil Engg., Vol. 110, pp. 1419-1446.
11. Curran, P.J., (1987), Remote Sensing Methodologies and Geography. International Journal of Remote Sensing, Vol. 8, pp. 1255-1275.
12. DeMers, M.N., (2000). Fundamental of Geographical Information Systems. 2ⁿ ed, John Wiley & Sons, New York.
13. Dickinson, W.T., Holland, M.E., and Smith, G.L., (1967). An experimental rainfall-runoff facility. Colo. State Univ. Fort Collins, Hydrol. Pap. 25.
14. Dooge, J.C.I., (1959). A general theory of the unit hydrograph. J. Geophys. Res, 64, pp 241-256.
15. Drayton, R.S., Wilde, B.M., and Harris, J.K., (1992). Geographical information system approach to distributed modeling. Hydrological Processes Vol. 6(3), pp. 36:-368.

16. Golany, P., and Larson, C.L., (1971). Effects of channel characteristics on time parameters for small watershed runoff hydrographs. Water Resources Research Center, Bull. 31, University of Minnesota, Minneapolis.
17. Gorte, B., (1998). Probabilistic Segmentation of Remotely Sensed Images. ITC publication nr 63. ITC, Enschede. 143 pp.
18. Gray, D. M., (1973). Handbook on the Principles of Hydrology". Water Information Center, Inc, New York.
19. Haan, C.T., Barfield, B.J., and Hayes, J.C., (1994). Design Hydrology and Sedimentology for Small Catchments. Academic Press, Inc., pp. 38.
20. Henderson, F.M., and Wooding, R.A., (1964). Overland flow and groundwater flow from a steady rainfall of finite duration. J. Geophys. Res., Vol. 69(8), pp. 1531-1540.
21. Hengl, T., Gruber, S., and Shrestha, D.P., (2003). Digital terrain Analysis in ILWIS, Lecture Note and User Guide. ILWIS Department, International Institute for Aerospace Survey & Earth Sciences Enschede, Netherland.
22. Hjelmfelt, A.T., (1978). Influence of infiltration on overland flow. J. Hydrol., Vol. 36, pp. 179-185.
23. Huggins, L.F., and Burney, J.R., (1982). Surface runoff, storage, and routing in Hydrologic Modeling of Small Watersheds, eds. C. T. Haan, H. P. Johnson, D. L. Brakensiek, ch. 5, 169-225. St. Joseph, Mich.: ASAE.
24. ITC (1997). User's guide for ILWIS 2.1 for Windows, The Integrated Land and Water Information System. ILWIS Departement, International Institute for Aerospace Survey & Earth Sciences Enschede, Netherland.
25. Jain, M.K., and Seth, S.M., (1997). Rainfall-Runoff Modelling of a Himalayan catchment using a Distributed Approach. Institution of Engineers (India) Journal, Vol. 78, pp. 89 – 92.
26. Jain, M.K., Kothyari, U.C., and Rangga Raju, K.G., (2002). Estimation of Temporal Variation of Sediment Yield using GIS. J. Hydrology, Vol 47, pp. 693-706.
27. Jensen, J.R., (1996). Introductory Digital Image Processing: A remote sensing perspective, 2nd Edition. NJ: Prentice-Hall.
28. Jensen, John R., (2002). Remote Sensing of The Environment an Earth Resources Prespective. Prentice Hall A Division of Simon & Schuster Englewood Clift, New Jersey.
29. Julien, P.Y., and Moglen, G.E., (1990). Similarity and length scale for spatially varied overland flow. Water Resour. Res., Vol. 26(8), pp. 1819-1832.
30. Kilgore, Jennifer Leigh (1997). Development and Evaluation of a GIS-Based Spatially Distributed Unit Hydrograph Model. Thesis submitted to the Faculty of the Virginia Polytechnic Institute and State University, Virginia.

31. Larson, C.L., (1965). A two-phase approach to prediction of peak rates and frequencies of runoff for small ungaged watersheds. Stanford Univ. Dep. Civ. Eng. Tech. Rep. 53.
32. Lighthill, M.J., and Whitham, G.B., (1955). Kinematic waves 1. Proc. R. Soc. London, Ser. A, Vol. 229, pp. 281-316.
33. Linsley, R.K., Kohler, M.A., and Paulhus, J.H., (1975). Hydrology for Engineers. New York: McGraw Hill Book Company.
34. Logicon Geodynamics, Inc., (1997). Multispectral Imagery Reference Guide. VA: Logicon Geodynamics, Inc.
35. Machmeier, R.E., and Larson, C.L., (1968). Runoff hydrographs for mathematical watershed model. J. Hydraul. Div. ASCE, Vol. 94(6), pp. 1453-1474.
36. Maidment, D.R., (1993). Developing a spatially distributed unit hydrograph by using GIS. In Kovar, K. and Nachnehel, H. *Eds), Application of Geographic Information System in Hydrology and water Resources Management. IASH Publ.. Vol. 211. p: 181-192.
37. Maidment, D.R., Olivera, F., Calver, A., and Eartheral, A., (1996). Unit hydrograph derived from spatially distributed velocity field. Hydrological Processes, Vol. 10, pp. 831 – 844.
38. McDonnell, R.A., (1996). Including the spatial dimension: Using geographical information systems in hydrology. Prog. Physical Geography Vol. 20(2), pp. 159-177.
39. Muzik, I., (1995). GIS derived distributed unit hydrograph, a new tool for flood modeling. In Developments in Computer Aided Design and Modeling for Civil Engineering, ed. B. H. V. Topping, 243-247. Edinburgh, UK: Civil-Comp Press.
40. Muzik, I., (1996). Flood modeling with GIS-derived distributed unit hydrographs. Hydrological Processes, Vol. 10, pp 1401-1409.
41. O'Callaghan. J.K., Mark, D.M., (1984). The extraction of drainage networks from digital elevation data. Compute, Vision, Graphics, and Image Process, Vol. 28, pp. 323-344.
42. Ogden, F.L., and Julien, P.Y., (1993). Runoff sensitivity to temporal and spatial rainfall variability at runoff plane and small basin scales. Water Resour. Res., Vol. 29(8), pp. 2589-2597.
43. Olivaera, F. and Maidment, D.R., (1999). Geographic Information Systems (GIS) based spatially distributed model for runoff routing. Water Resources Research, Vol. 35 (4), pp .1155-1164.
44. Ponce, Victor Miquel, (1989). Engineering Hydrology Principles and Practice. Prentice Hall A Division of Simon & Schuster Englewood Clifft, New Jersey.

45. Ramirez, Jorge A., (2000). Prediction and Modeling of Flood Hydrology and Hydraulics. Chapter 11 of *Inland Flood Hazards: Human, Riparian and aquatic Communities* Eds. Ellen Wohl. Cambridge University Press, Colorado.
46. Rodriguez-Iturbe, I., and Valdes, J.B., (1979). The geomorphological structure of hydrologic response. *Water Resources Res.* Vol. 15(6), pp. 1409-1420.
47. Saghafian, B., (1992). Hydrologic analysis of watershed response to spatially varied infiltration. Ph.D. Dissertation, Civil Engineering Department, Colorado State University, Fort Collins.
48. Saghafian, B., and Julien, P.Y., (1995). Time to Equilibrium for Spatially Variable Watersheds. *Journal of Hydrology*, Elsevier Science, Vol. 172, 231 – 245.
49. Saghafian, B., Julien, P.Y., and Rajaie, H., (2002). Runoff Hydrograph Simulation Based on Time Variable Isochrone Technique. *Journal of Hydrology*, Elsevier Science, Vol. 261, pp. 193 - 203.
50. Schaake, J.C., (1965). Synthesis of the inlet hydrograph. Ph.D. Dissertation, Department of Sanitary Engineering and Water Resources, The Johns Hopkins University, Baltimore, MD.
51. Sherman, L.K., (1932). Streamflow from rainfall by the unit-graph method. *Eng. NewsRecord* Vol 108, pp. 501-5
52. Singh, Vijay P., (1988). *Rainfall-Runoff Modelling, Volume I*. Prentice Hall A Division of Simon & Schuster Englewood Clifft, New Jersey.
53. Singh, Vijay P., (1988). *Watershed Modelling, Volume II*. Prentice Hall A Division of Simon & Schuster Englewood Clifft, New Jersey.
54. Todini, E., (1988). Rainfall-runoff Modeling – Past, Present and Future, *Journal of Hydrology*, Vol .100, pp. 341-352.
55. Wooding, R.A., (1965a). A hydraulic model for the catchment-stream problem, I. Kinematic-wave theory. *J. Hydrol.*, Vol. 3, pp. 254-267.
56. Wooding, R.A., (1965b). A hydraulic model for the catchment-stream problem, II. Numerical solutions. *J. Hydrol.*, 3: 268-282.
57. Wooding, R.A., (1966). A hydraulic model for the catchment-stream problem, III. Comparison with runoff observations. *J. Hydrol.*, Vol. 4, pp. 21-37.
58. Woolhiser, D.A., (1969). Overland flow on a converging surface. *Trans. ASAE*, Vol 12(4), pp. 460-462.

APPENDIX A-1

CALCULATION OF RAINFALL EXCESS

EVENT 1

Rainfall (cm)	Phi Index	Rainfall Excess (cm)
0.3	0.205	0.10
0.49	0.205	0.29
0.11	0.205	0
0.5	0.205	0.30
0	0.205	0
0.13	0.205	0
0.13	0.205	0
Total Rainfall Excess =		0.675
Depth Surface Runoff =		0.675

EVENT 2

Rainfall (cm)	Phi Index	Rainfall Excess (cm)
0.27	1.252	0
0.33	1.252	0
0.52	1.252	0
0	1.252	0
0.2	1.252	0
1.51	1.252	0.26
0.45	1.252	0
0.26	1.252	0
Total Rainfall Excess =		0.258
Depth Surface Runoff =		0.258

EVENT 3

Rainfall (cm)	Phi Index	Rainfall Excess (cm)
0.17	0.200	0
0.27	0.200	0.07
0.14	0.200	0
0.26	0.200	0.06
0.41	0.200	0.21
0.43	0.200	0.23
0.44	0.200	0.24
0.13	0.200	0
0.15	0.200	0
0.11	0.200	0
0.08	0.200	0
Total Rainfall Excess =		0.810
Depth Surface Runoff =		0.810

EVENT 4

Rainfall (cm)	Phi Index	Rainfall Excess (cm)
0.13	0.379	0
0.2	0.379	0
0.69	0.379	0.31
0.23	0.379	0
0.02	0.379	0
0.02	0.379	0
Total Rainfall Excess =		0.311
Depth Surface Runoff =		0.311

EVENT 5

Rainfall (cm)	Phi Index	Rainfall Excess (cm)
0.33	0.297	0.03
0.46	0.297	0.16
1.08	0.297	0.78
0.56	0.297	0.26
0.38	0.297	0.08
0.09	0.297	0
0.03	0.297	0
Total Rainfall Excess =		1.326
Depth Surface Runoff =		1.326

EVENT 6

Rainfall (cm)	Phi Index	Rainfall Excess (cm)
0.17	0.167	0
0.29	0.167	0.12
0.13	0.167	0
0.14	0.167	0
0.68	0.167	0.51
0.36	0.167	0.19
0.05	0.167	0
0.06	0.167	0
0.37	0.167	0.20
0.05	0.167	0
0.21	0.167	0.04
0.15	0.167	0
0.07	0.167	0
Total Rainfall Excess =		1.081
Depth Surface Runoff =		1.081

EVENT 7

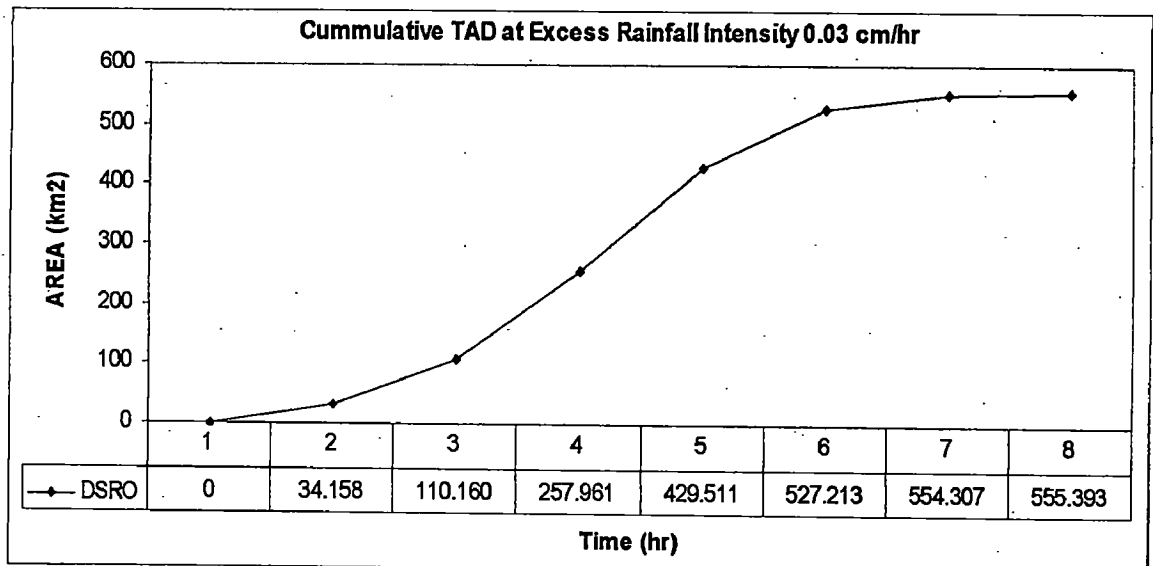
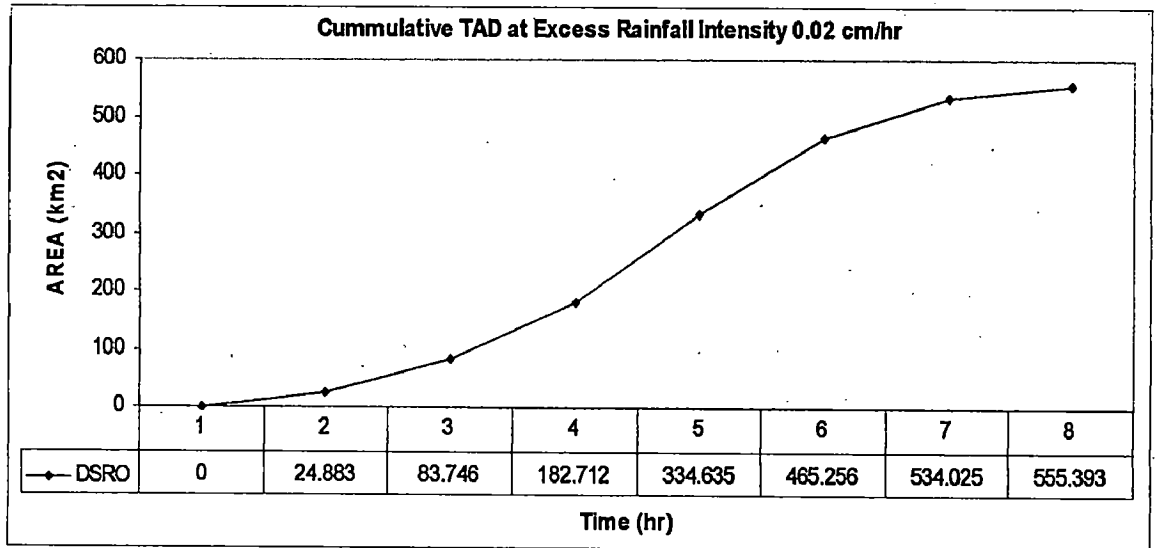
Rainfall (cm)	Phi Index	Rainfall Excess (cm)
0.33	0.078	0.25
0.50	0.078	0.42
0.35	0.078	0.27
0.32	0.078	0.24
0.62	0.078	0.54
0.38	0.078	0.30
0.09	0.078	0
0.01	0.078	0
0.00	0.078	0
0.00	0.078	0
0.00	0.078	0
0.04	0.078	0

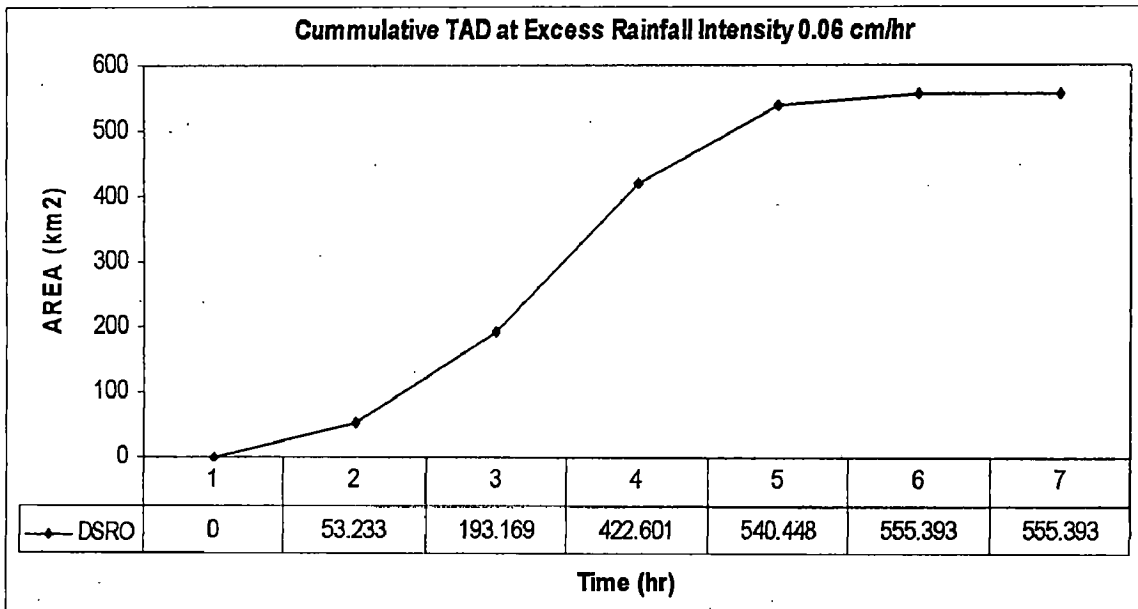
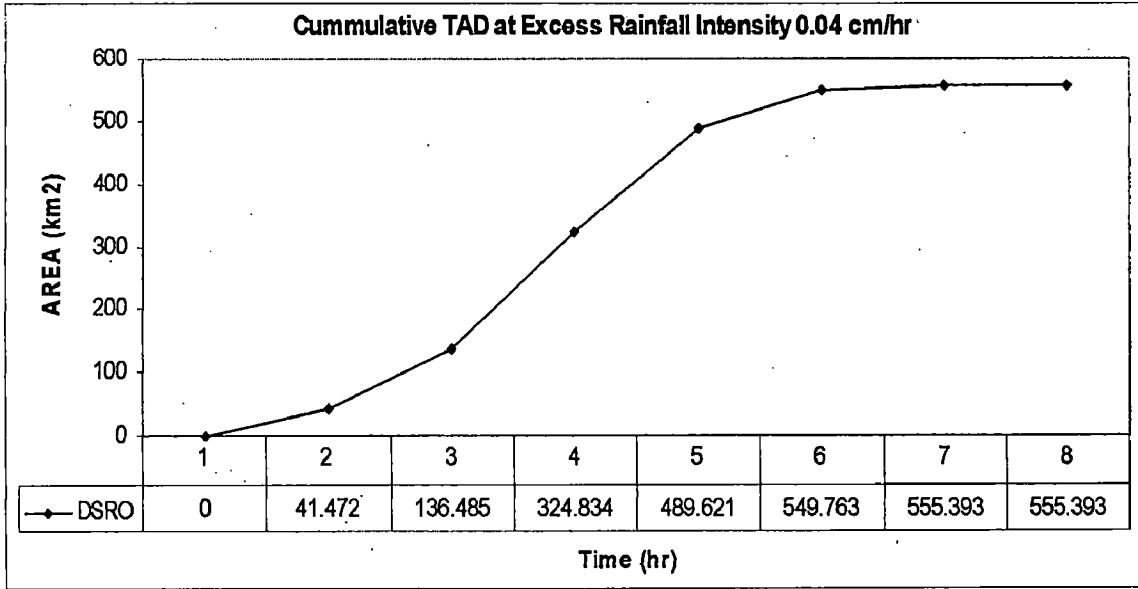
EVENT 7

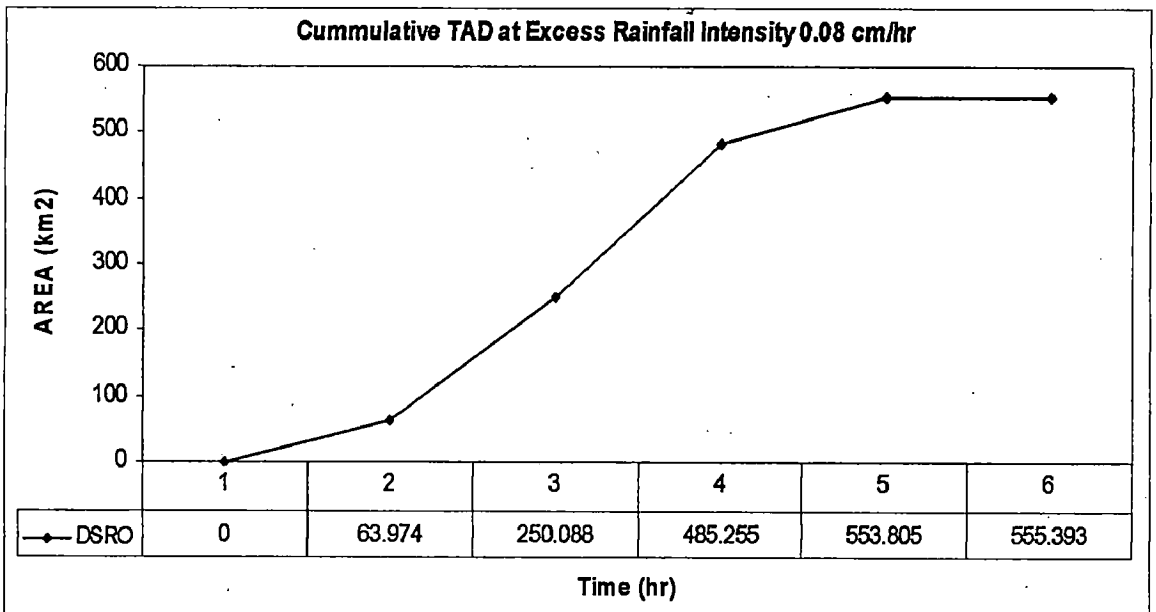
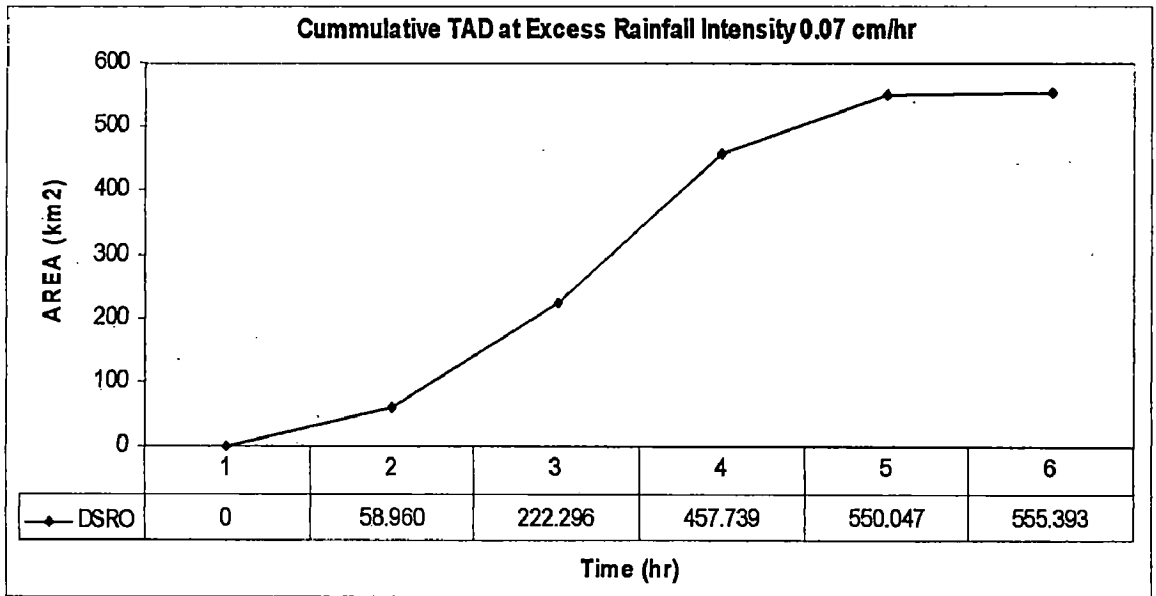
Rainfall (cm)	Phi Index	Rainfall Excess (cm)
0.07	0.078	0
0.43	0.078	0.35
0.56	0.078	0.48
1.10	0.078	1.02
0.46	0.078	0.38
0.17	0.078	0
0.16	0.078	0
0.27	0.078	0.19
0.19	0.078	0
Total Rainfall Excess =		4.759
Depth Surface Runoff =		4.759

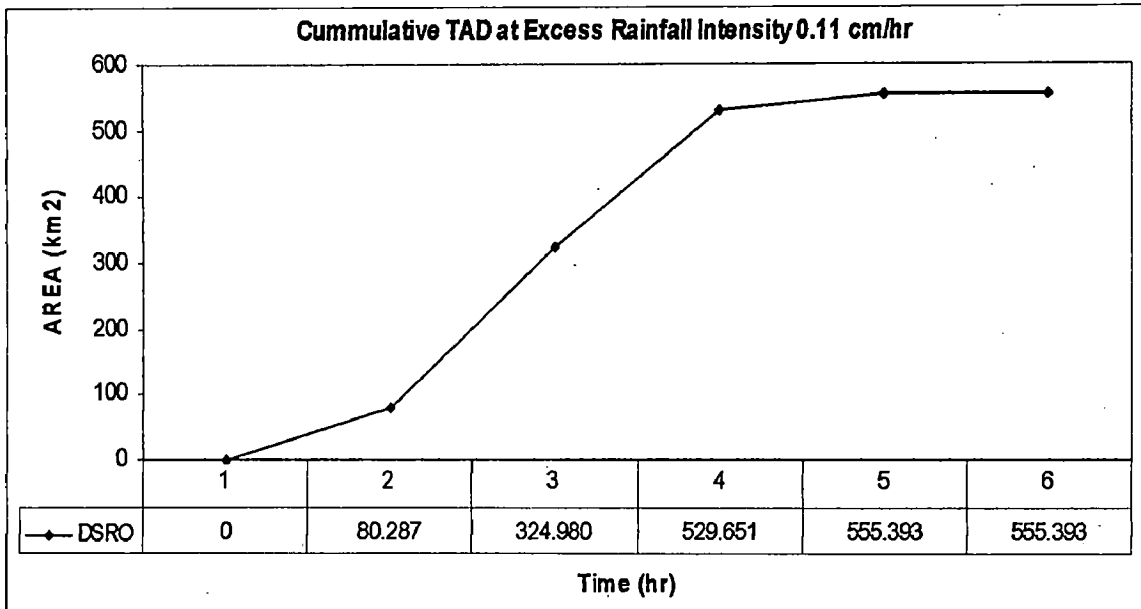
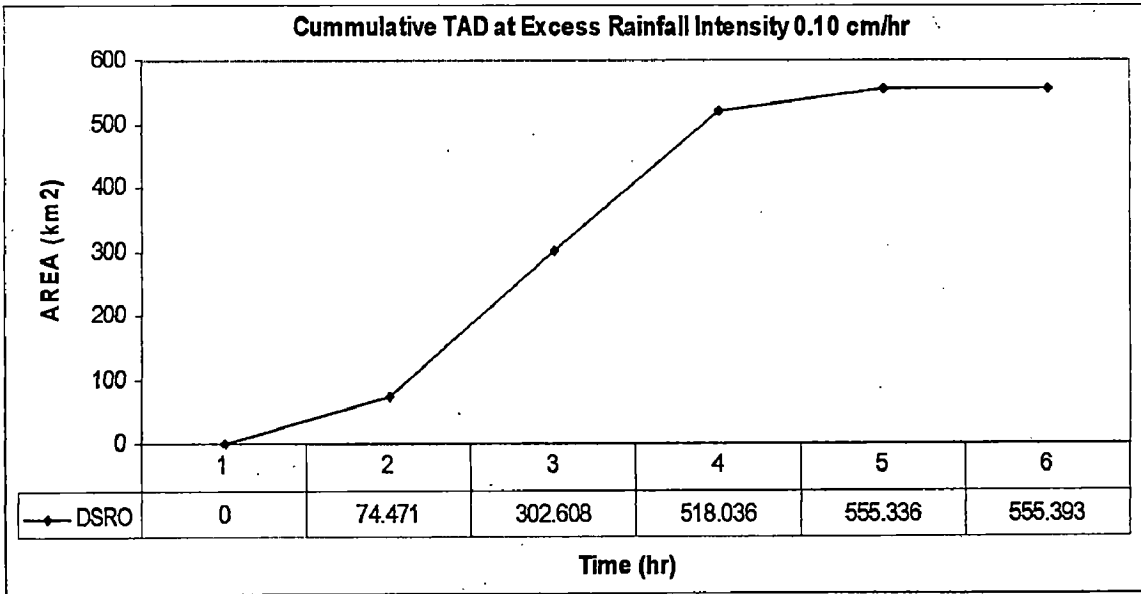
APPENDIX A-2

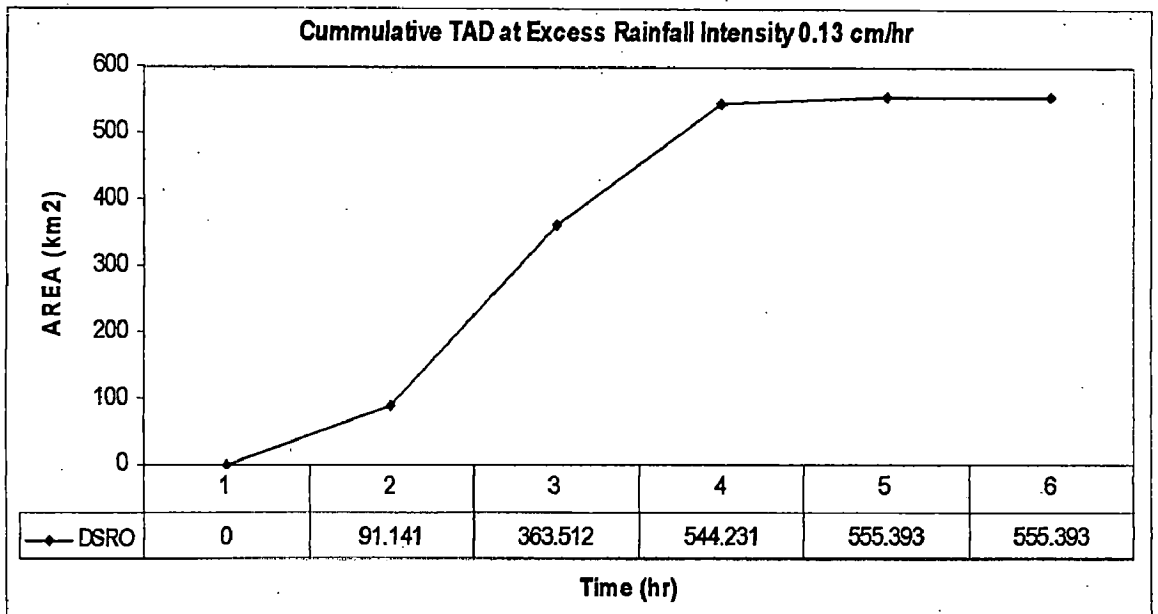
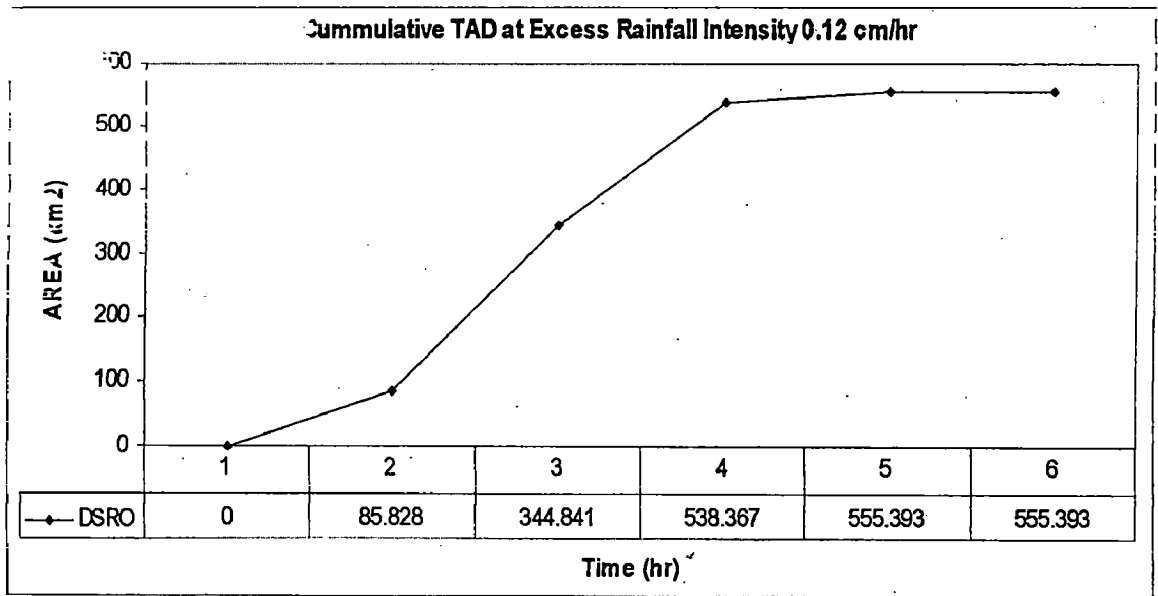
GRAPH OF S-HYDROGRAPH FOR EVERY RAINFALL EXCESS INTENCITY



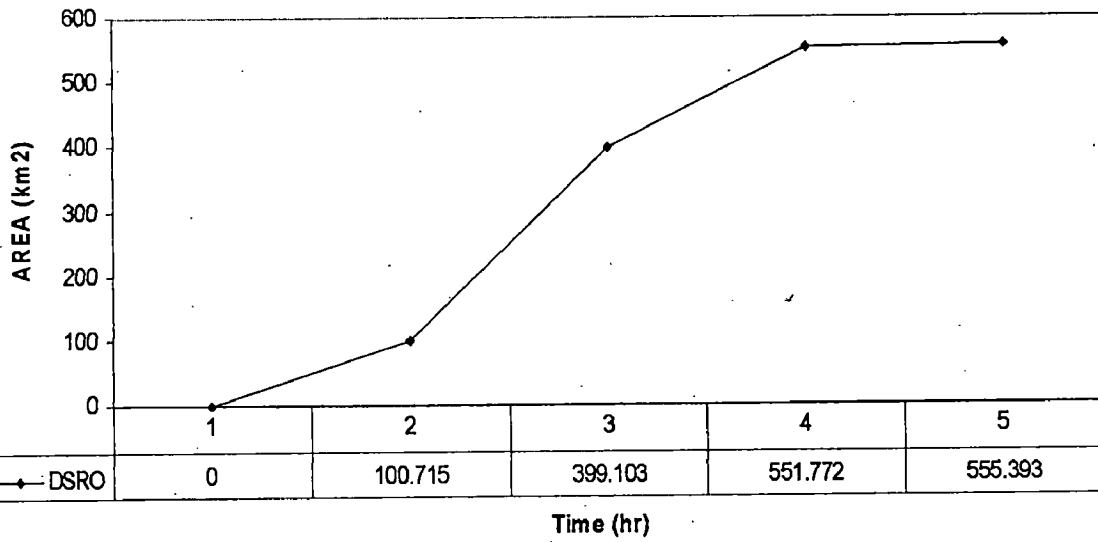




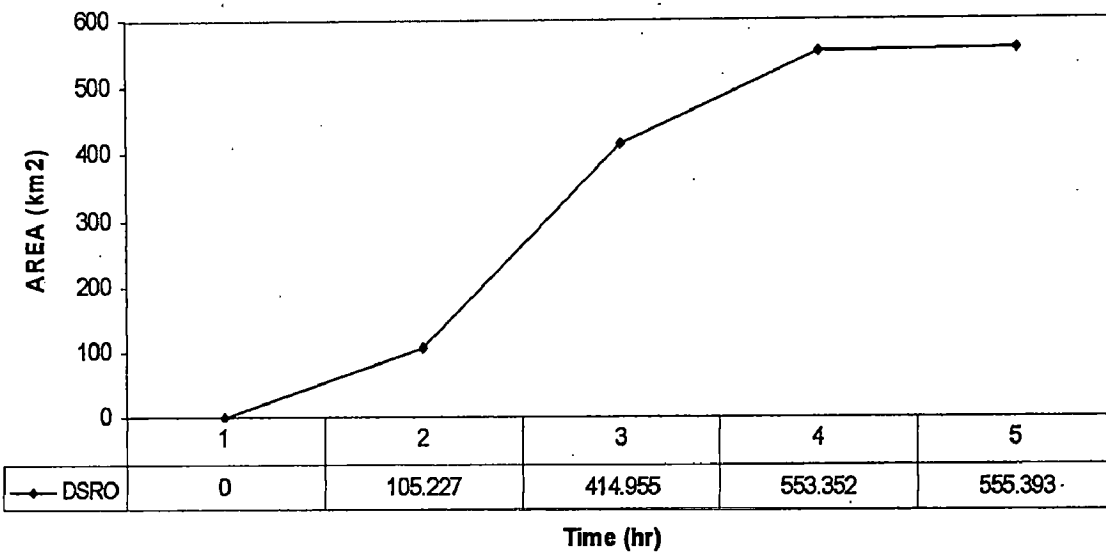


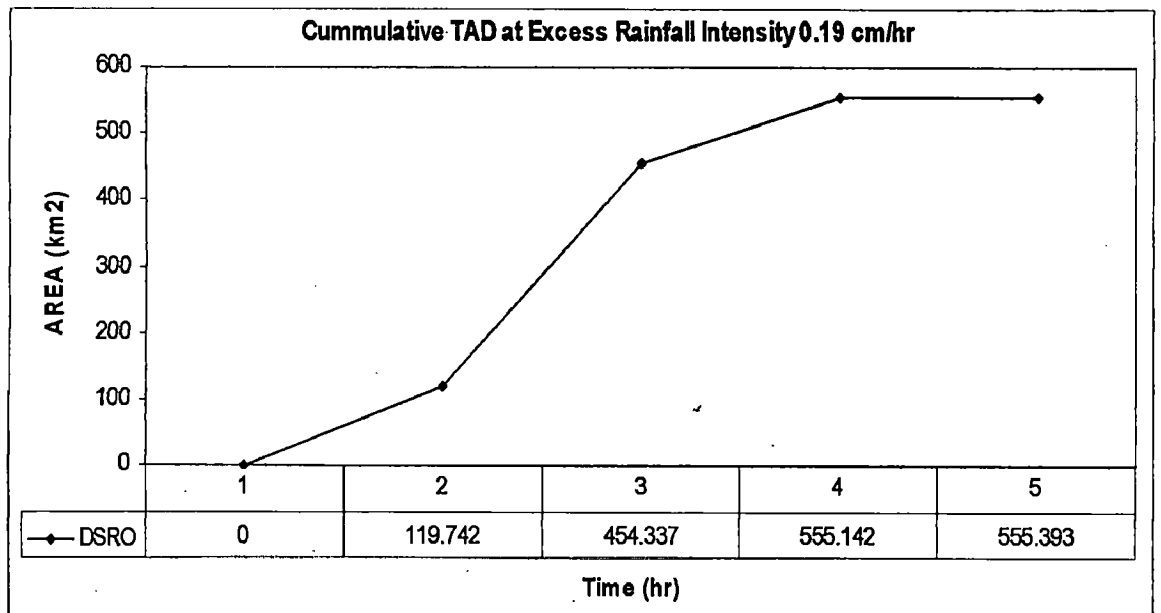
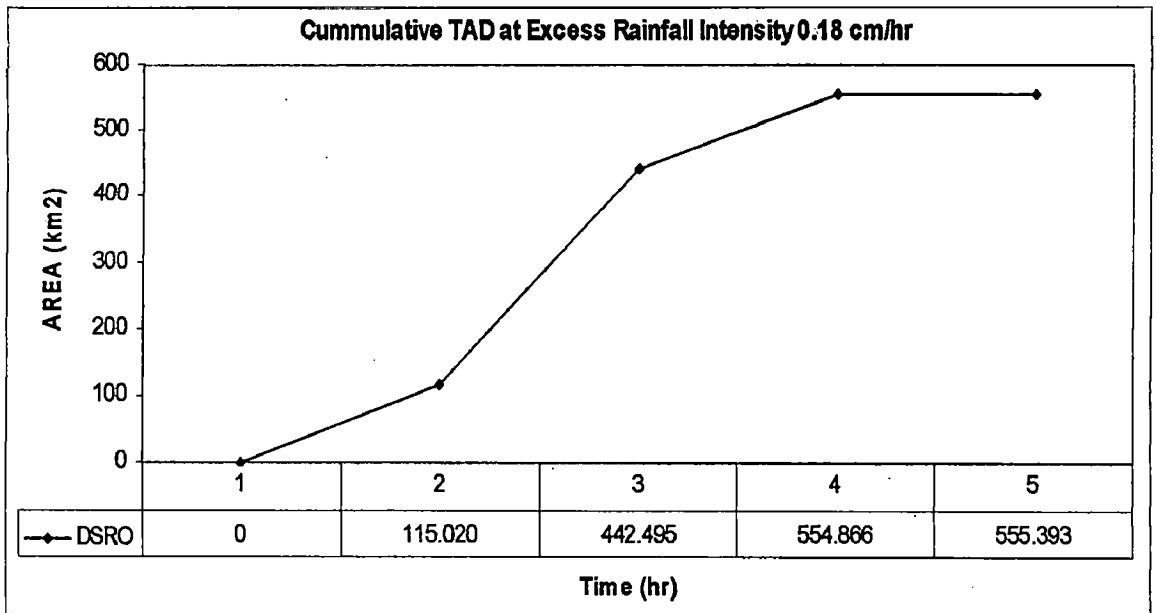


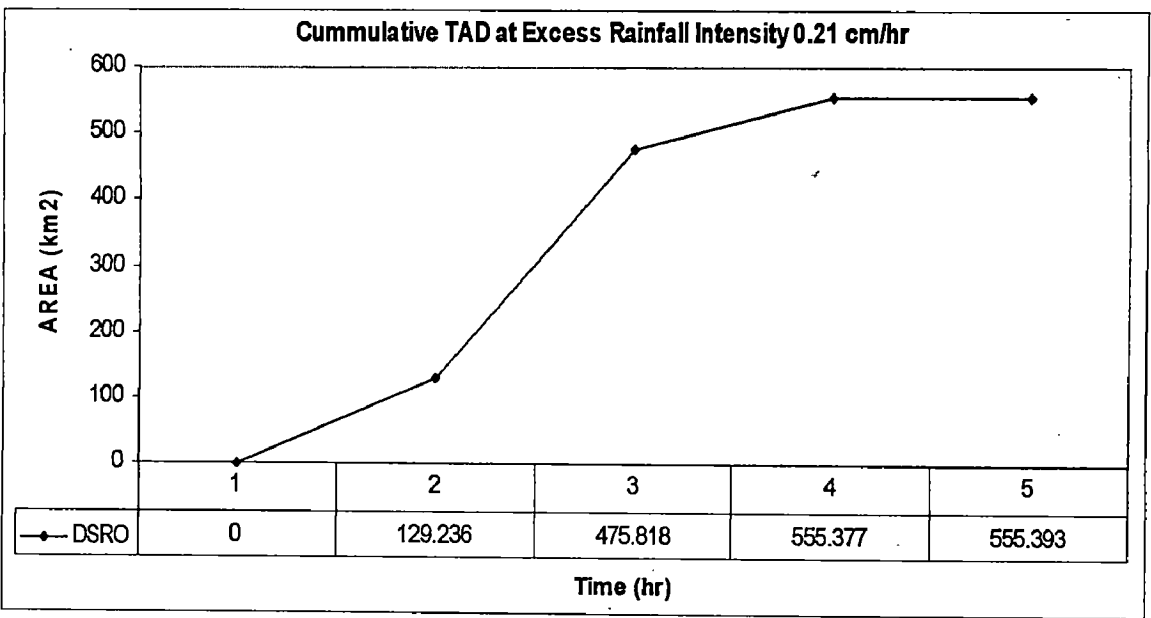
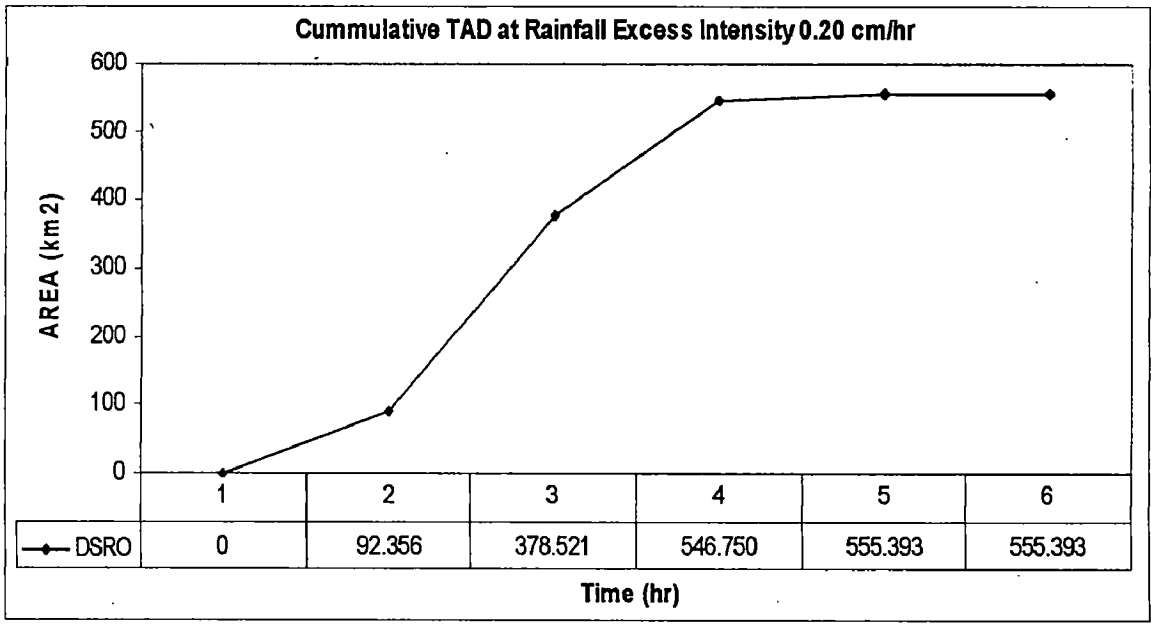
Cummulative TAD at Excess Rainfall Intensity 0.15 cm/hr

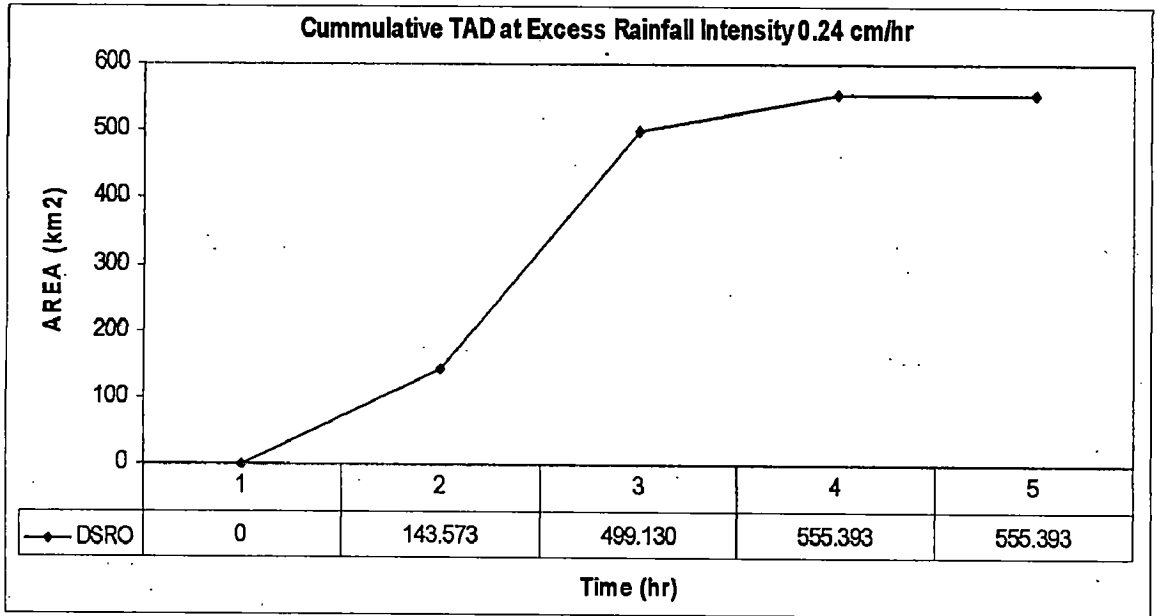
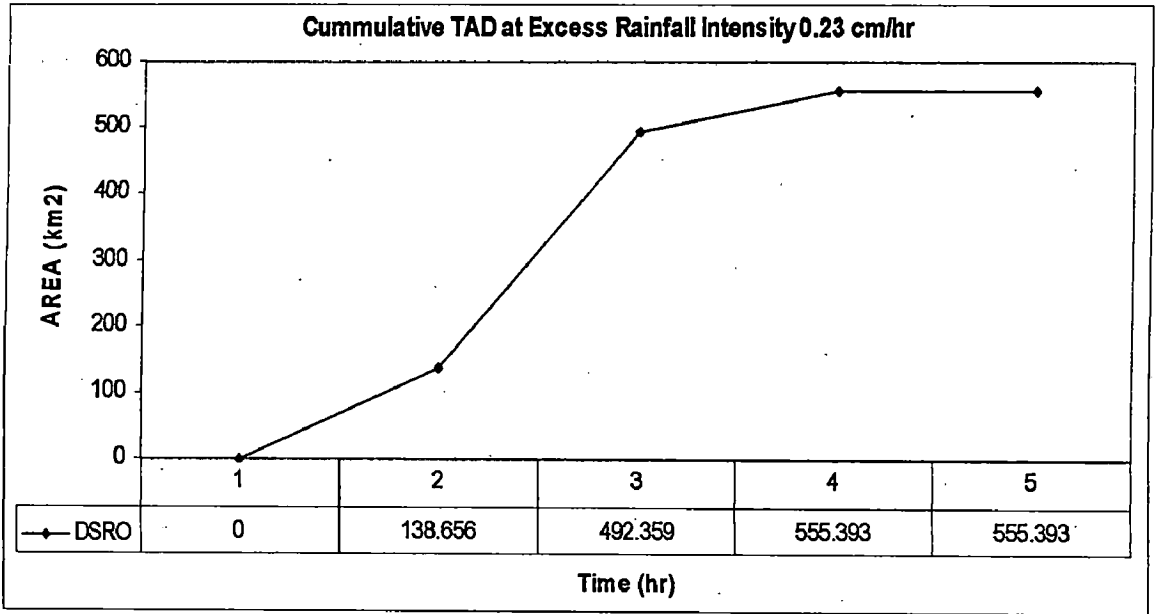


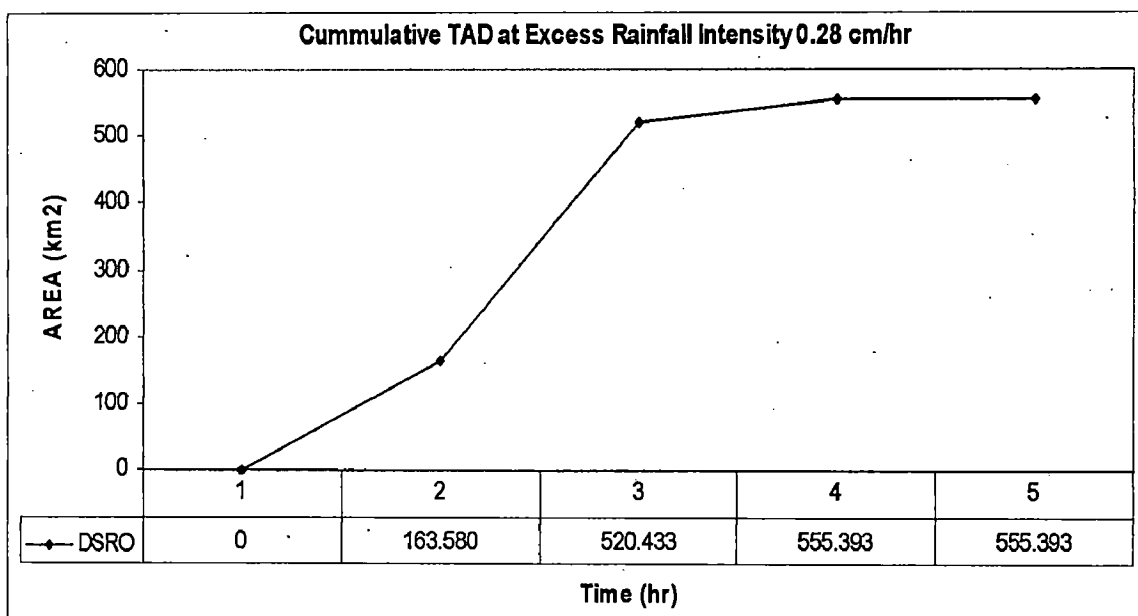
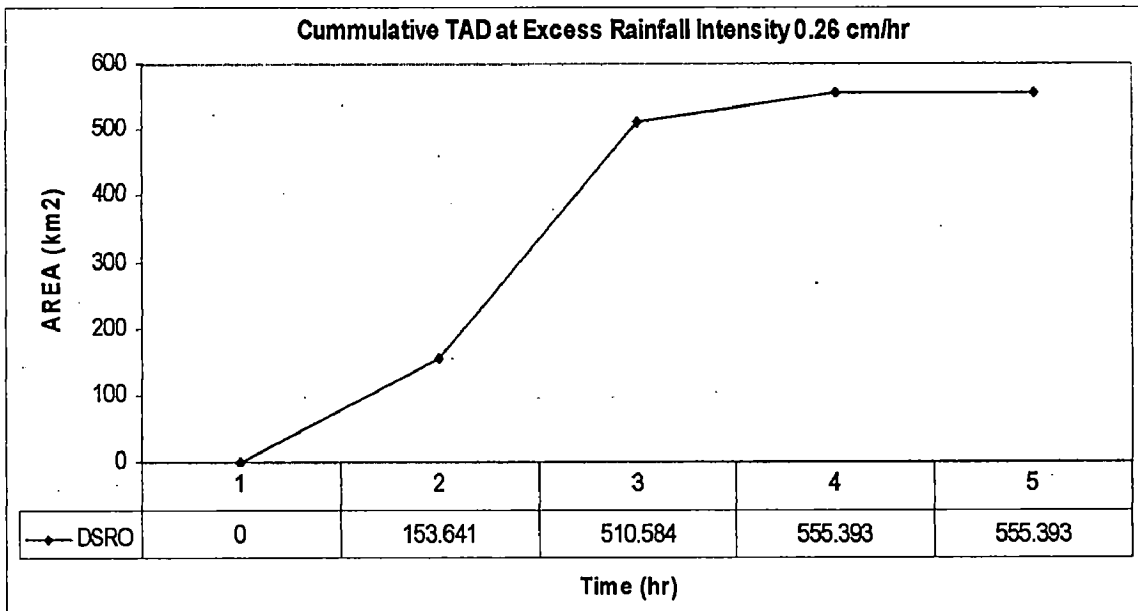
Cummulative TAD at Excess Rainfall Intensity 0.16 cm/hr

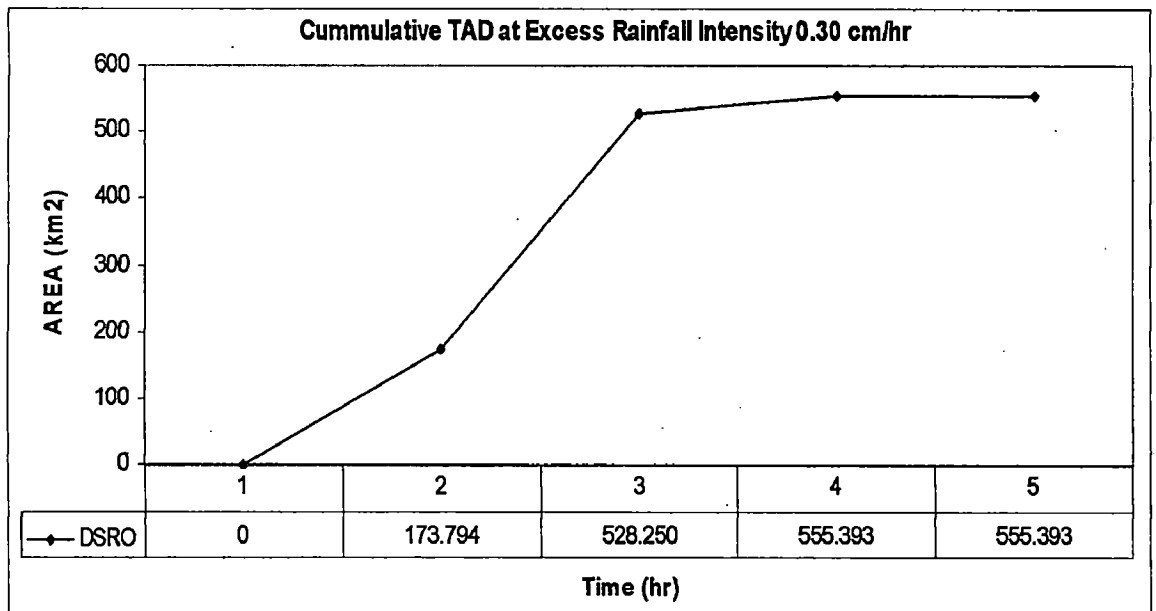
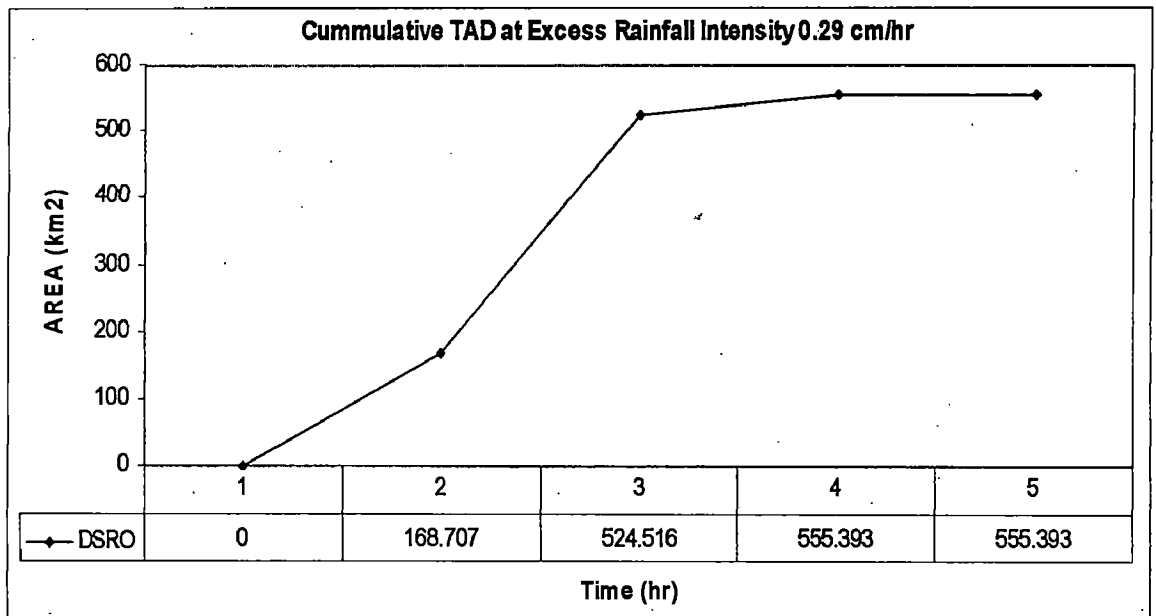


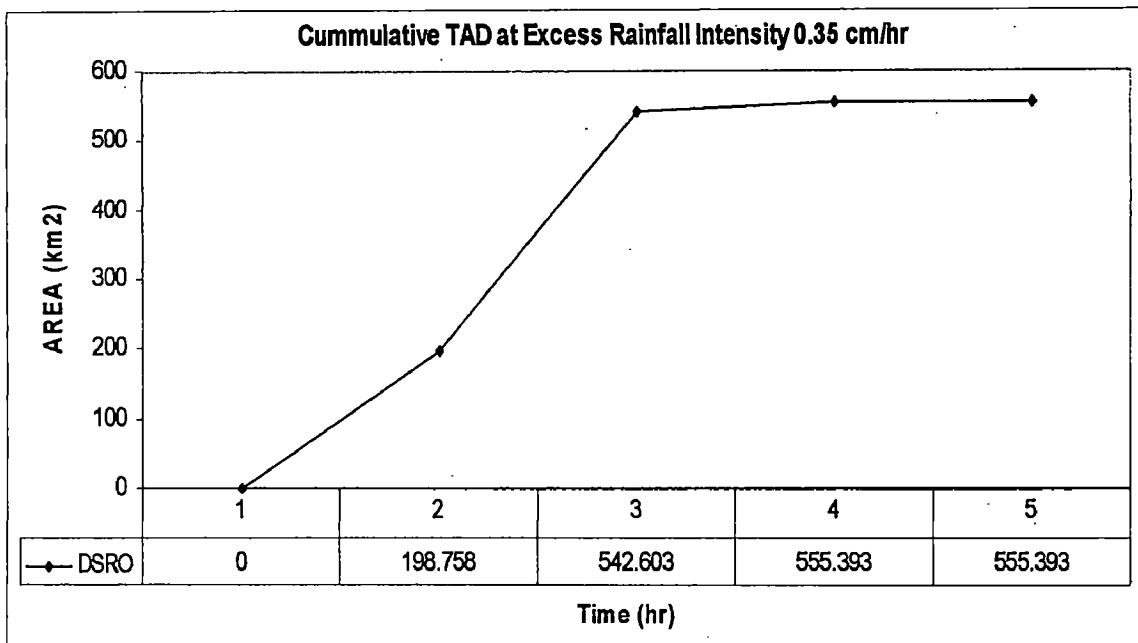
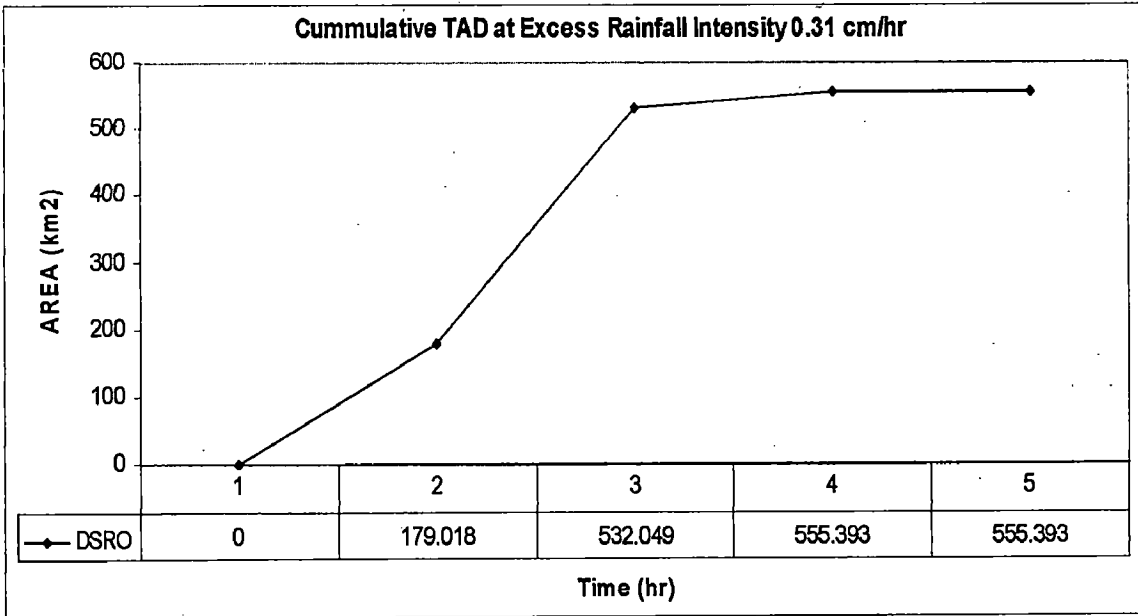


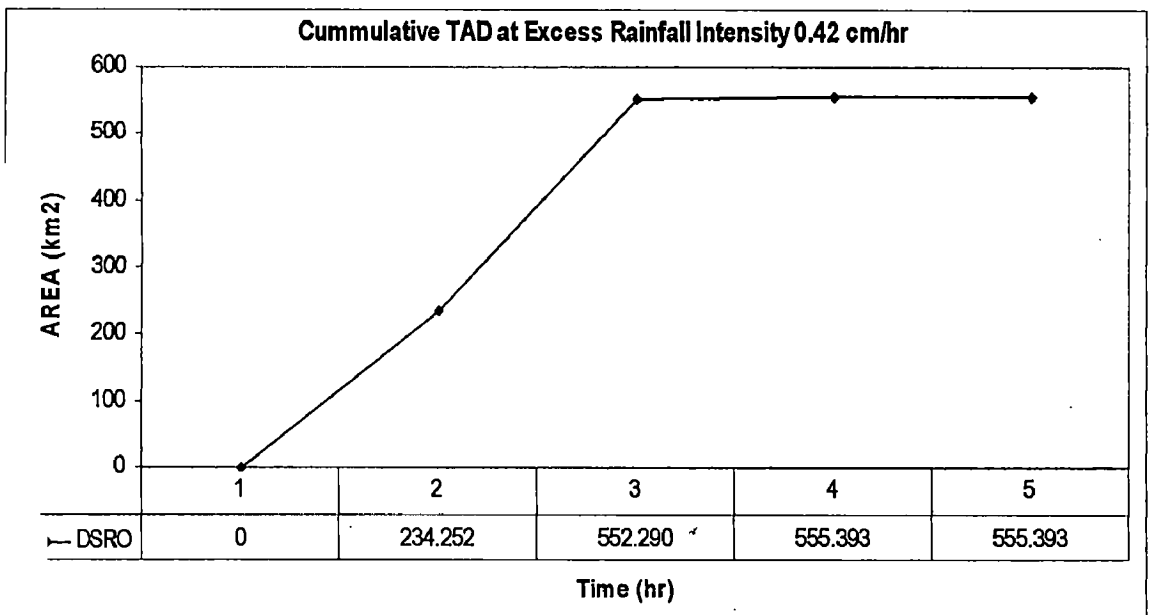
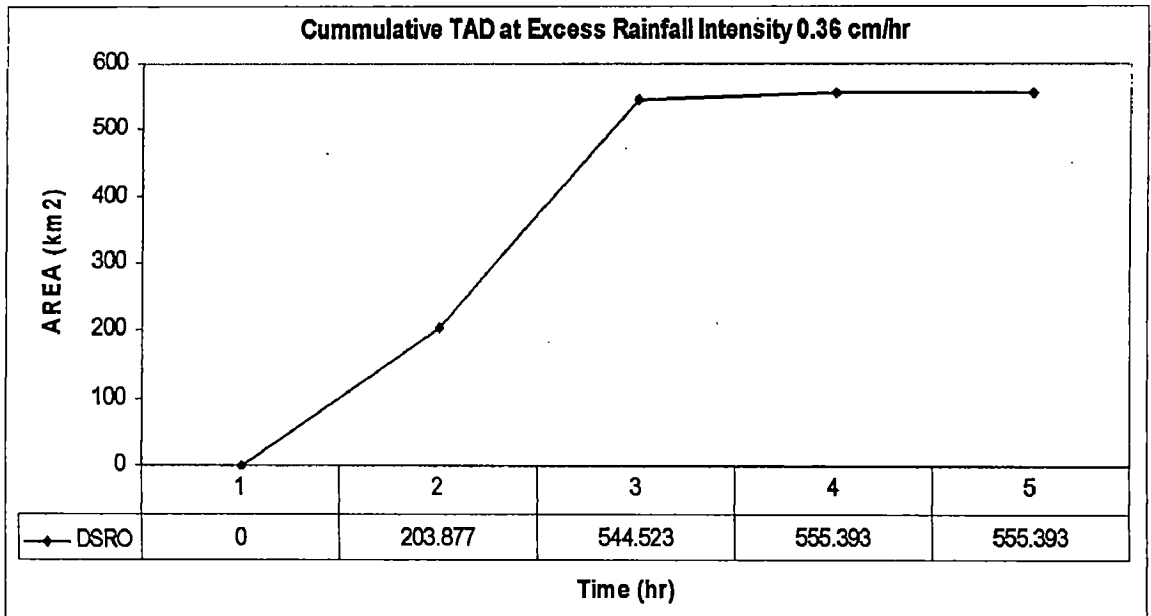




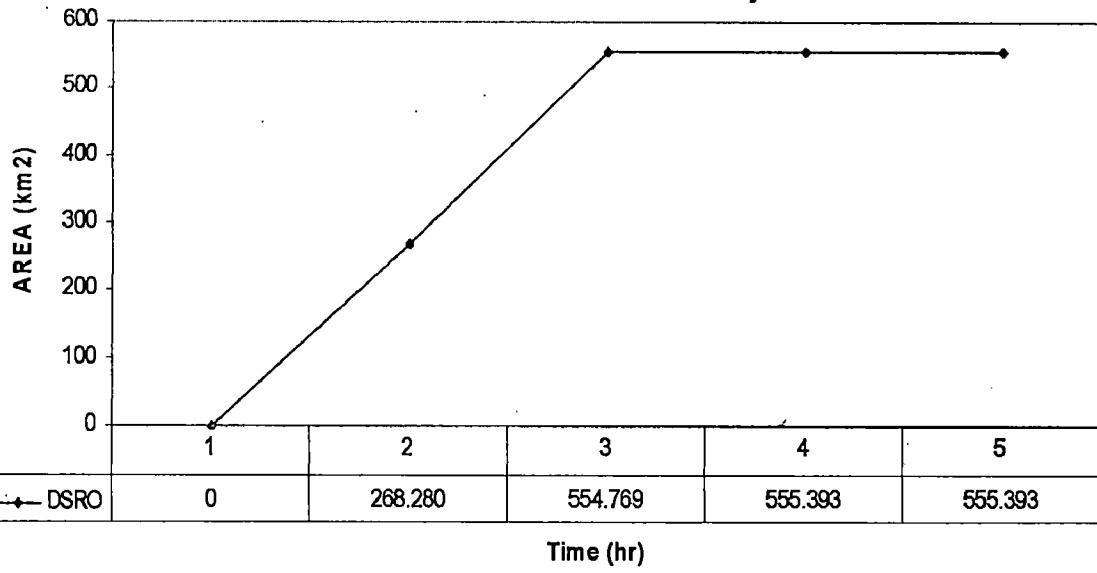




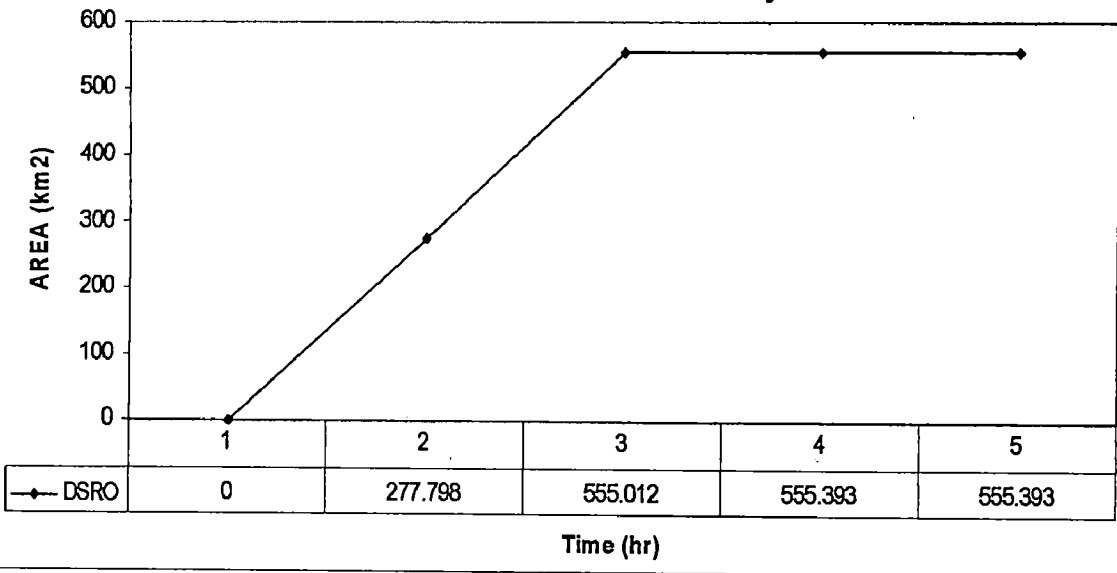


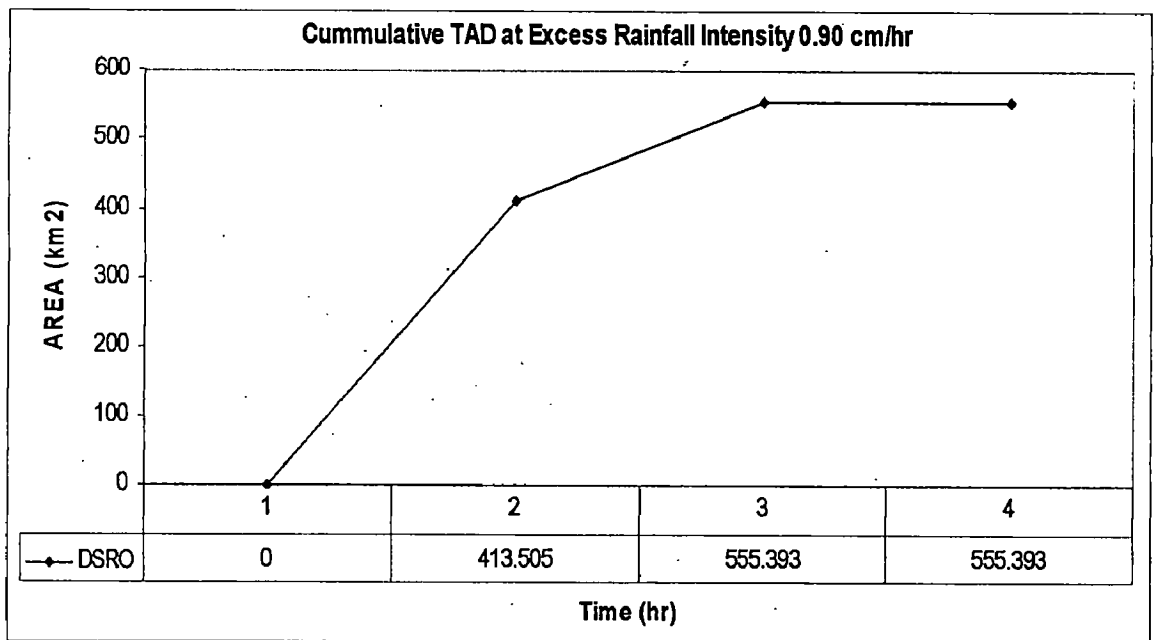
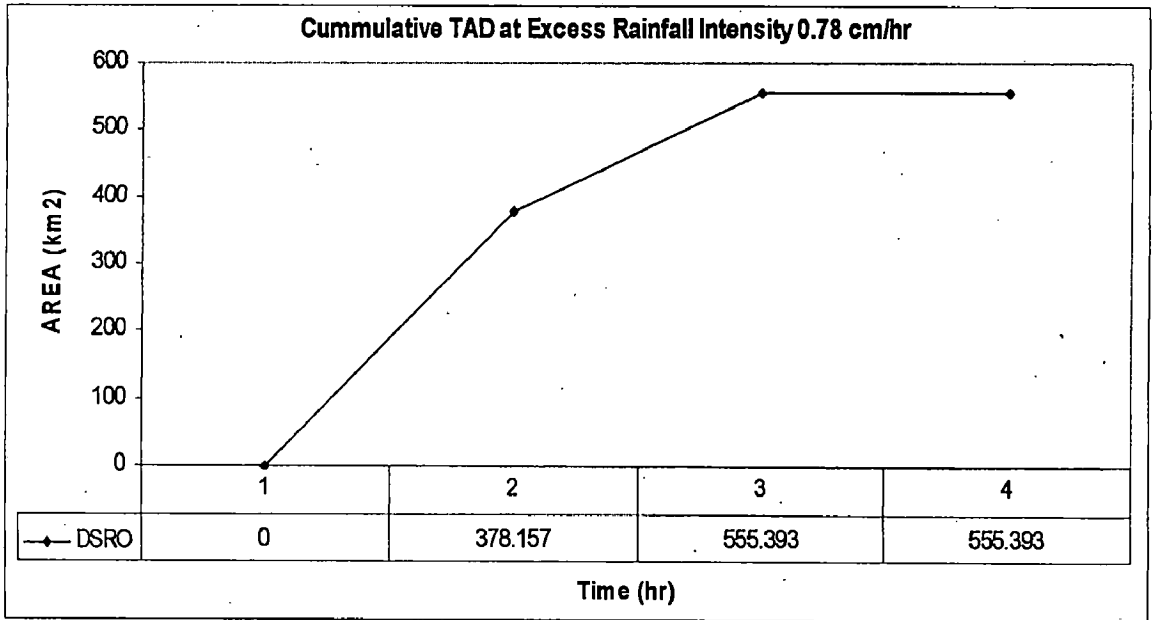


Cummulative TAD at Excess Rainfall Intensity 0.49 cm/hr



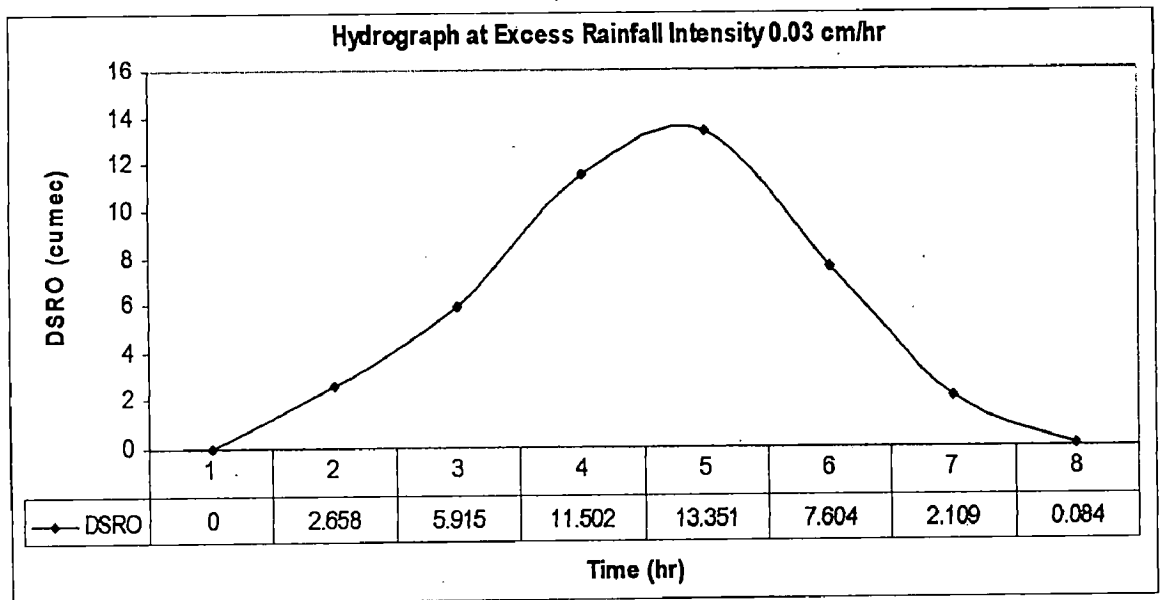
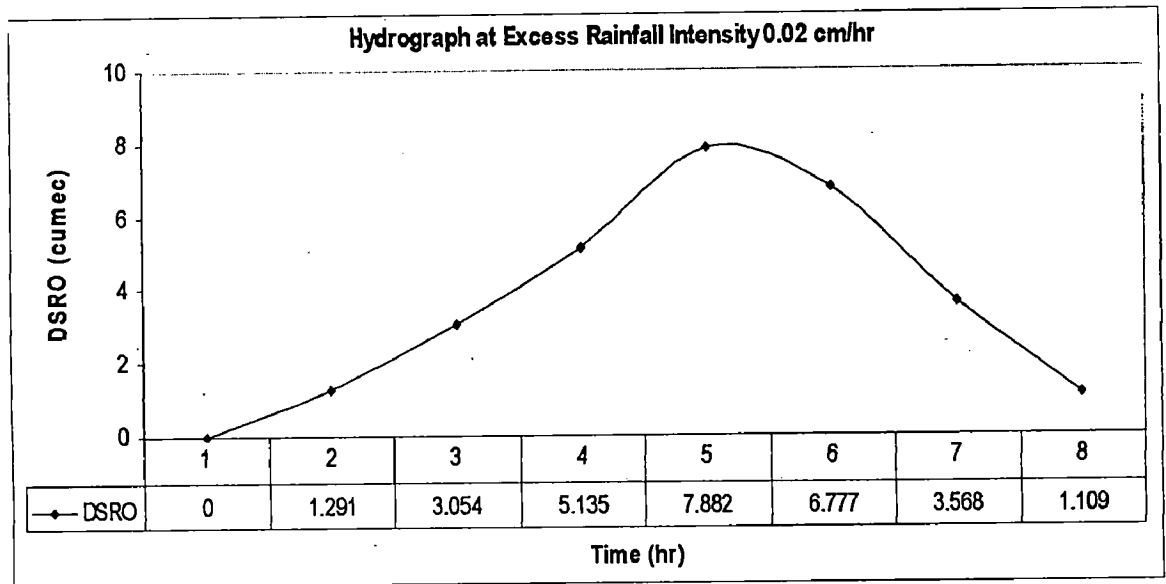
Cummulative TAD at Excess Rainfall Intensity 0.51 cm/hr

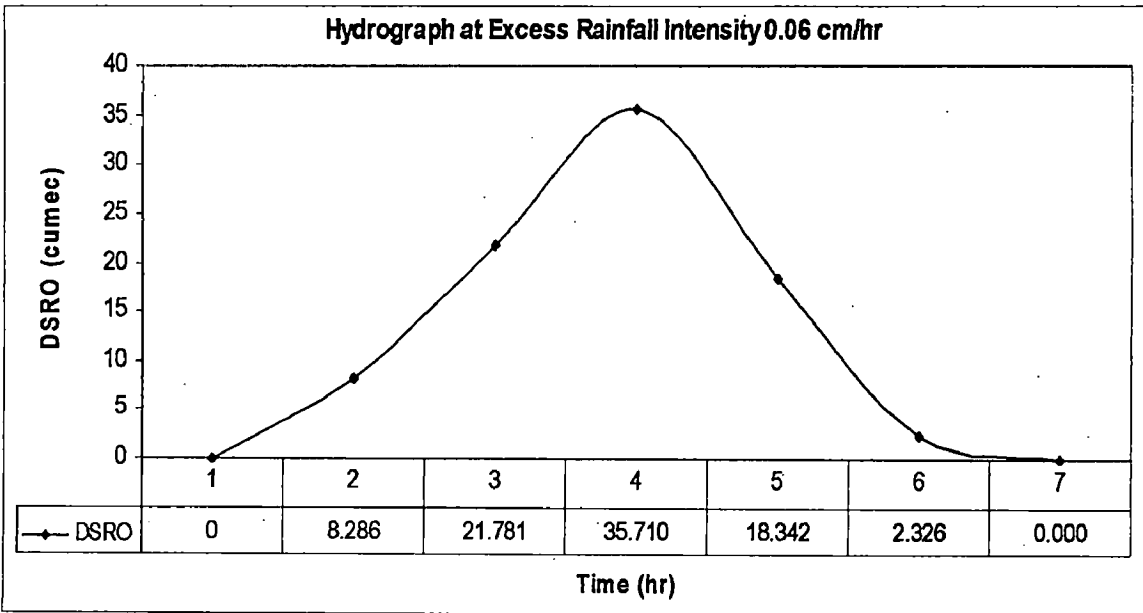
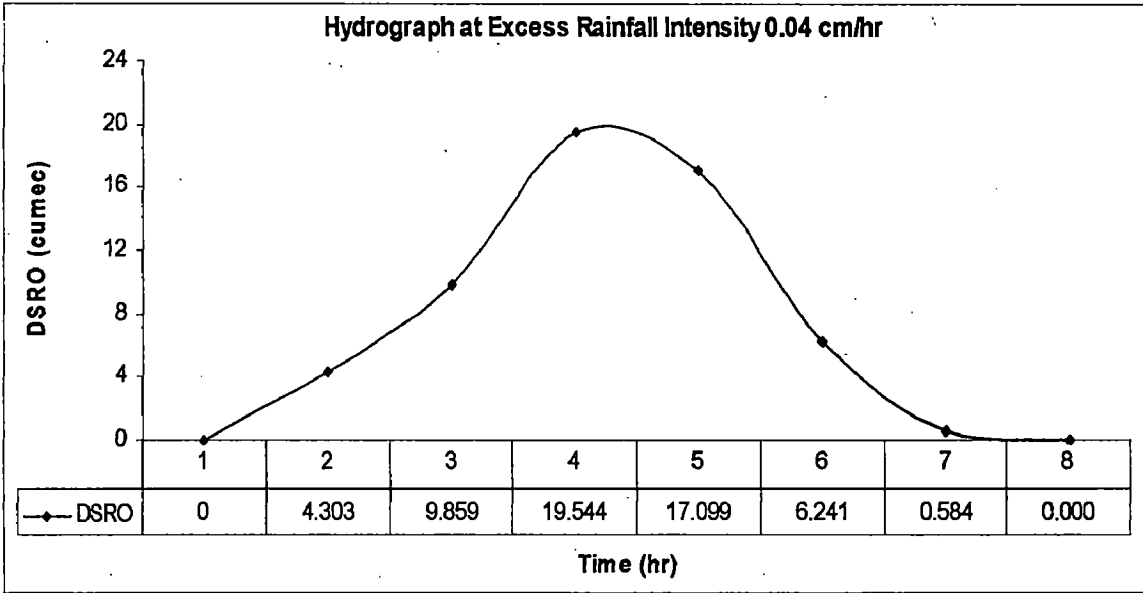


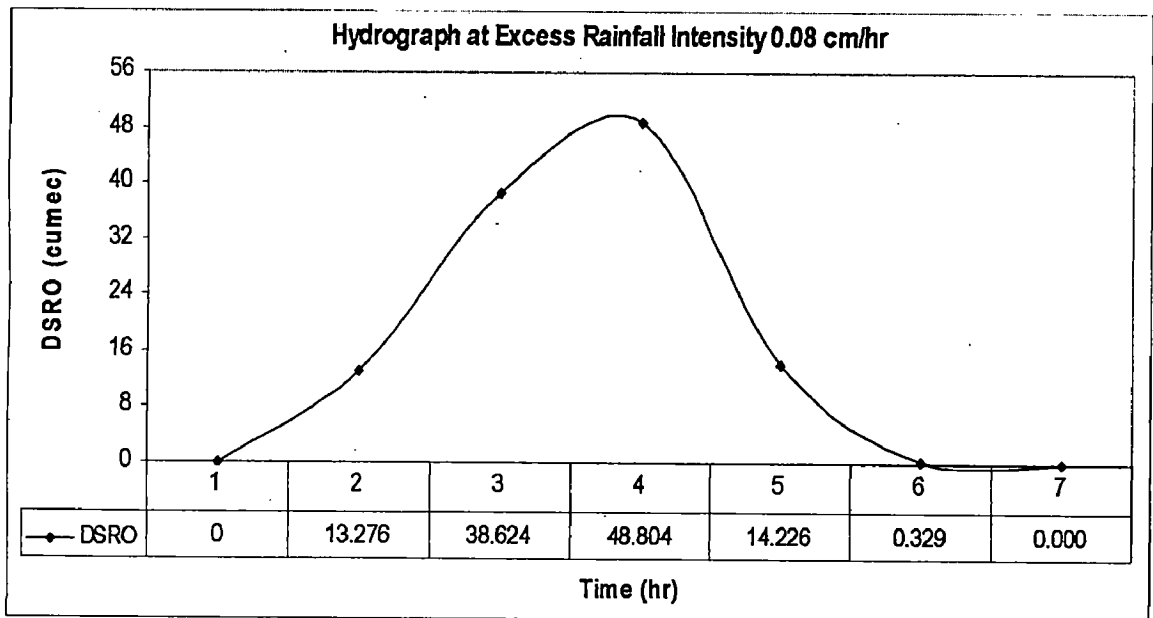
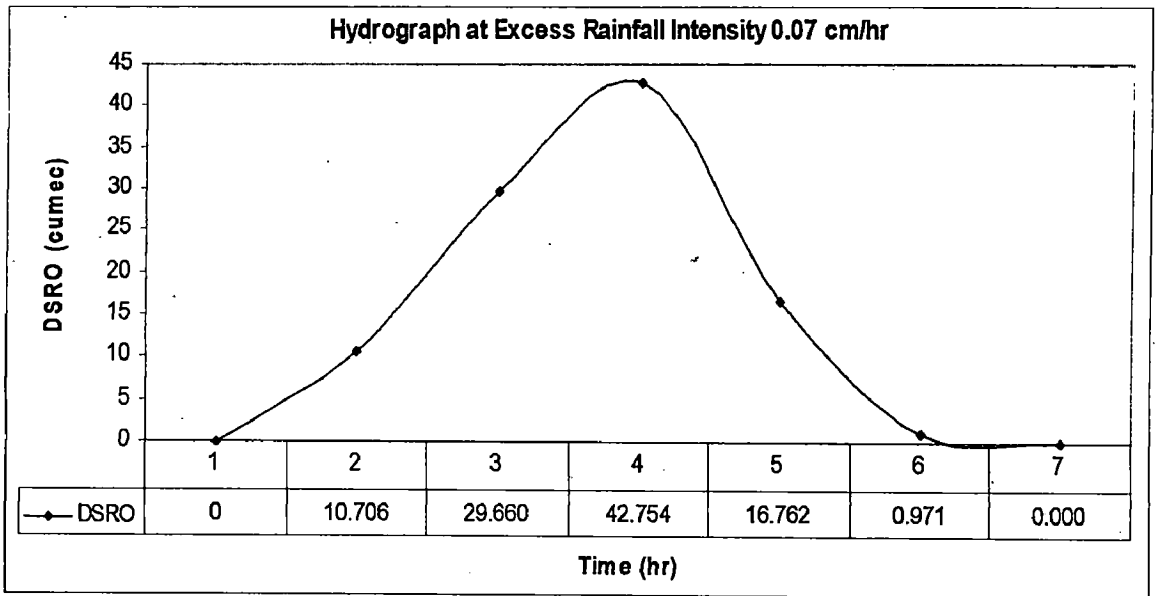


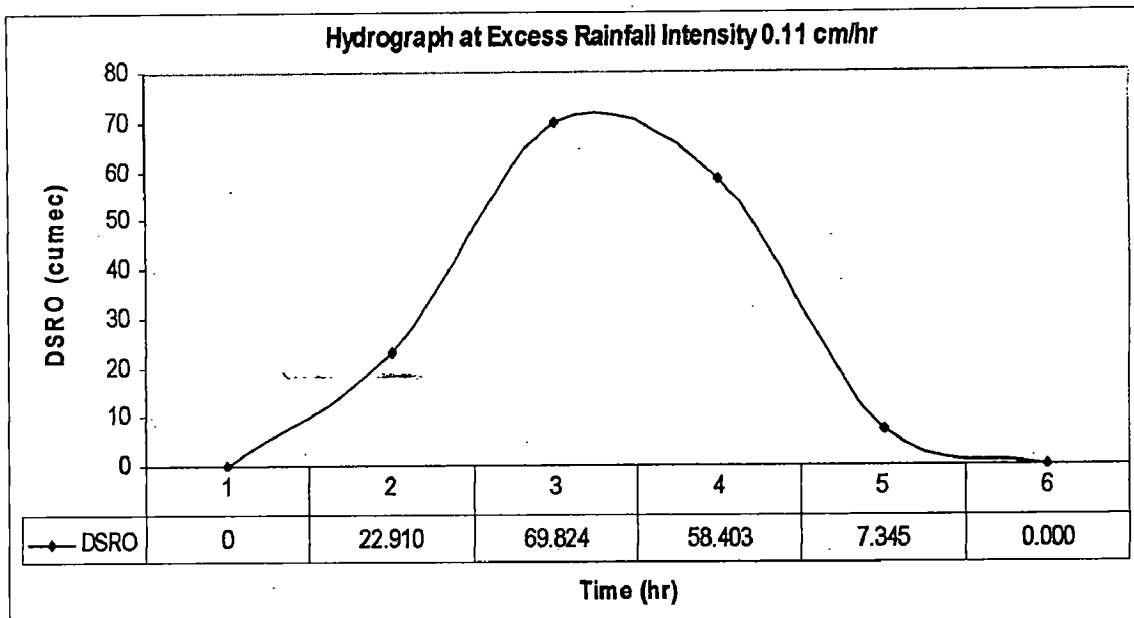
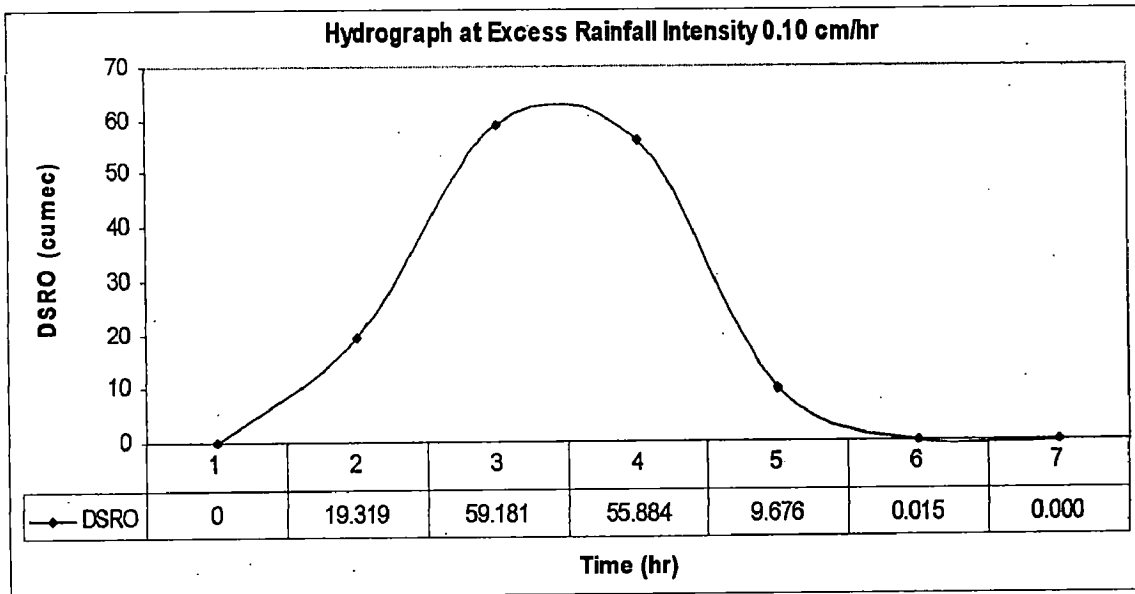
APPENDIX A-3

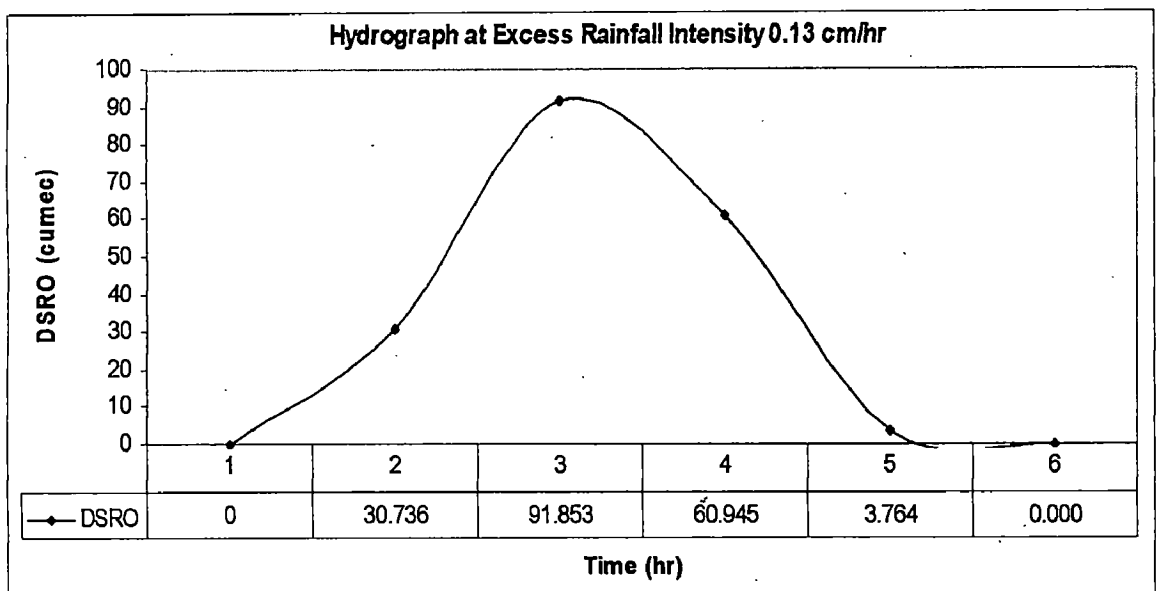
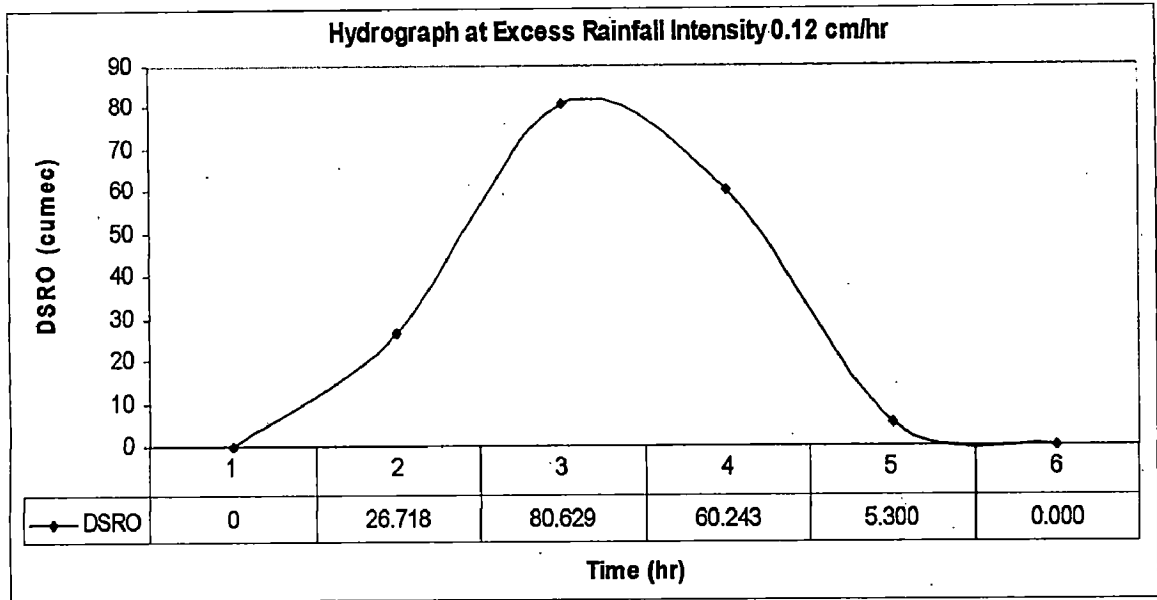
GRAPH OF DSRO DUE TO RAINFALL EXCESS

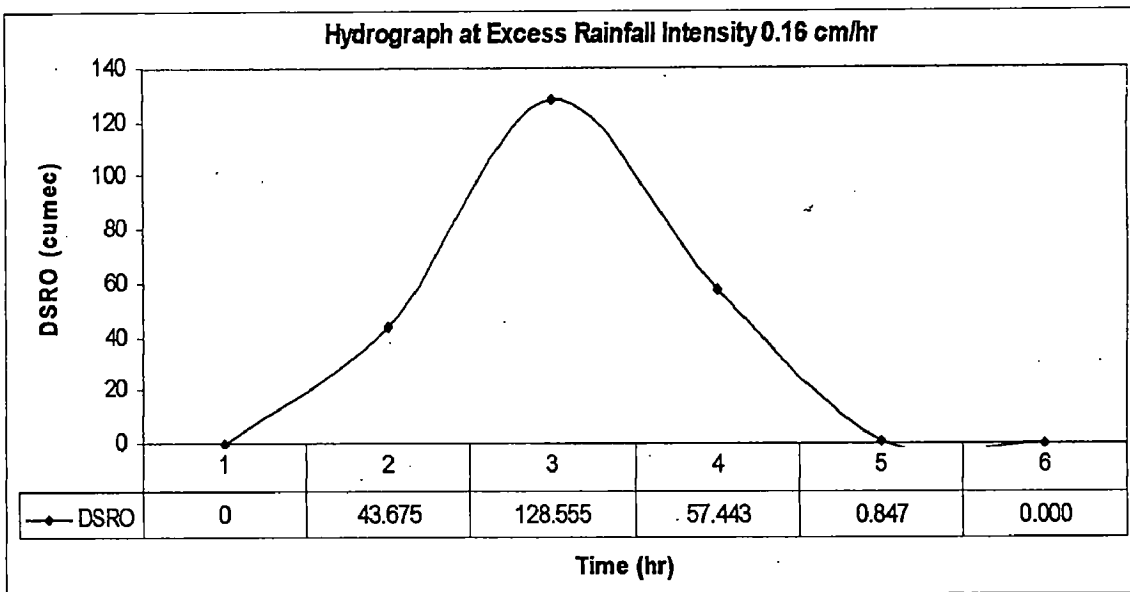
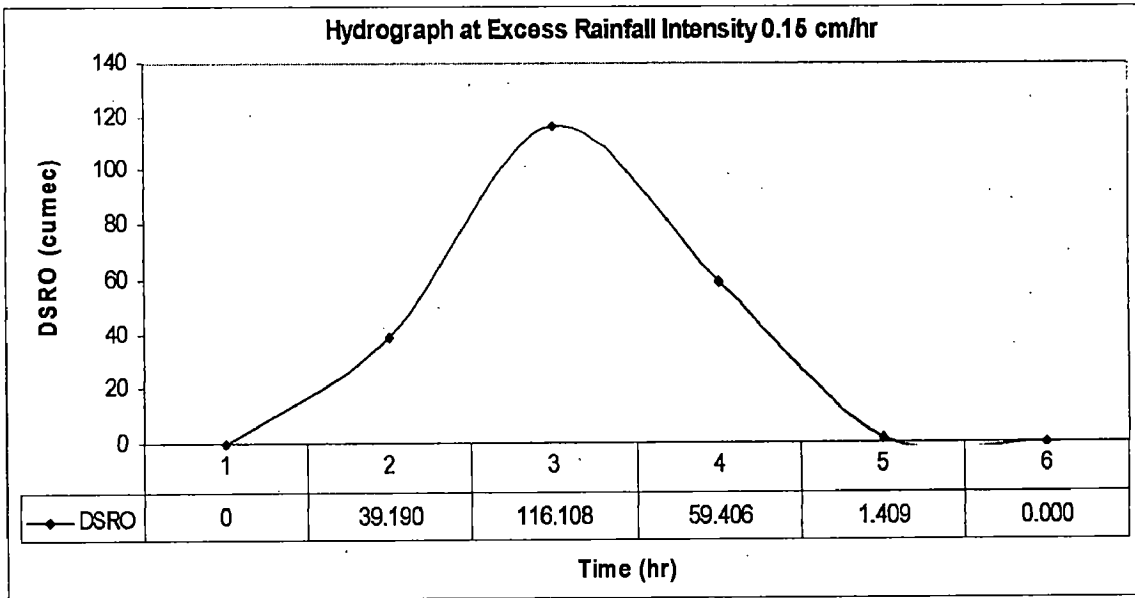


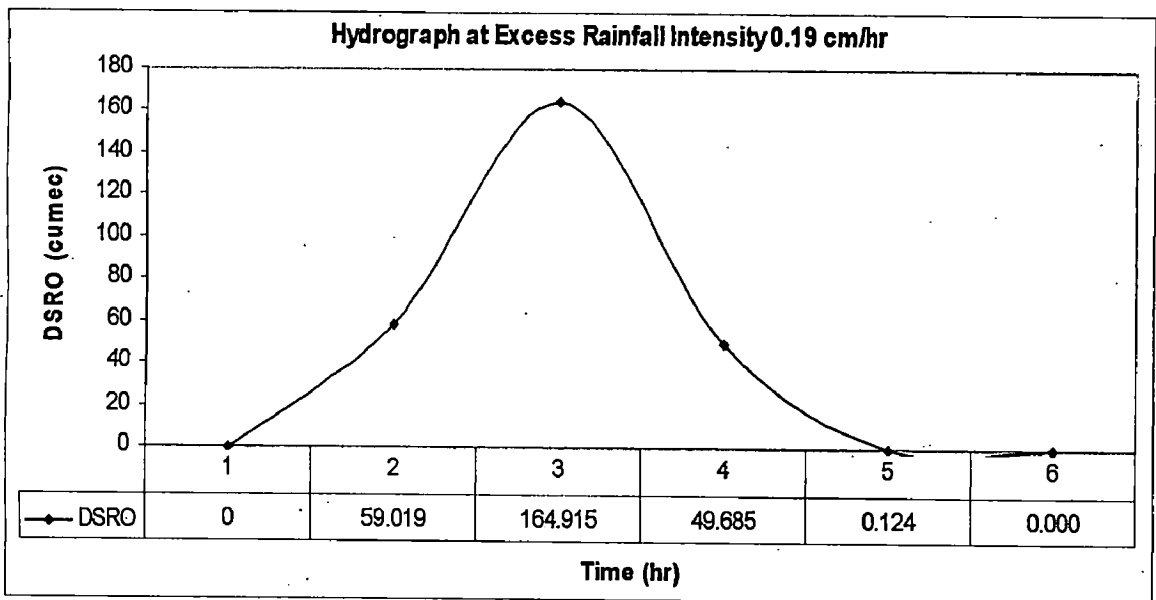
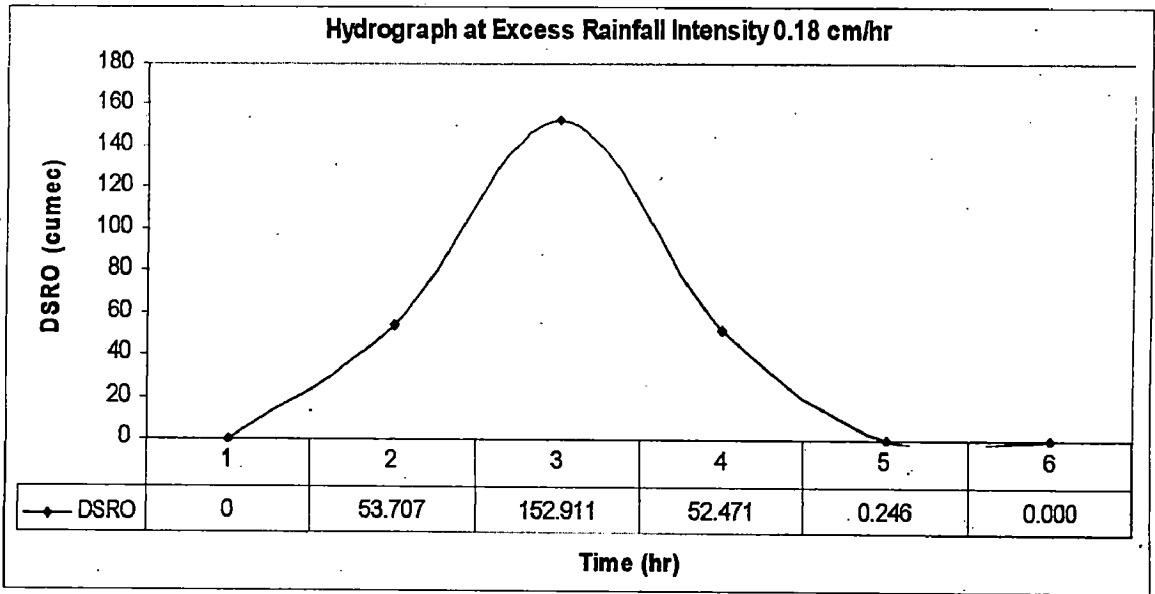


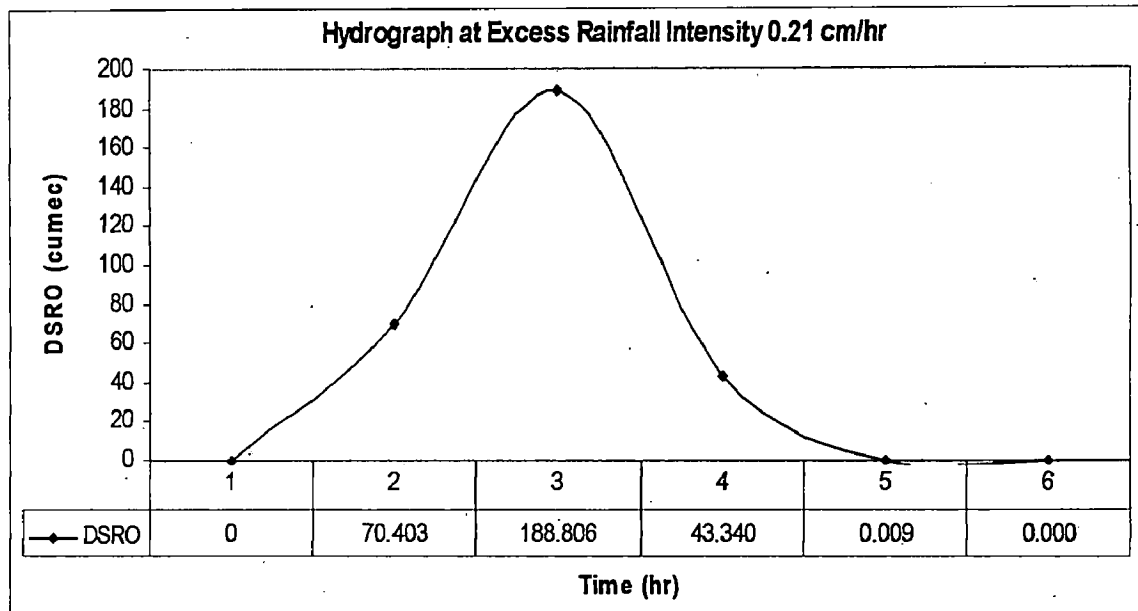
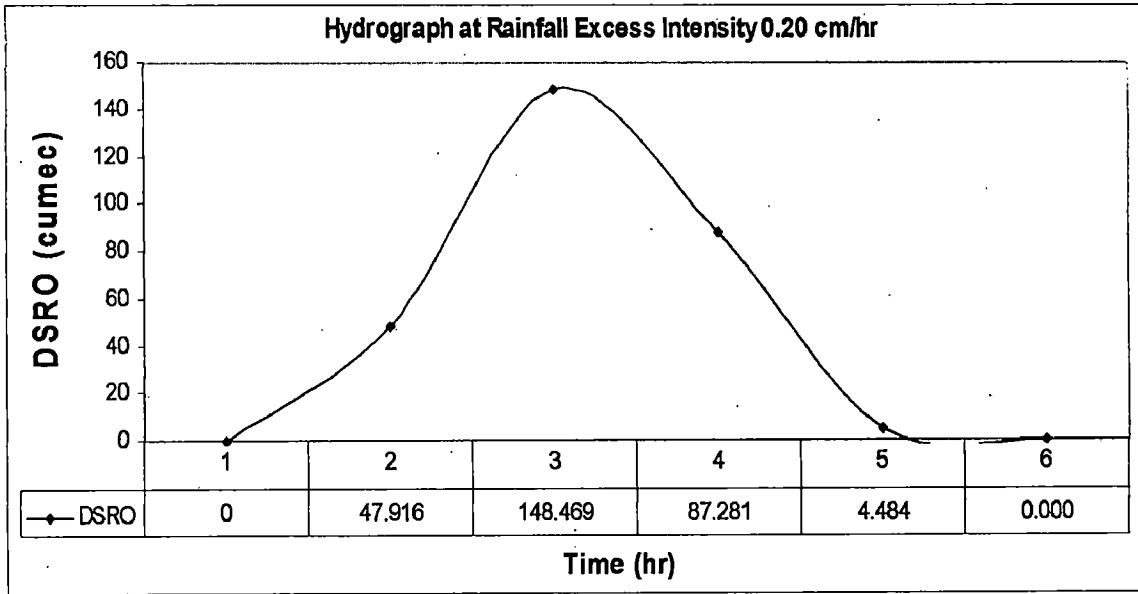


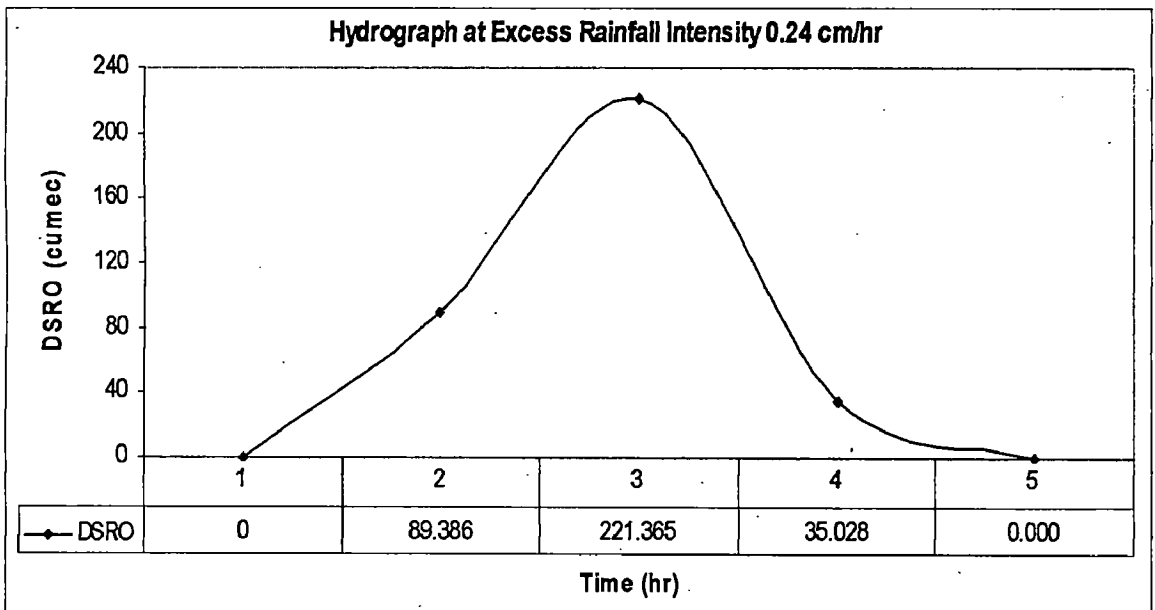
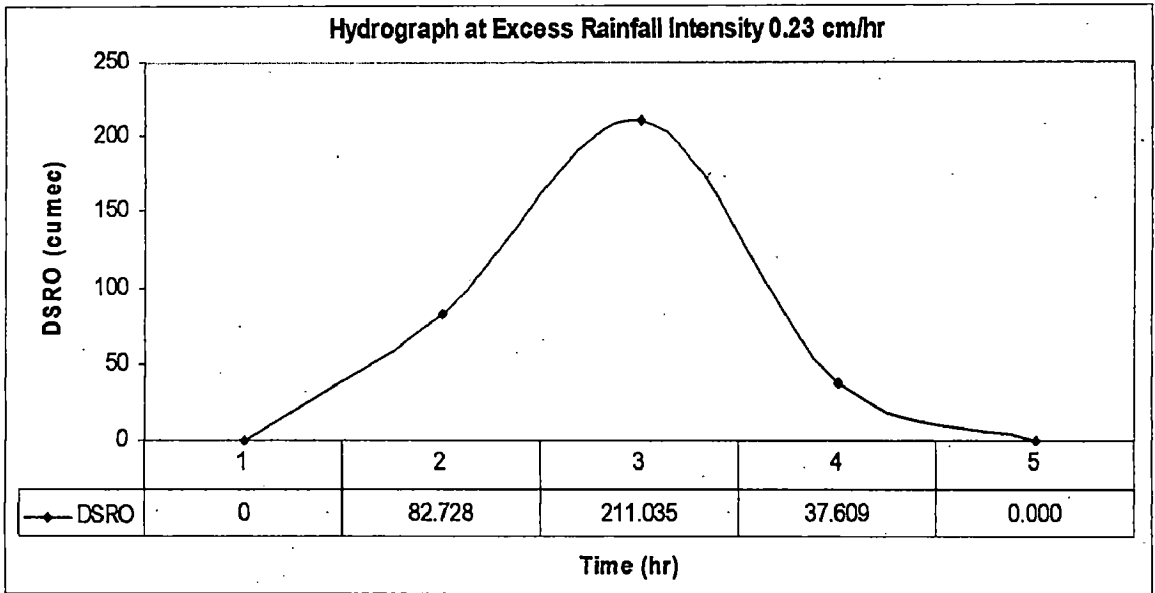


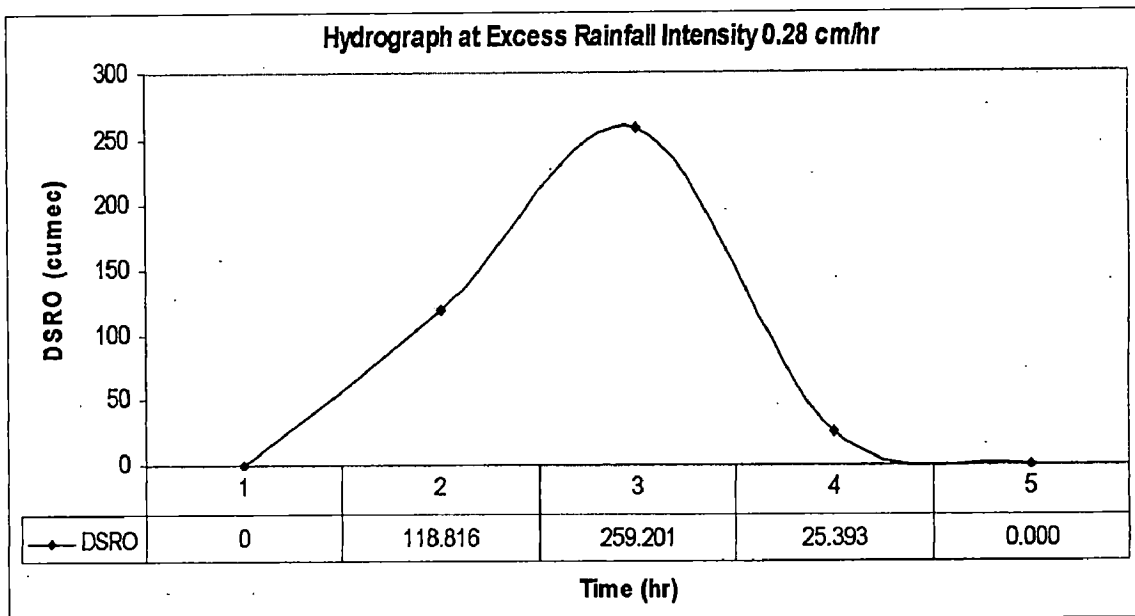
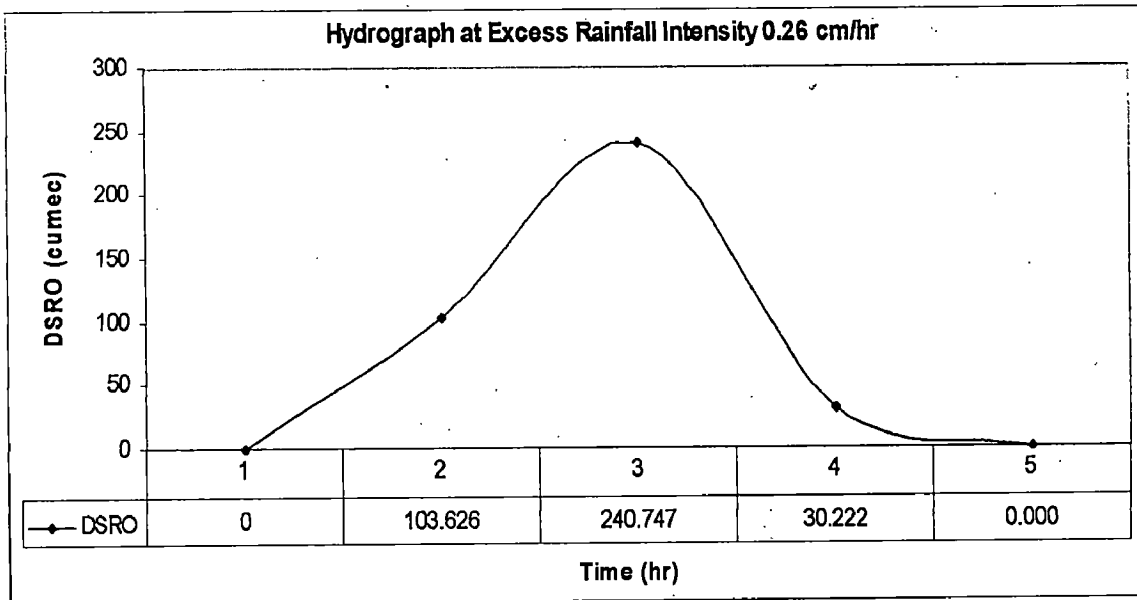


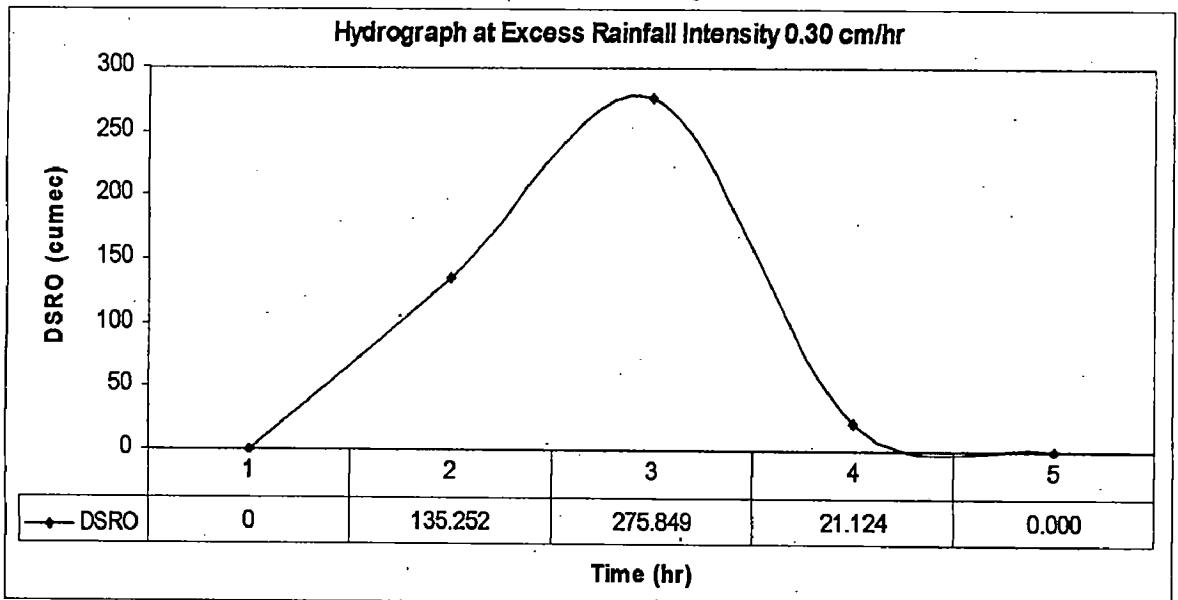
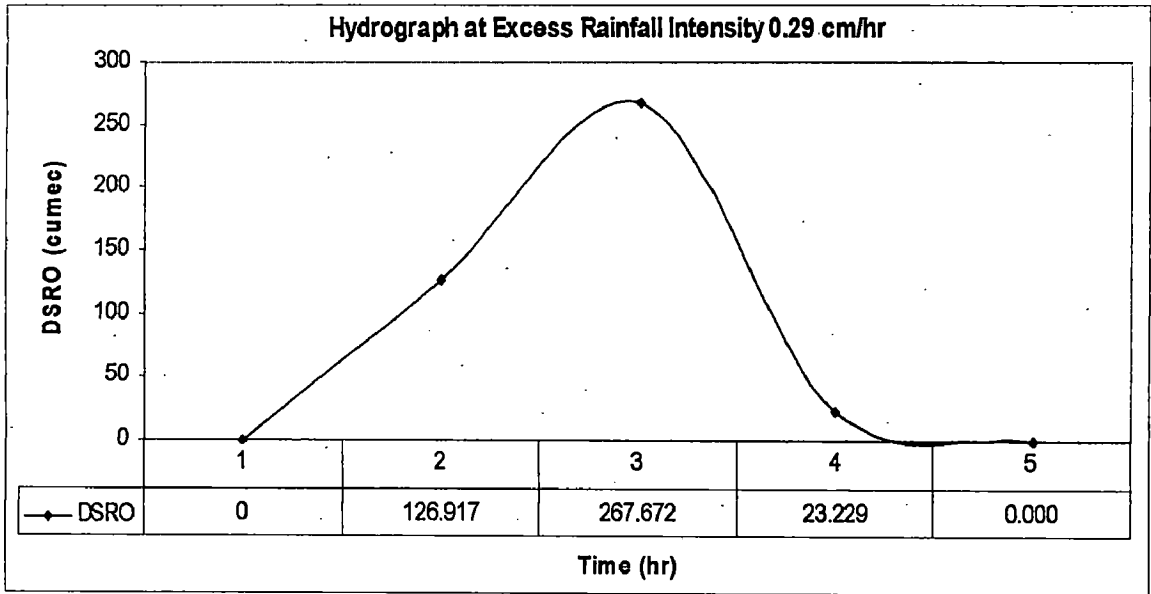


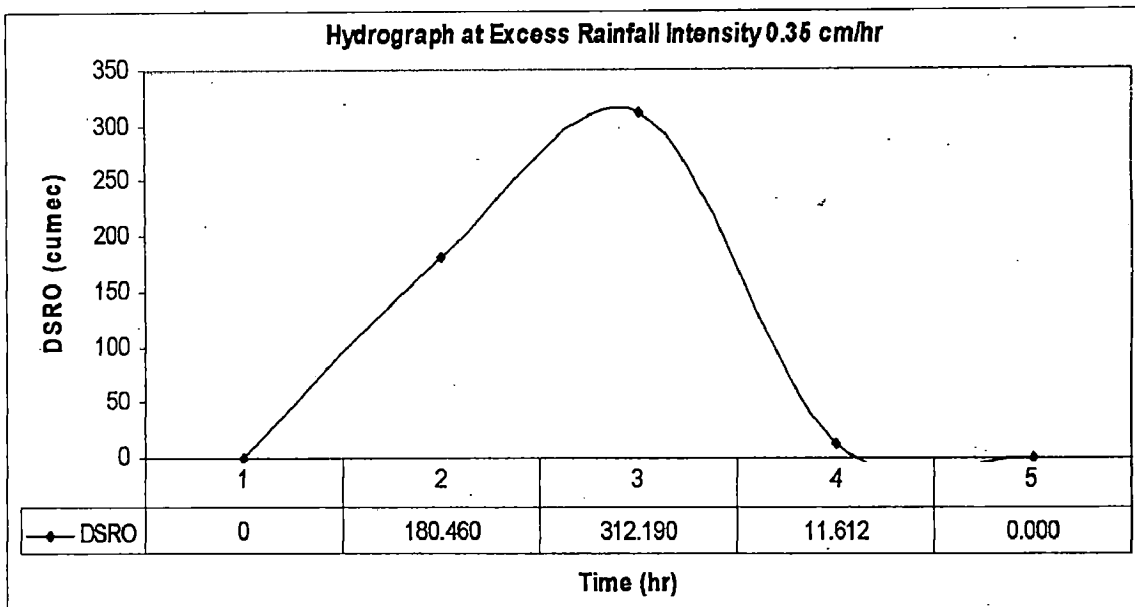
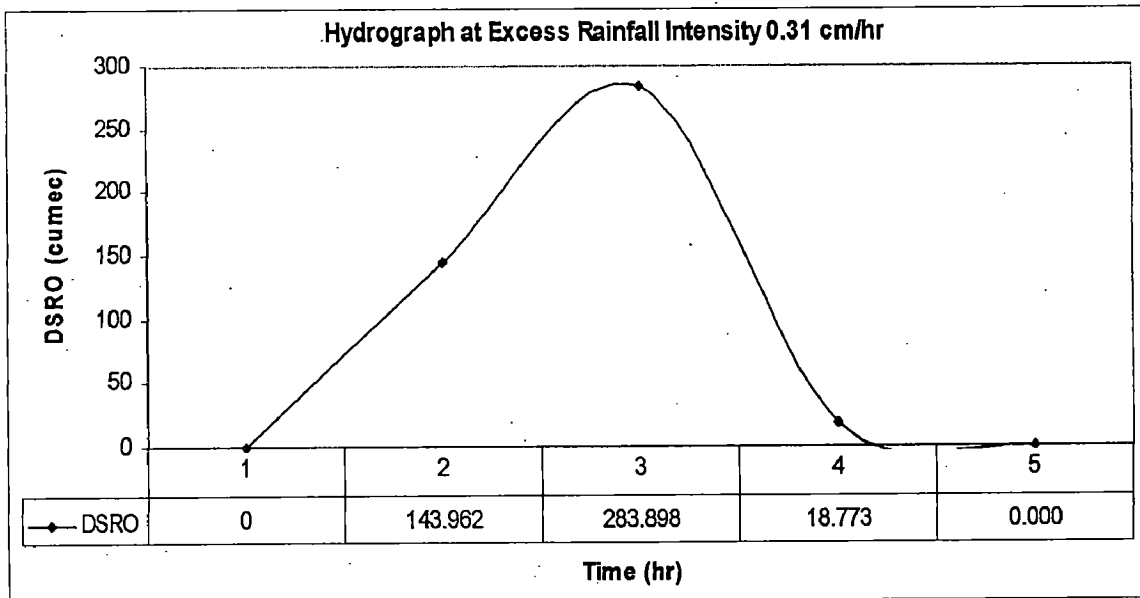


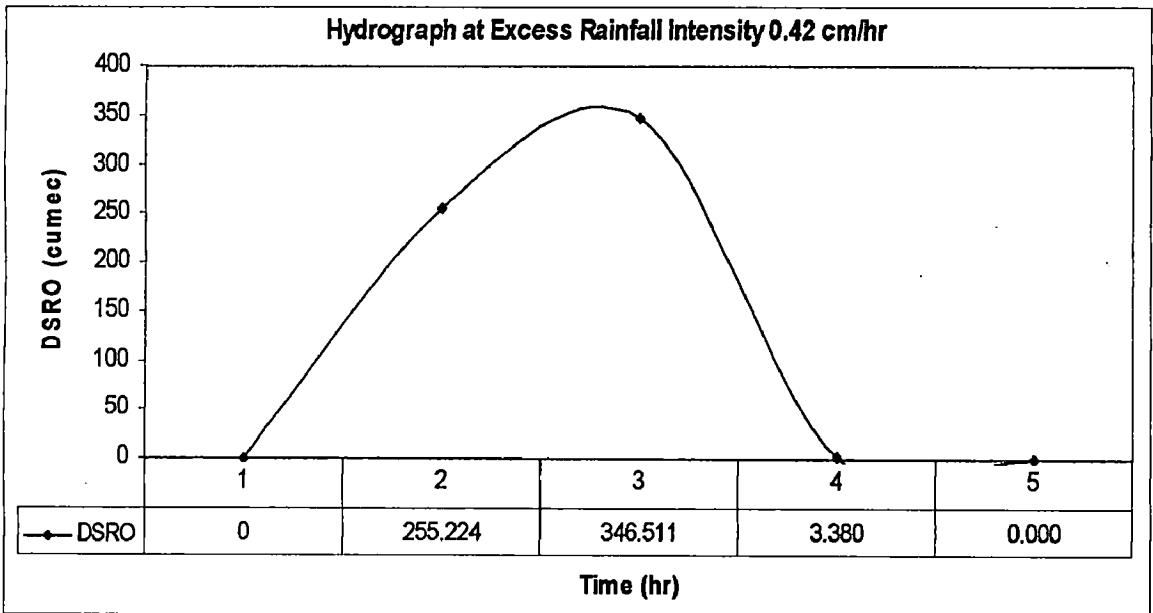
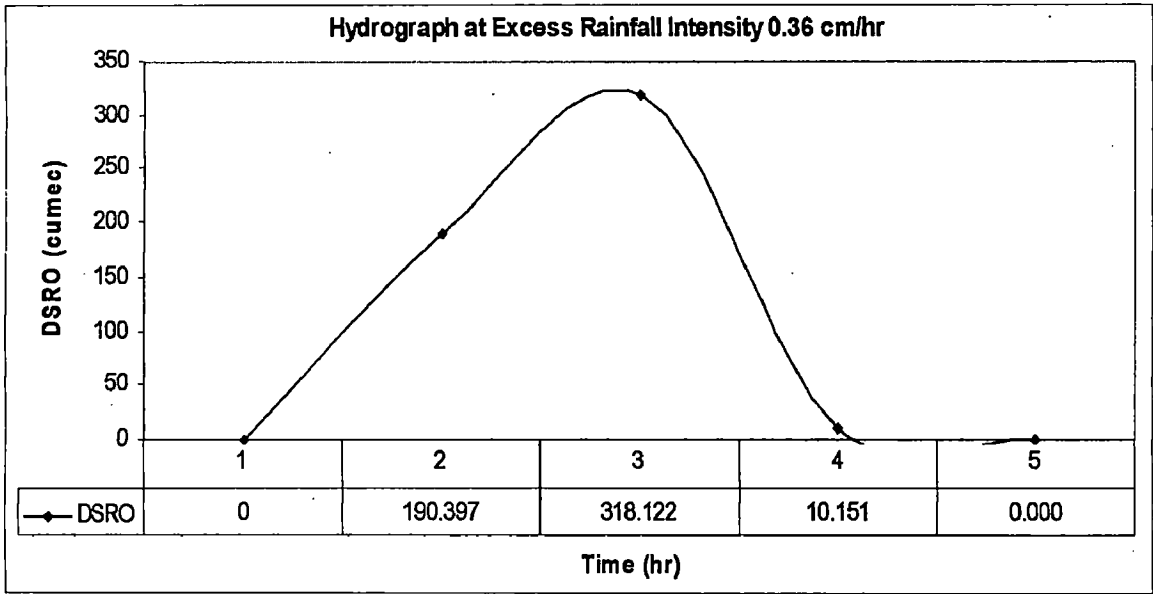


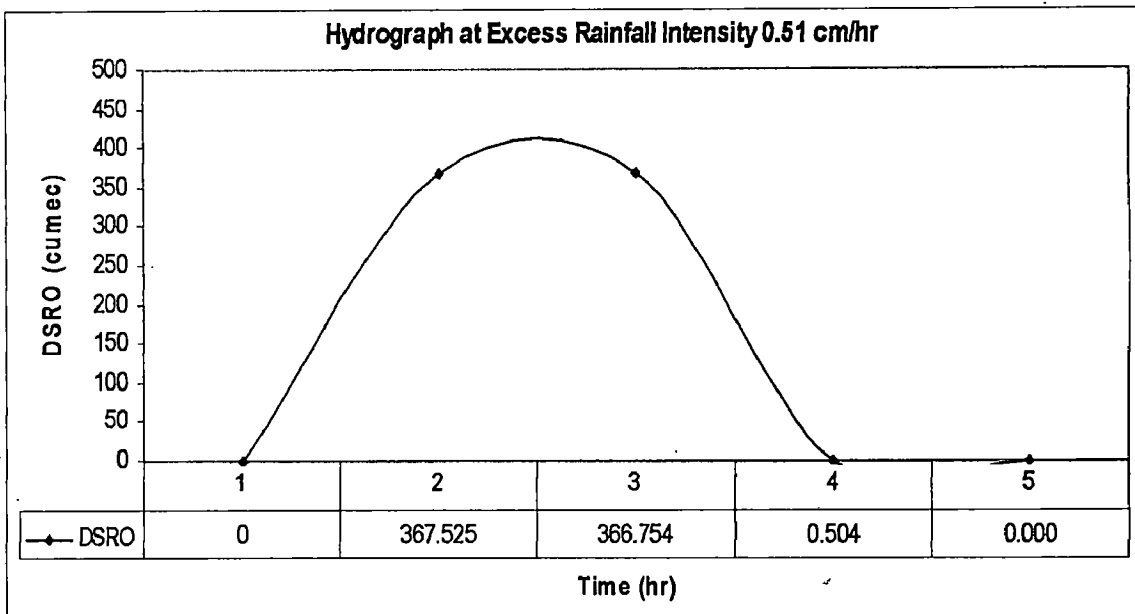
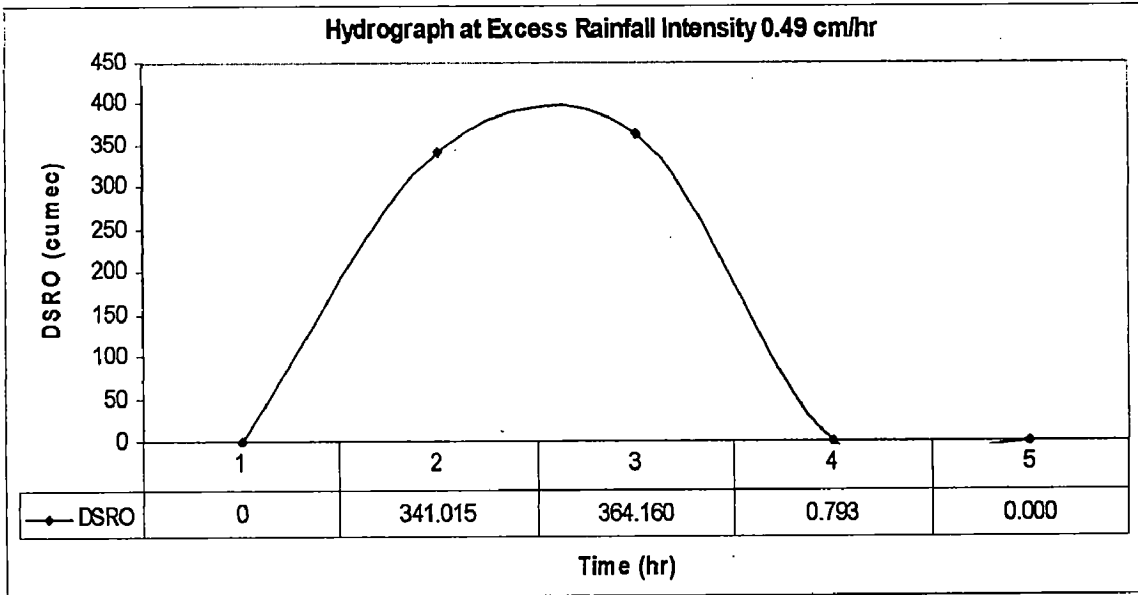


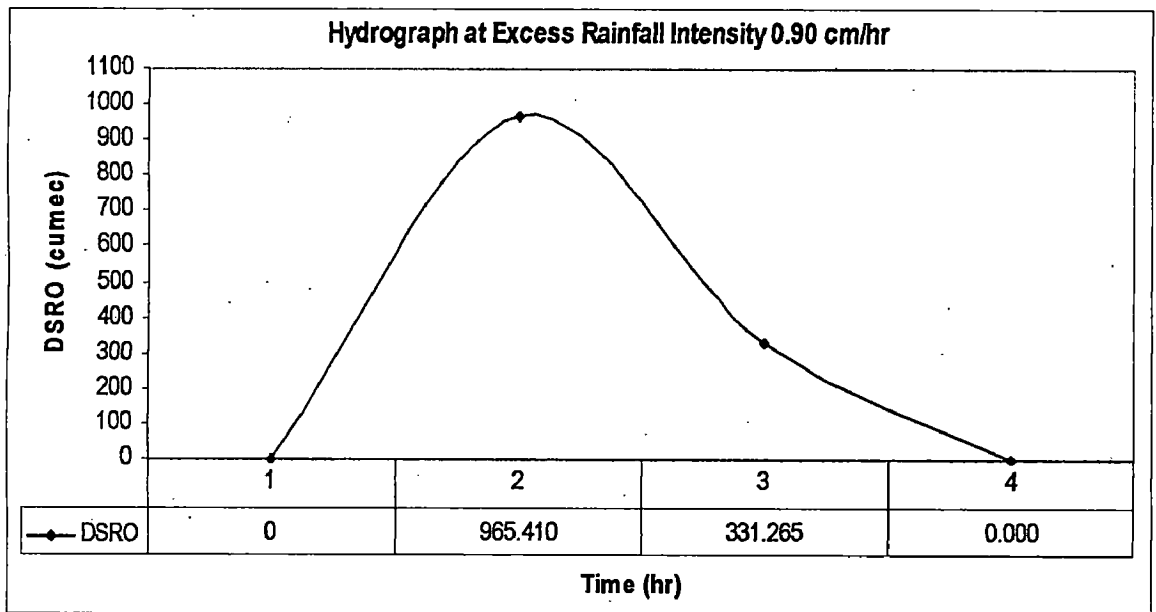
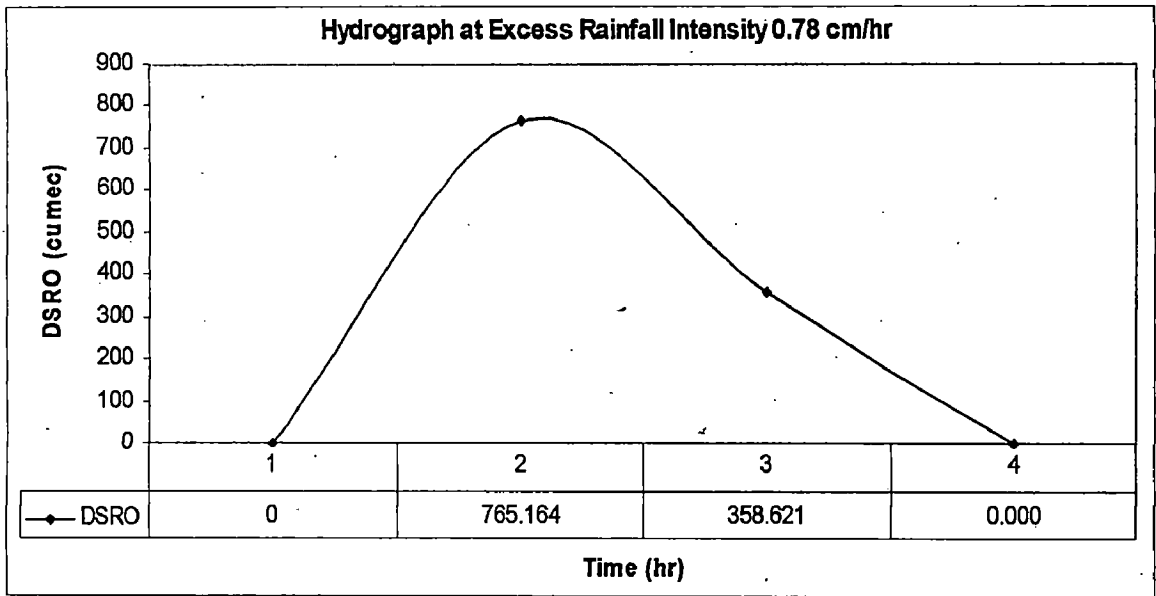












APPENDIX A-4

CALCULATION OF TOTAL DSRO FOR 7 STORM

CALCULATION TOTAL DSRO USING CONVOLUTION METHOD FOR EVENT 1

Time (hr)	DSRO with Excess Rainfall Intensity					Total Direct Surface Runoff
	0.10 cm/hr	0.29 cm/hr	0	0.30 cm/hr	0	
0	0.00					0.00
1	12.00	0.00				12.00
2	40.00	126.92	0.00			166.92
3	62.00	267.67	0.00	0.00		329.67
4	55.00	23.23	0.00	135.25	0.00	213.48
5	20.00	0.00	0.00	275.85	0.00	295.85
6	2.00	0.00	0.00	21.12	0.00	23.12
7	0.80	0.00	0.00	0.00	0.00	0.80
8	0.21	0.00	0.00	0.00	0.00	0.21
9	0.00	0.00	0.00	0.00	0.00	0.00
10		0.00	0.00	0.00	0.00	0.00

CALCULATION TOTAL DSRO USING CONVOLUTION METHOD FOR EVENT 2

Time (hr)	DSRO with Excess Rainfall Intensity						Total Direct Surface Runoff
	0	0	0	0	0	0.26 cm/hr	
0	0.0						0.0
1	0.0	0.0					0.0
2	0.0	0.0	0.0				0.0
3	0.0	0.0	0.0	0.0			0.0
4	0.0	0.0	0.0	0.0	0.0		0.0
5	0.0	0.0	0.0	0.0	0.0	0.0	0.0
6	0.0	0.0	0.0	0.0	0.0	103.6	103.6
7	0.0	0.0	0.0	0.0	0.0	240.7	240.7
8		0.0	0.0	0.0	0.0	30.2	30.2
9			0.0	0.0	0.0	0.0	0.0
10				0.0	0.0	0.0	0.0
11					0.0	0.0	0.0
12						0.0	0.0

**CALCULATION TOTAL DSRO USING CONVOLUTION METHOD
FOR EVENT 3**

Time (hr)	DSRO with Excess Rainfall Intensity							Total Direct Surface Runoff
	0	0.07 cm/hr	0	0.06 cm/hr	0.21 cm/hr	0.23 cm/hr	0.24 cm/hr	
0	0.00							0.00
1	0.00	0.00						0.00
2	0.00	7.00	0.00					7.00
3	0.00	17.00	0.00	0.00				17.00
4	0.00	29.00	0.00	5.00	0.00			34.00
5	0.00	42.75	0.00	11.00	70.40	0.00		124.16
6	0.00	38.00	0.00	19.00	188.81	82.73	0.00	328.53
7	0.00	19.00	0.00	29.20	43.34	211.04	89.39	391.96
8		5.00	0.00	35.61	0.01	37.61	221.37	299.59
9		0.40	0.00	24.00	0.00	0.00	35.03	59.43
10		0.10	0.00	13.60	0.00	0.00	0.00	13.70
11		0.00	0.00	3.00	0.00	0.00	0.00	3.00
12			0.00	0.40	0.00	0.00	0.00	0.40
13				0.30	0.00	0.00	0.00	0.30
14				0.00	0.00	0.00	0.00	0.00

**CALCULATION TOTAL DSRO USING CONVOLUTION METHOD
FOR EVENT 4**

Time (hr)	DSRO with Excess Rainfall Intensity						Total Direct Surface Runoff
	0	0	0.31 cm/hr	0	0	0	
0	0.00						0.00
1	0.00	0.00					0.00
2	0.00	0.00	0.00				0.00
3	0.00	0.00	143.96	0.00			143.96
4	0.00	0.00	283.90	0.00	0.00		283.90
5	0.00	0.00	18.77	0.00	0.00	0.00	18.77
6	0.00	0.00	0.00	0.00	0.00	0.00	0.00
7	0.00	0.00	0.00	0.00	0.00	0.00	0.00
8		0.00	0.00	0.00	0.00	0.00	0.00
9			0.00	0.00	0.00	0.00	0.00
10				0.00	0.00	0.00	0.00
11					0.00	0.00	0.00
12						0.00	0.00

**CALCULATION TOTAL DSRO USING CONVOLUTION METHOD
FOR EVENT 5**

Time (hr)	DSRO with Excess Rainfall Intensity							Total Direct Surface
	0.03 cm/hr	0.16 cm/hr	0.78 cm/hr	0.26 cm/hr	0.08 cm/hr	0	0	Runoff
0	0.00							0.00
1	1.24	0.00						1.24
2	2.60	38.00	0.00					40.60
3	4.20	129.00	765.16	0.00				898.36
4	5.80	80.00	358.62	103.63	0.00			548.05
5	7.90	18.00	0.00	240.75	8.00	0.00		274.64
6	10.50	1.00	0.00	30.22	23.22	0.00	0.00	64.95
7	12.40	0.50	0.00	0.00	39.50	0.00	0.00	52.40
8	13.35	0.00	0.00	0.00	48.80	0.00	0.00	62.15
9	12.60		0.00	0.00	35.00	0.00	0.00	47.60
10	9.49			0.00	11.00	0.00	0.00	20.49
11	6.80				2.00	0.00	0.00	8.80
12	4.20				0.50	0.00	0.00	4.70
13	2.00				0.00	0.00	0.00	2.00
14	0.80					0.00	0.00	0.80
15	0.00						0.00	0.00

APPENDIX A-5

GRAPH OF DIRECT SURFACE RUNOFF FOR 7 STORM

